DESIGN OF A C-BAND DUAL-POLARIZED STRIP-FED APERTURE COUPLED STACKED PATCH PLANAR ANTENNA ARRAY FOR POINT-TO-POINT COMMUNICATION

A THESIS SUBMITTED TO

THE GRADUATE SCHOOL OF ENGINEERING AND SCIENCE

OF BILKENT UNIVERSITY

IN PARTIAL FULFILLMENT OF THE REQUIREMENTS FOR

THE DEGREE OF

MASTER OF SCIENCE

IN

ELECTRICAL AND ELECTRONICS ENGINEERING

By

Caner ASBAŞ

August 2017

DESIGN OF A C-BAND DUAL-POLARIZED STRIP-FED APERTURE COUPLED STACKED PATCH PLANAR ANTENNA ARRAY FOR POINT-TO-POINT COMMUNICATION

By Caner ASBAŞ

August 2017

We certify that we have read this thesis and that in our opinion it is fully adequate, in scope and in quality, as a thesis for the degree of Master of Science.

Vakur B. ERTÜRK (Advisor)

Ergin ATALAR

Hatice Özlem AYDIN ÇİVİ

Approved for the Graduate School of Engineering and Science:

Ezhan KARAŞAN
Director of the Graduate School

ABSTRACT

DESIGN OF A C-BAND DUAL-POLARIZED STRIP-FED APERTURE COUPLED STACKED PATCH PLANAR ANTENNA ARRAY FOR POINT-TO-POINT COMMUNICATION

Caner ASBAŞ
M.S. in Electrical and Electronics Engineering
Advisor: Vakur B. ERTÜRK
August 2017

Point-to-point (P2P) communication is utilized where each communication node knows the physical or electrical positions of the other. In this type of communication, only two nodes transmit/receive message between each other and no other node is included in this process. P2P communication offers some advantages such as lower power consumption, better information safety, lower vulnerablity to jamming and better channel capacity usage. With these properties, it is preferred frequently in military.

Directional antennas with high gain and low side lobe level (SLL) are desired for P2P communication in order to achieve higher effective communication distance, lower power consumption and to decrease the interference between channels, respectively. Another requirement is caused by Multiple-Input-Multiple-Output capability, which is a technique to use dual or circularly polarized transreceiver antennas instead of using separate transmitter and receiver antennas in the system. For dual-polarized MIMO antennas, high cross polarization isolation values are desired to separate the transmitting and receiving channels in order to prevent them effecting each other.

In this study, a C-band dual-polarized strip-fed aperture coupled stacked patch antenna array for P2P communication is designed. To satsify the requirements of P2P communication, the reflection coefficient of the designed antenna is -10dB. The gain is 20dB and SLL is better than -15dB in the cardinal and intercardinal planes of the antenna for both polarizations. Additionally, 40dB cross polarization isolation can be achieved. The idea is based on planar array of strip-fed dual-polarized aperture coupled patch antennas with stripline feed networks. By

adjusting the amplitude distribution on the feed network, -15dB SLL in both cardinal and intercardinal planes is achieved for both polarizations. In order to block the coupling between feed networks for different polarizations and prevent distortion on amplitude and phase distributions, stripline feed networks are chosen. In this way, cross polarization isolation can be increased as well. Hence, a novel antenna element, dual-polarized strip-fed aperture coupled stacked patch antenna is proposed. The parameters that affect the impedance behaviour of this type of antenna are investigated and examined in detail. Required feed networks to achieve -15dB SLL in cardinal and intercardinal planes are designed. The proposed antenna elements are placed in array sturucture, connected to feed networks and the resulted antenna array is optimized and analyzed.

Keywords: Point-to-point (P2P) communication, side lobe level (SLL) reduction, aperture coupled patch antenna, strip-fed antenna.

ÖZET

NOKTADAN NOKTAYA TELEKOMÜNİKASYON İÇİN C BANT DUAL POLARİZE ŞERİT BESLEME AÇIKLIK BAĞLAŞIMLI DÜZLEMSEL BİR YIĞINLANMIŞ YAMA ANTEN DİZİSİ TASARIMI

Caner ASBAŞ
Elektrik ve Elektronik Mühendisliği, Yüksek Lisans
Tez Danışmanı: Vakur B. ERTÜRK
Ağustos 2017

Noktadan noktaya telekomünikasyondan, her bir iletişim düğümü diğerinin fiziksel ya da elektriksel konumunu bildiğinde faydalanılır. Bu tip iletişimde, sadece iki düğüm birbiri arasında mesaj alır ya da gönderir ve başka bir düğüm bu sürece dahil edilmez. Noktadan noktaya telekomünikasyon; düşük güç sarfı, gelişmiş bilgi güvenliği, düşük karıştımaya açıklık ve gelişmiş kanal kapasite kullanımı gibi birtakım avantajlar sunar. Bu özellikleriyle noktadan noktaya telekomünikasyon askeri uygulamalarda sıklıkla tercih edilmektedir.

Noktadan noktaya telekomünikasyon için görece yüksek etkin iletişim mesafesi ile düşük güç sarfını sağlamak ve kanallar arası girişimi düşürmek amacıyla yüksek kazançlı ve düşük yan kulak seviyeli yönlü antenler tercih edilmektedir. Diğer bir gereksinim, sistemde ayrı ayrı gönderme ve alma antenleri yerine dual yada dairesel polarize alma/gönderme antenleri kullananmaya dayanan bir teknik olan Çoklu Girdi Çoklu Çıktı (MIMO) metodundan kaynaklanmaktadır. Dual polarize MIMO antenleri için alma ve gönderme kanallarının birbirini etkilemesinin önlenmesi ve birbirinden ayrılması amacıyla yüksek çapraz polarizasyon izolasyonu tercih edilmektedir.

Bu çalışmada, noktadan noktaya telekomünikasyon için C bant dual polarize şerit besleme açıklık bağlaşımlı düzlemsel bir yığınlanmış yama anten dizisi tasarlanmıştır. Noktadan noktaya telekomünikasyon gereksinimlerini karşılamak amacıyla tasarlanan antenin yansıma katsayısı -10dB'dir. Anten kazancı 20dB'dir ve yan kulak seviyesi anayön ve arayön düzlemlerinde her iki polarizasyon için -15dB'dir. Ayrıca 40dB çapraz polarizasyon izolasyona ulaşılmıştır. Bu

çalışmadaki fikir, şerit besleme hat ağına sahip bir şerit beslemeli dual polarize açıklık bağlaşımlı yama anten düzlemsel dizisidir. Besleme hattı ağındaki genlik ve faz dağılımı ayarlanarak her iki polarizasyon için anayön ve arayön düzlemlerinde -15dB yan kulak seviyesi sağlanmıştır. Farklı polarizasyonlar arasındaki bağlaşımı ve genlik ile faz dağılımındaki bozulmaları engellemek için şerit hat besleme ağı seçilmiştir. Böylece çapraz polarizayon izolasyonu da arttırılmıştır. Bu sebeple, yeni bir anten elemanı, dual polarize şerit besleme açıklık bağlaşımlı yığınlanmış yama anten önerilmiştir. Bu tip antenin empedans davranışını etkileyen parametreler tespit edilmiş ve detaylıca incelenmiştir. Anayön ve arayön düzlemlerinde -15dB yan kulak seviyesini sağlamak için gerekli besleme ağı tasarlanmıştır. Önerilen anten elemanları dizi ortamına yerleştirilmiş, besleme ağına bağlanmış ve elde edilen anten dizisi optimize ve analiz edilmiştir.

Anahtar sözcükler: Noktadan noktaya telekomünikasyon, yan kulak seviyesi azaltımı, açıklık bağlaşımlı yama anten, şerit beslemeli anten.

To my father passed away in 2017...

Acknowledgement

I would like express my gratitude to my supervisor Prof. Vakur B. ERTÜRK for his supervision and support throughout my studies. I would also thank Prof. Dr. Ergin ATALAR and Prof. Dr. Özlem AYDIN ÇİVİ, the members of my jury, for accepting to read and review my thesis.

I would like to express my gratidute to Aselsan Inc. for letting me conduct my research, and giving me permission to use the facilities. I am grateful to Mehmet Erim İNAL, Özkan SAĞLAM and Kadir İŞERİ for their valuable comments and support. I would also like to thank Turkish Scientific and Technological Research Council - Science Fellowships and Grant Programmes Department, TÜBİTAK-BİDEB, for their financial assistance in my graduate study.

I would also like to extend my graditudes to my elder sister Nilay, my mother Nuray and my father Ahmet for their encouragement and endless support.

Contents

List of Figures

List of Tables

Chapter 1

Introduction

Point-to-point (P2P) communication is utilized where each communication node knows the physical or electrical positions of the other. A telephone call or a telegraph message can be regarded as simple examples for P2P communication. In P2P communication, only two communicated nodes transmit/receive message between each other and no other node is included in this process. In this aspect, P2P communication is in contrast to point-to-multipoint (P2MP) communication or broadcasting where one node transmits messages to many nodes at the same time [1].

Although digital communication by electromagnetic waves seems a recent development in terms of communication, it dates back to ancient times. The first recorded P2P communication was performed during Trojan War by King Agamemnon using torches and signal fires to send messages to his wife [2]. However, modern P2P communication was started in 1816 in France. This system was based on transmitting electric sparks via wires and constituted an initial point for modern telegraphs. Over the years, wired systems have been substituted with wireless systems. In 1896, the first point-to-point wireless communication link was established [3]. Nowadays, wireless link communication has a significant role in P2P communication.

P2P communication has various advantages over P2MP communication. First of all, since the position of the node to be communicated is known, all the available power can be tried to be delivered to this node. In this way, the power consumption can be decreased with respect to P2MP communication or broadcasting that transmits the available power to all communication nodes [4]. This situation also results in higher effective communication distance. Interference is another point that should be considered. With P2P communication, links are allocated to determined communications and lower interference in these links can be reached compared to P2MP communication [5]. Also, limitation with only two communication nodes provides the system with information safety since it is not preferred to deliver signals through the directions where the communicated node is not located. Lower vulnerability to jamming can be regarded as another advantage of P2P communication [6]. With wireless P2P, it is desired to get signals from the direction of the node to be communicated, and received signals from other directions are kept under a limit value. In this way, jamming vulnerability is decreased. Because of the aforementioned features, P2P communication is preferred frequently in military.

On the other hand, P2P communication has some disadvantages. The only available propagation mode for P2P communication is line-of-sight (LoS) propagation. Other mechanisms such as skywave or ground wave propagations cannot be benefitted in this type of communication. This fact limits us with two different conditions. The first one is about available frequencies for P2P communication. Low frequencies such as middle frequency (MF) and high frequency (HF), where ground wave and skywave propagations are dominant, cannot be used for P2P communication. On the other hand, due to higher frequencies such as Ka- or Ku-band, signals become more vulnerable to free path loss and this limits the effective distance for P2P communication. Therefore, middle frequency bands such as C-band and E-band are frequently prefered in order to provide higher effective communication depending on the application. Secondly, due to LoS propagation, it is required to ensure that line of sight should not include obstacles and sources of fade.

The above-mentioned advantages and disadvantages lead some requirements

for the antennas used for P2P communication. Firstly, since the position of the node to be communicated is known, antennas should be directional. Otherwise, all the available power cannot be transmitted only to the node, but it is transmitted through some other directions as well. In addition to that, bidirectional antennas cannot be used as the information safety cannot be ensured because undesired nodes can receive signals from other directions. Another requirement is caused by the interference effect. In order to decrease the interference between communications performed in separate links, the side lobe level (SLL) should be kept under an acceptable level. Moreover, SLL is also important in terms of jamming. When the SLL is high, the node becomes vulnerable to be jammed in the directions where the node to be communicated is not located. As it is mentioned, low frequency bands such as HF are not proper for P2P communication. On the other hand, higher frequency bands suffer more from path loss. That means middle frequencies such as E-band or C-band are more appropriate for P2P communication.

Another desired requirement in P2P communication is Multiple-Input Multiple-Output (MIMO) capability. MIMO is a technique used to multiply the channel link capacity by using transmitting and receiving antennas at both the source (transmitter) and the destination (receiver) at the same time [7]. In order to achieve such MIMO capability, one can use dual or circularly polarized transreceiver antennas instead of using separate transmitter and receiver antennas in a system. Hence, the physical space is reduced, which is another desired feature. However, note that dual-polarized antennas require high cross polarization isolation to separate the transmitting and receiving channels. Otherwise, channels obtain signals from each other and the quality of communication decreases. On the other hand, when circularly polarized antennas are used, axial ratio (a parameter that indicates the difference between orthogonal components of the antenna gain) becomes important. A higher axial ratio value (which is undesired) means antenna gain cannot be divided equally or closely into the components and we receive/transmit less signal power via one polarization. This fact yields again a low communication quality. The choice whether circular or dual linear polarization must be used is usually determined by the requirements of the radio of the

communication system.

In the literature, there are various types of antennas used for P2P communication. Reflector antennas are one of the types of antennas for this purpose. They have high gain, low SLL and high cross polarization isolation. With these properties, they are useful for P2P communication. On the other hand, they are bulky structures, not low profile and not easy to install due to their paraboloid reflector components. A variety of reflector antennas is proposed for P2P communication in [8]-[16]. In [8], the proposed antenna is a C-band Gregorian reflector antenna of diameter 2.4m with a reflection coefficient of -17dB and a cross polarization isolation of 25dB. In [9], a C-band, dual-gridded reflector antenna is proposed. The anntenna in this work has 26dBi gain and 33dB cross polarization isolation. [10] presents conceptual information about C-, Ka- and Ku-band dual-gridded reflector antennas. In [11], the design of a reflector antenna in L-band with a -25dB SLL and a 29dBi gain is presented. However, the dimensions of this antenna is 8m x 2m and it is a bulky structure. [12] presents a solution for Brasilsat B3 case which provides the cities in the Amazon region with satellite communication. The antenna in this study is a dual C- and Ku-band reflector with a diameter of 2.4m. In [13], the design of a reflector antenna in S-band is presented. This antenna has -14dB reflection coefficient and 38dBi gain. The diamater for this antenna is 2.6m. In [14], a feed antenna for a reflector antenna in S-band is proposed. [15] proposes a C-band multifeed reflector antenna. Moreover, [16] is another solution for Brasilsat case. The proposed antenna in [16] is a C-band reflector antenna with a 29dBi gain and a 33dB cross polariation isolation. On the other hand, horn antenna is another type of antenna preferred in P2P communication. It has similar properties with a reflector antenna. However, horn antennas are not low profile and easy to install. [17]-[20] can be given as examples of studies for horn antennas that are used in P2P communication. In [17], the proposed antenna is a C/X dual-band horn antenna with a reflection coefficient lower than -16.5dB, though it additionally includes a reflector antenna that has a 2.7m diameter. In [18], a C-band horn antenna is proposed. The horn is hexagonal shaped with a reflection coefficient lower than -17dB and a cross polarization level lower than -28dBi. The proposed antenna in [19] is an L/C

band corrugated dual-slot horn. It has a reflection coefficient lower than -20dB and its cross polarization level is lower than -20dB. [20] proposes a horn antenna with a mode converter in C-band. The dimension of the antenna is 24cm x 30cm. Gain of it is higher than 19dBi and its VSWR is better than 1.5. -9dB SLL in E-plane and -20dB SLL in H-plane are achieved in [20] as well.

Antenna arrays are another option and may even be prefered in P2P communication. They allow us to synthesis desired patterns by adjusting amplitude and phase distribution on the array elements. Different types of antenna elements such as Vivaldi antenna, dipole antenna or patch antenna can be used as the single element in an antenna array depending on the physical and electrical requirements. Among the available elements for antenna arrays, microstrip patch antennas offer some advantages. It is possible to design low profile and easy to install antenna arrays, called panel antennas, with patch antennas. [21]-[28] give examples for such panel antennas. [21] proposes an antenna whose operating frequency band is 2.5GHz - 2.7GHz. Its reflection coefficient is -10dB, it has a cross polarization level of -10dB and its gain is 8dB. Furthermore, this antenna is dual-polarized, that means it is capable of MIMO. In [22], the design of another dual-polarized antenna for P2P communication is presented. It works at 5.5GHz. It is a 4x4 planar array and 40dB cross polariation isolation is achieved in this work. In [23], a planar dual-polarized antenna similar to previous studies is presented. However, the operating frequency is 2.6GHz. The proposed array in [24] is a 6x6 planar antenna array with a Wilkinson power divider as its feed network. It is composed of circularly polarized antennas that are dual-fed square stacked patch antennas and the axial ratio is better than 1.5dB. The operating frequency is reported as 1.9GHz - 2.6GHz band. 7dB gain, -21 dB reflection coefficient (better than 1.2 VSWR) and 23dB cross polarization isolation are achived in this band. In [25], 40dB gain is achieved with a -15dB reflection coefficient (better than 1.5 VSWR) by using 16x32 elements. The dimensions of the antenna array is 80cm x 42cm. [26] proposes an antenna array which consists of patches fed by dogbone slots. The feeding is nonuniform to perform beam shaping. The array is single polarized and a -30dB reflection coefficient (better than 1.1 VSWR) can be reached. [27] proposes a dual-polarized and dual-band (X- and S-band) antenna

array which consists of patch and ring-resonant antennas. The S-band antenna is a 2x1 ring-resonant antenna array with a 9.5dB gain, -22dB reflection coefficient (better than 1.2 VSWR), 25dB cross polarization isolation and -10dB SLL. The X-band antenna is a 4x8 circular patch series fed antenna array with a 18dB gain, -19dB reflection coefficient, 30dB cross polarization isolation. In [28], the proposed antenna is a dual-polarized aperture coupled patch 2x2 antenna array with a -13dB reflection coefficient. Moreover, its cross polarization isolation is 22dB and SLL is -13dB. In the literature, other antenna arrays which constist of other types of antenna elements than patch antennas can be found for P2P communication. In [29], an array of grid elements with -10dB reflection coefficient, 17dB gain and -12dB SLL between 77GHz and 85GHz is proposed. Horn antennas are also used as array elements. For instance in [30], the design of 6x24 horn antenna array at Ku-band is presented. Rectangular waveguides in [31] and monopulse antennas in [32] are other antenna elements used for arrays in P2P communication. On the other hand, proper antenna elements for array structure in P2P communication are still being studied in the literature. In [33], a microstrip fed microstrip triband antenna is proposed. This antenna operates at 1.8GHz, 2.4GHz and 3.5GHz for wireless communication applications. Its gain is 2dB. In [34], the antenna is a dual-polarized slot coupled stacked patch antenna. It is fed by H-shaped slots and its cross polariation isolation is 36dB.

The aim of this thesis is to propose a C-band strip-fed dual-polarized aperture coupled stacked patch antenna array for P2P communication. The operation band is chosen as 4.4GHz to 5GHz. In order to satisfy the requirements for P2P communication, the minimum gain is aimed to be 20dB and the desired cross polarization isolation is 40dB. Additionally, SLL is desired to be at least is -15dB for both cardinal and intercardinal planes unlike similar works where SLL is limited to 15dB only in cardinal planes. Note that cardinal planes can be defined as the cuts for ϕ=0° and ϕ=90° when antenna is placed on the xy-plane as the direction of antenna placement is x- and y-directions [35]. The intercardinal planes are the cuts except cardinal planes, i.e, planes for ϕ=45° and ϕ=135°. Moreover 10° 3dB beamwidth is aimed. The proposed antenna is a planar array of strip-fed dual-polarized aperture-coupled patch antenna that has stripline feed networks

with required amplitude and phase distribution. By adjusting the amplitude distributions, -15dB SLL in both cardinal and intercardinal planes can be reached for both polarizations. By considering the beamwidth and gain requirements, the approximate size of the antenna array should be 5.8λ, and hence we can satisfy these requirements via 6 by 6 antennas with an interelement spacing of 0.96λ. This structure provides us with conformal and easy to install geometry. However, a dual-polarized aperture coupled stacked patch antenna with stripline feed does not exist in literature although there are some works on single polarized ones as in [36]. The main contribution of this thesis is the design of a strip-fed dual-polarized aperture coupled stacked patch antenna. In this way, the feed networks for different polarizations can be separated with ground planes and proper amplitude and phase distribution to constitute the desired array factor can be achieved. If microstrip feed network and microstrip fed aperture coupled patch antenna were chosen for the array, the amplitude and phase distributions of feed networks for different polarizations would be distorted due to coupling between them when they are stacked, and the resulted array factor would not satisfy the requirements of P2P communication. Briefly, this work includes three steps that are to design the feed network with the desired amplitude and phase distributions, to design the single antenna element that is compatible with the structure of the feed network, and to make antenna elements and feed network operate together properly in array environment.

In Chapter 2, structure of the proposed single antenna element is presented. Also, the parameters that affect the behavior of the single antenna element are investigated. The final design of the single element is also provided in this chapter. In Chapter 3, firstly the required amplitude and phase distributions are determined. Then, the feed network that realizes the desired distribution is designed systematically. In Chapter 4, the single elements are placed in the array configuration and the feed network is connected, thereby finalizing the design process of the antenna array. Finally, conclusions and future work are presented in Chapter 5.

Chapter 2

Single Element Design

Aperture coupled patch antennas were first proposed by Pozar in [37]. These antennas consist of two substrates; one of them contains radiating element, and the other one includes the feed network. Over the years, dual-polarized aperture coupled patch antennas have been presented as discussed in [38] and [39]. These antennas are based on microstrip technology. Due to the feed network used, dual-polarized aperture coupled patch antennas with stripline technology are required for this work. However, available antennas in the literature are single polarized. Therefore, in this thesis, we propose a novel antenna type which is dual-polarized strip-fed aperture coupled stacked patch antenna.

The simulations in this chapter are performed via HFSS® in a computer having 32GB RAM and 2.8GHz Intel® i7 microprocessor. In the simulation model, all metallic surfaces (patches, ground planes etc.) are modelled as copper. The antenna element is fed by waveports. A vacuum box in the shape of rectangular parallelpiped is defined around the antenna element. The minimum distance from the single antenna element to the vacuum box is $\lambda/4$ for the minimum frequency in the solution band. The solution frequency is chosen as the maximum frequency in the solution band. For the adaptive solution, maximum number of passes is determined as 15 and maximum of Delta S is determined as 0.02.

2.1 Proposed Single Element Structure

The details of the proposed antenna structure are depicted from Fig. 2.1 to Fig. 2.5.

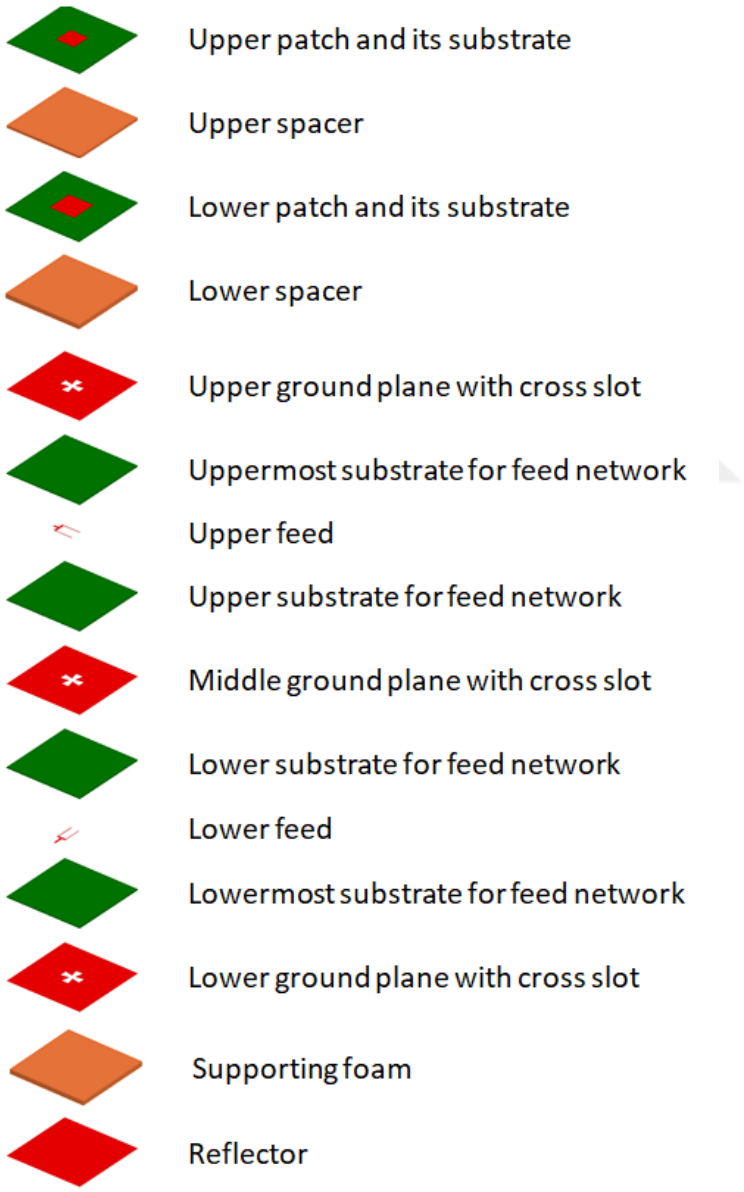

Figure 2.1: Exploded view of the proposed single antenna element

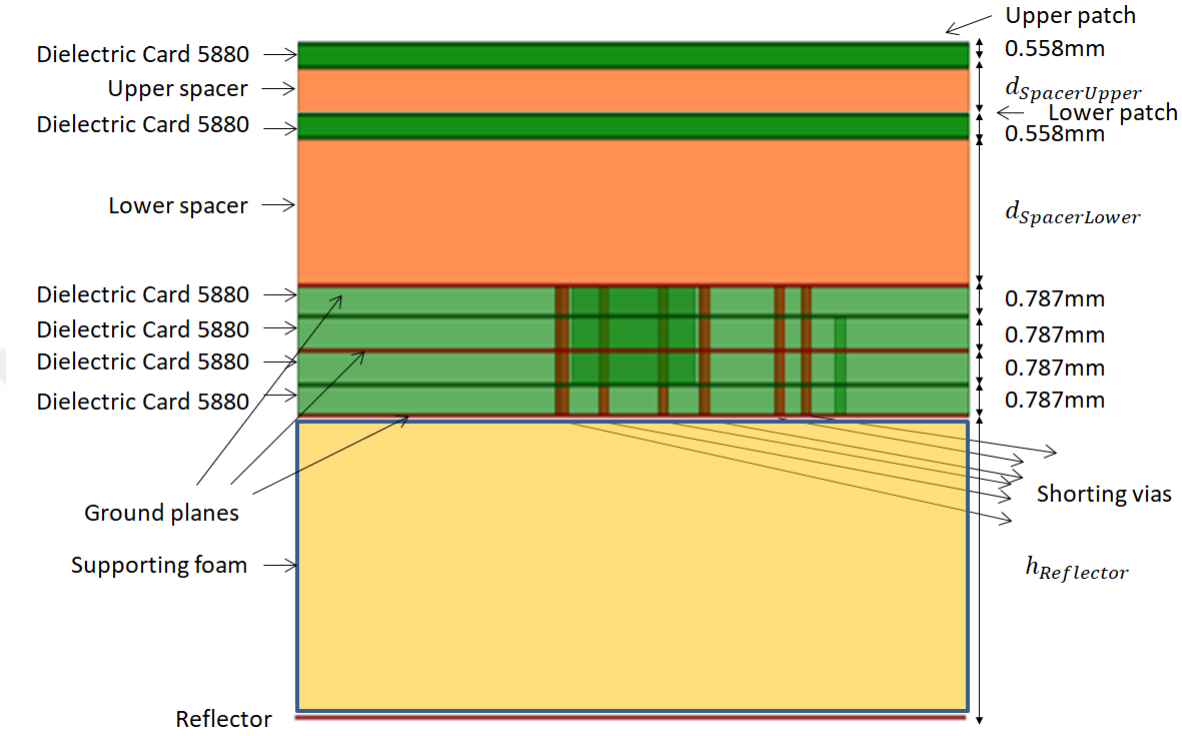

Figure 2.2: Side view of the proposed single antenna element

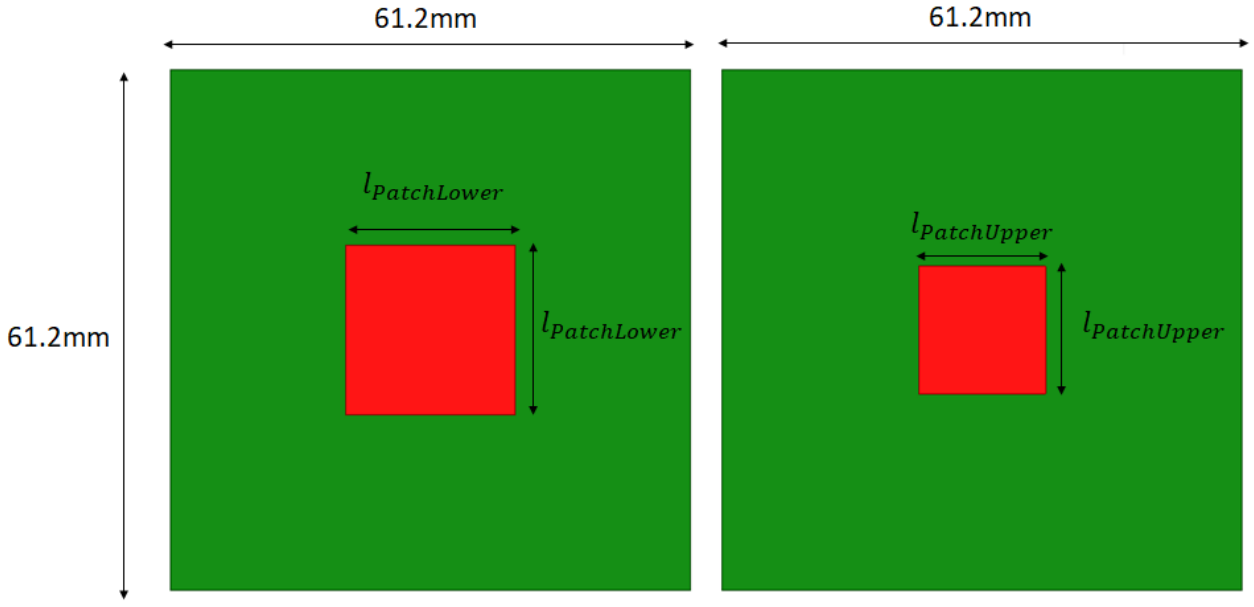

Figure 2.3: Lower (a) and upper (b) patch and their parameters

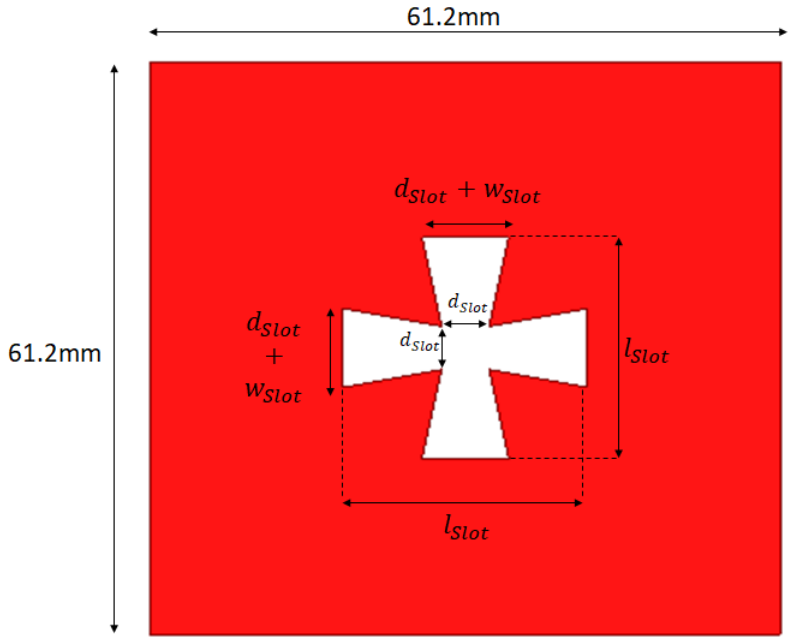

Figure 2.4: Top view of slots with their parameters

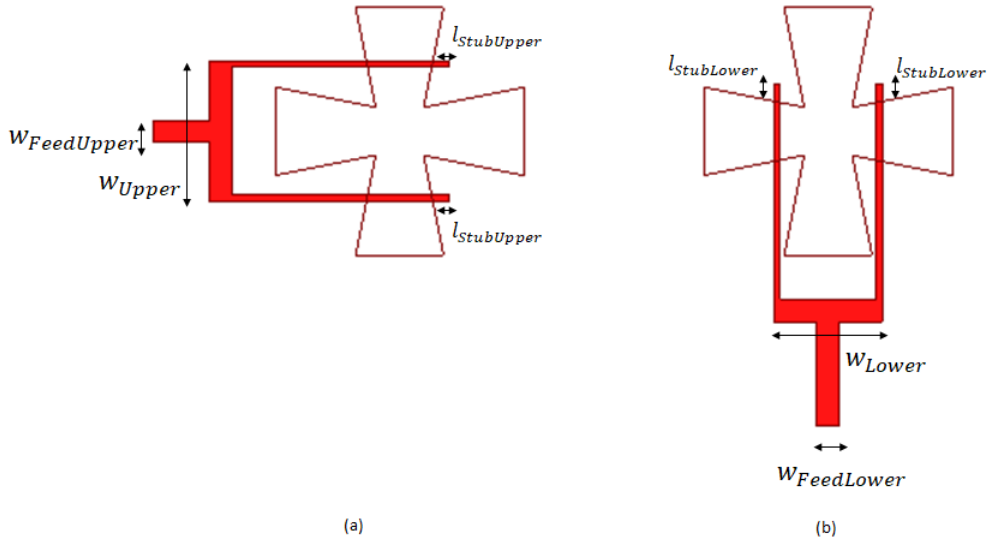

Figure 2.5: Upper (a) and lower (b) feed networks with their parameters with respect to slots

This structure can be regarded as a modified dual-polarized aperture coupled patch antenna. The first modification is about the ground planes. Since stripline based feed network is used, the single element is also changed to a stripline structure. However, in order to operate the slots properly, it is observed that all the ground planes should have identical slots as a result of simulations due to the symmetry requirement. These slots are designed in the form of dog-bone shaped. In this way, dilatation of the slot width becomes an extra parameter to tune the antenna to meet the desired specifications. The other modification is the reflector plane at the bottom of the configuration as shown in Fig. 2.2. This plane reflects the radiation at the back to the front. Also note that, stacked patches are used to obtain two different resonance frequencies. On the other hand, it is not easy to operate both patches and slots at the same time. At the frequency where patches start to operate and operating of slots is ceasing, a sharp change in the impedance behavior of the antenna element is observed. In order to eliminate the change in impedance and provide smoother impedance variation, all ground planes are shorted to each other by using vias. In this way, parallel plate waveguide modes can be supressed. The cross polarization isolation is another issue that should be handled in the design of the single element. Since stripline feed is used, high cross polarization isolation can be achieved. However, to keep it higher than 40dB it is required to reshape the feeds. Instead of using a single part stripline, the 50Ω stripline feed is divided into two 100Ω stripline branches. In this way, higher cross polarization isolation (40dB) can be achieved.

For each element, foam Rohacell®51 HF material is used as the spacer and the supporting foam. This material is a foam with low weight, low relative permittivity (which is 1.065) and has low tangent loss (lower than 0.0008) [40]. Since the feeding striplines are long in the feed network in order to divide the input power to 36 antenna elements, use of a substrate with high loss would result in lower antenna efficiency and lower gain. Therefore, the substrates are chosen as ROGERS 5880 Duroid®dielectric card. It is chosen because it is a low loss card with a tangent loss of 0.0004 [41].

2.2 Final Form of the Single Antenna Element

Every parameter in the proposed antenna structure causes a trade-off between reflection coefficients of upper and lower feed and cross polarization isolation. Therefore, they should be optimized with respect to the desired parameters (40dB cross polarization isolation and -10dB reflection coefficient) in the operation band (4.4GHz to 5GHz). As a result of systematic simulations, the values tabulated in Table 2.1 are chosen.

Parameter Name	Value(mm)	Value(λ_0)
$l_{PatchLower}$	20	0.313
$d_{SpacerLower}$	3.5	0.055
l_{Slot}	15.5	0.243
d_{Slot}	3	0.047
$l_{StubUpper}$	1.6	0.025
w_{Upper}	8	0.125
$h_{Reflector}$	16	0.251
w_{Slot}	2.5	0.039
w_{Lower}	6	0.094
$l_{StubLower}$	1.5	0.025
$l_{PatchUpper}$	15	0.392
$d_{SpacerUpper}$	2	0.031
$w_{FeedUpper}$	1.4	0.022
$w_{FeedLower}$	1.4	0.022

Table 2.1: Antenna design parameters with nominal values

Note that the characteristic impedance of the upper feed is tuned to 60Ω whereas it is tuned to 40Ω for the lower feed. Consequently, S-parameters and gain patterns for the cardinal and intercardinal planes as a result of the simulations are obtained as shown in Fig. 2.6 to Fig. 2.14. The simulations are performed from 4GHz to 5.5GHz with an increment of of 25MHz altohugh the operation band is 4.4GHz to 5GHz in order to observe the impedance characteristics of the antenna element widely.

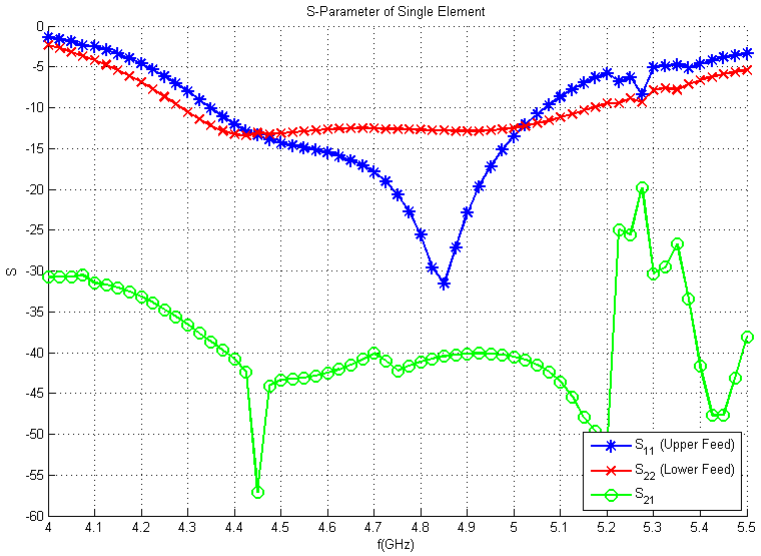

Figure 2.6: Simulated S-parameters of the finalized antenna element versus frequency

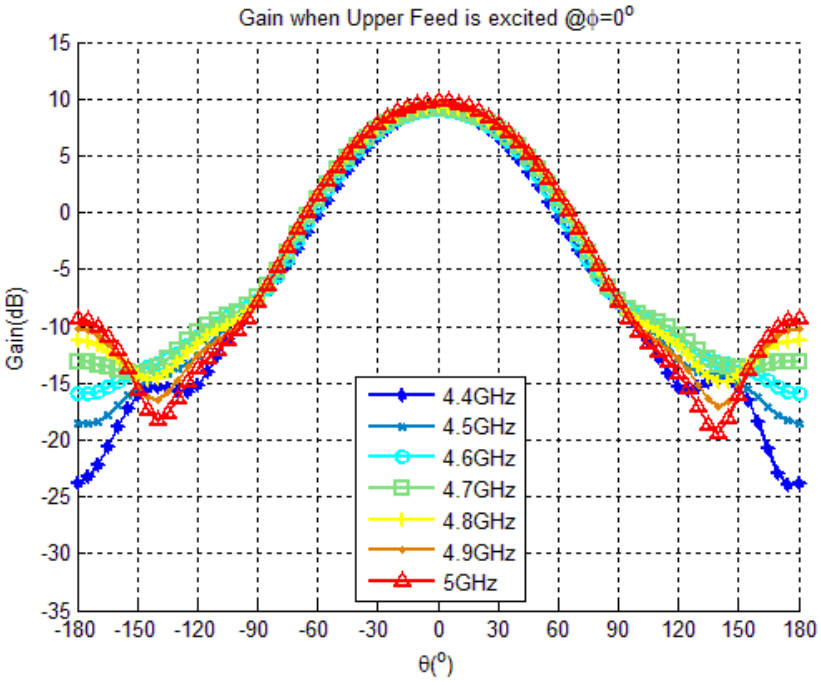

Figure 2.7: The gain behavior of a typical strip-fed aperture coupled stacked patch antenna versus θ at ϕ =0° plane when upper feed is excited

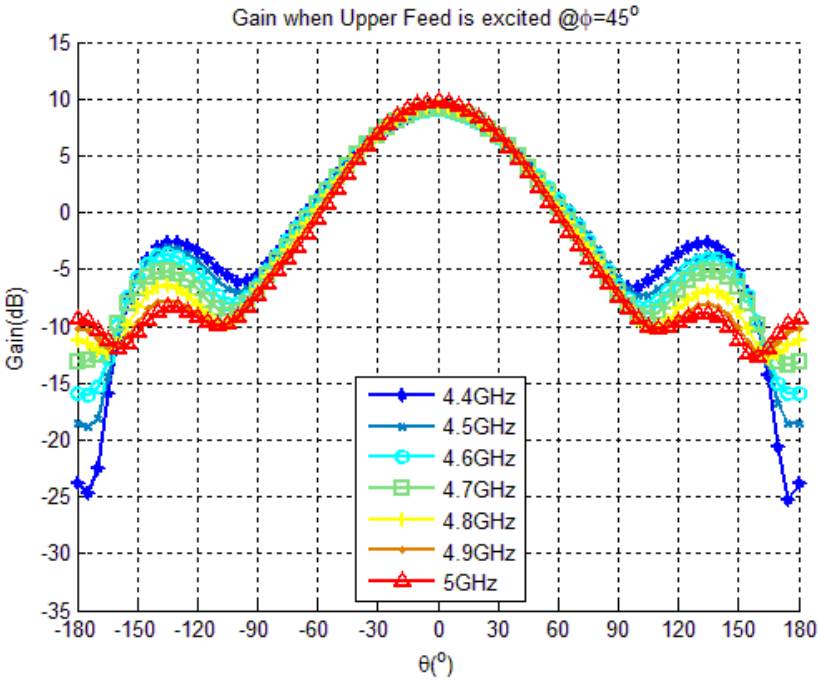

Figure 2.8: The gain behavior of a typical strip-fed aperture coupled stacked patch antenna versus θ at ϕ =45° plane when upper feed is excited

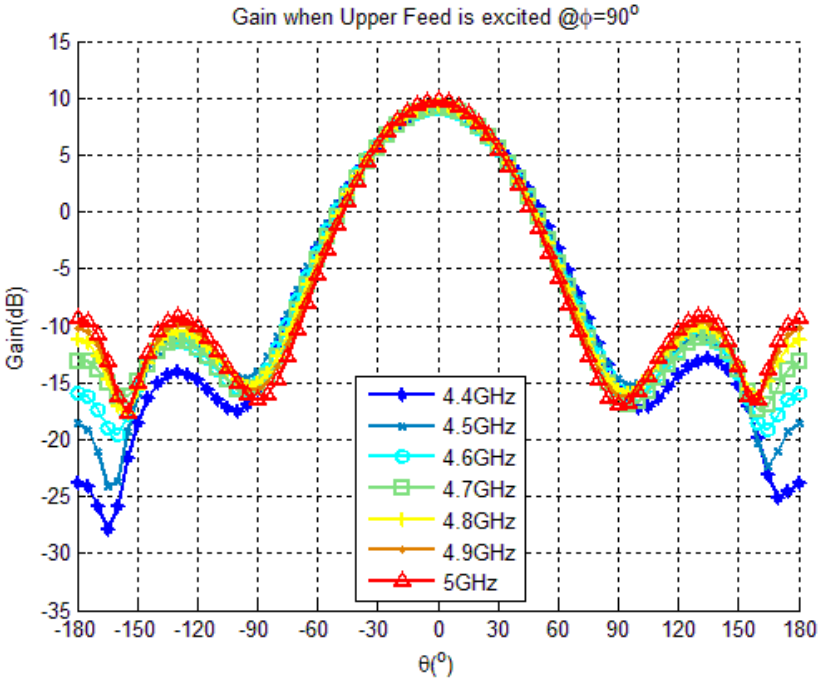

Figure 2.9: The gain behavior of a typical strip-fed aperture coupled stacked patch antenna versus θ at ϕ =90° plane when upper feed is excited

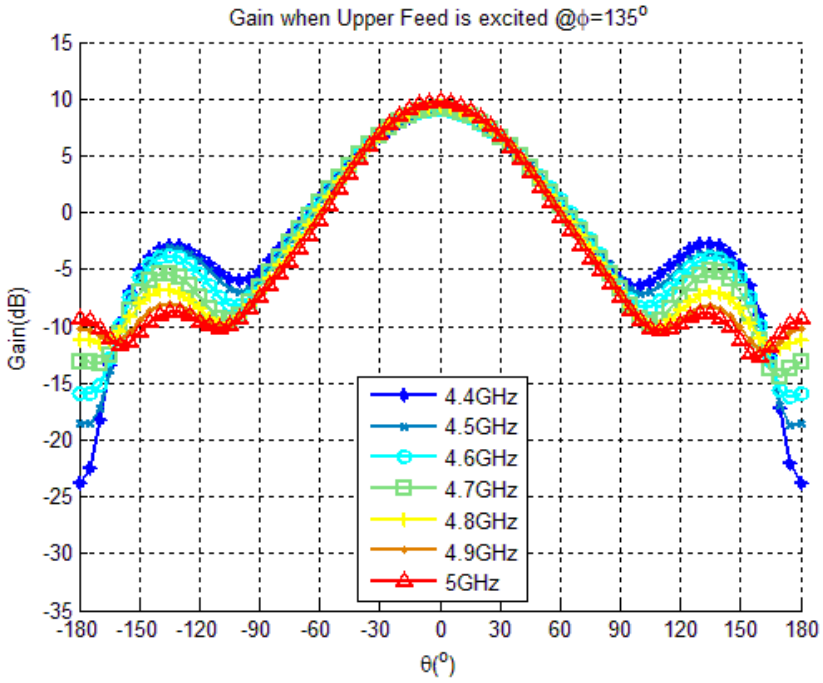

Figure 2.10: The gain behavior of a typical strip-fed aperture coupled stacked patch antenna versus θ at ϕ =135° plane when upper feed is excited

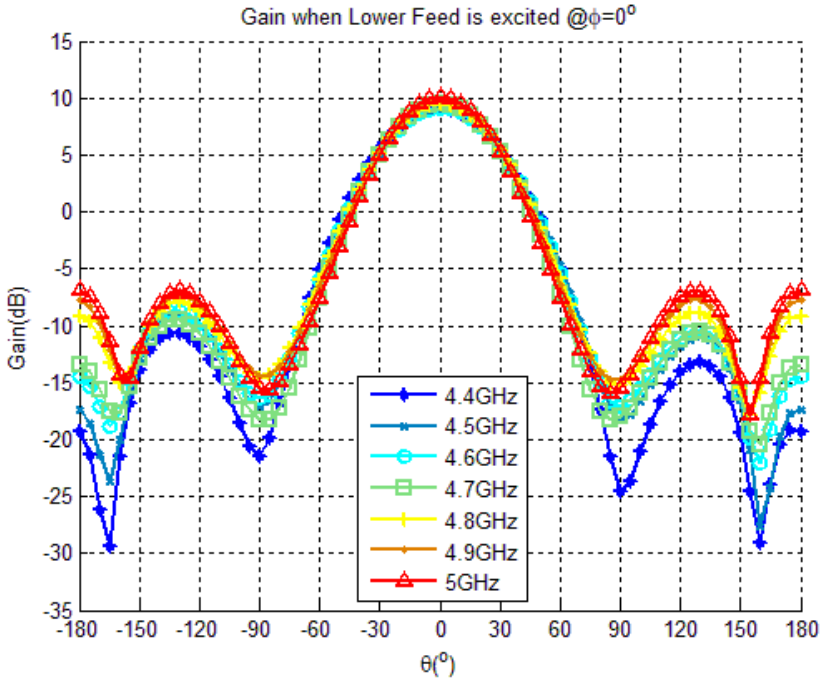

Figure 2.11: The gain behavior of a typical strip-fed aperture coupled stacked patch antenna versus θ at ϕ =0° plane when lower feed is excited

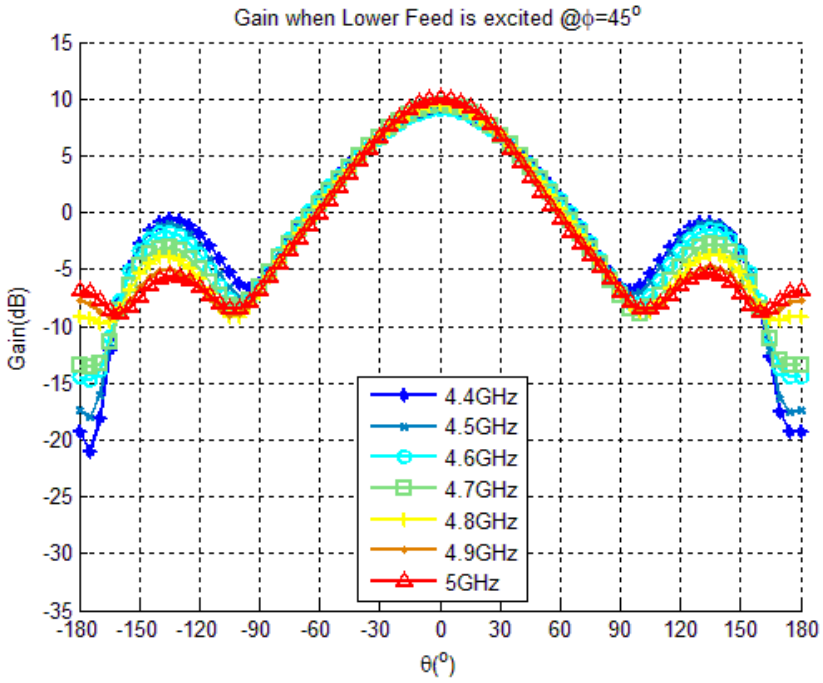

Figure 2.12: The gain behavior of a typical strip-fed aperture coupled stacked patch antenna versus θ at ϕ =45° plane when lower feed is excited

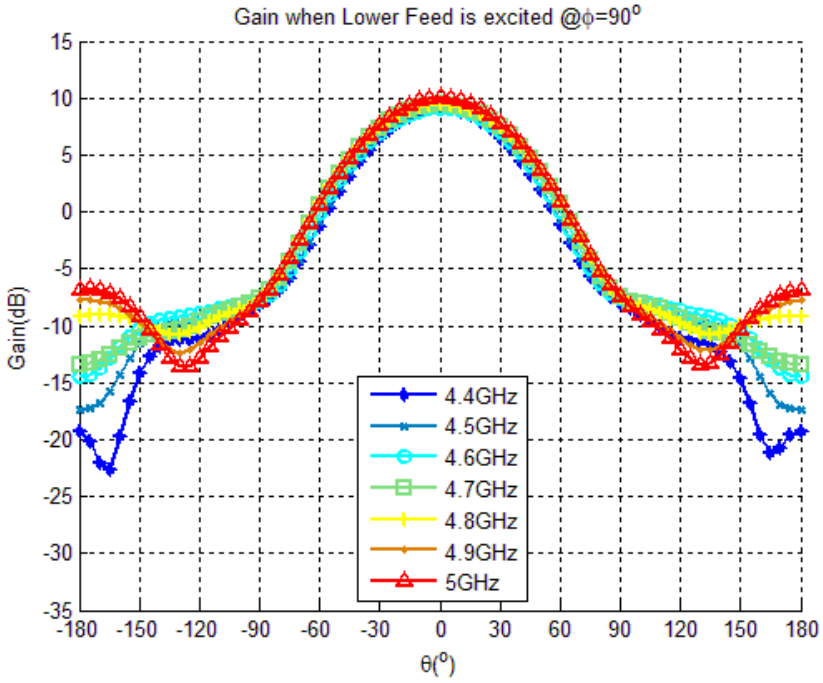

Figure 2.13: The gain behavior of a typical strip-fed aperture coupled stacked patch antenna versus θ at ϕ =90° plane when lower feed is excited

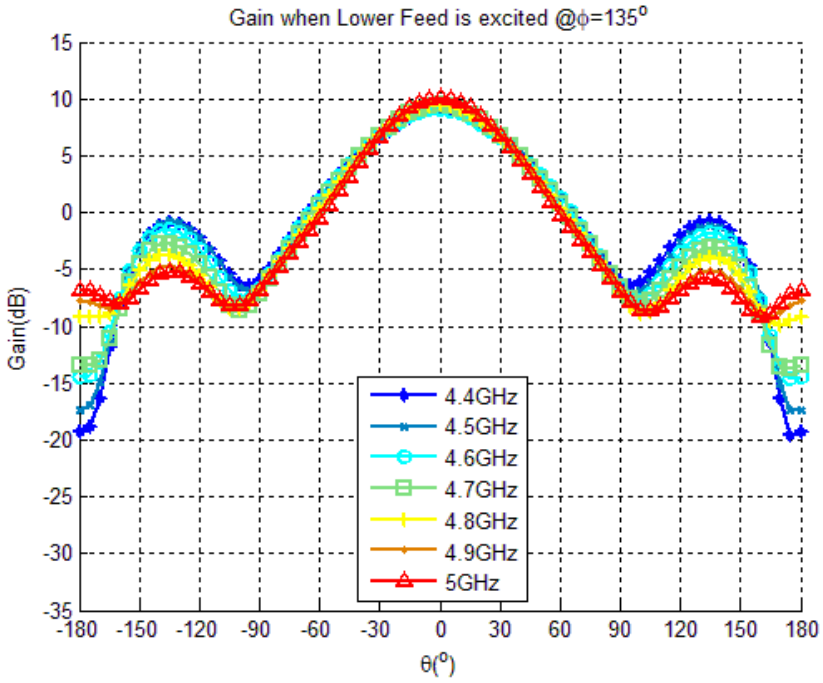

Figure 2.14: The gain behavior of a typical strip-fed aperture coupled stacked patch antenna versus θ at ϕ =135° plane when lower feed is excited

It can be seen from Fig. 2.6 that the reflection coefficients are lower than -10dB for both feed networks and the cross polarization isolation (i.e., S_{21}) is higher than 40dB. Moreover, desired patterns for both polarizations on the cardinal and intercardinal planes are obtained as seen in Fig. 2.7 to Fig. 2.14. Therefore, the initial design of a single antenna element (i.e., strip-fed aperture coupled stacked patch antenna) is completed. In the following subsections, parametric tests on critical parameters are performed to observe their full effects on the design.

2.3 Parametric Tests

In this section, the results of parametric tests for important variables are presented. In all these tests, all the parameters other than the parameter of interest are kept constant and equated to values in Table 2.1.

2.3.1 Lower Patch Length ($l_{PatchLower}$)

Since similar patterns and impedance characteristics for both polarizations are desired, the lower patch shown in Fig. 2.3(b) is designed as square. In Fig. 2.15, Fig. 2.16 and Fig. 2.17, the effect of lower patch length on the impedance characteristics is presented.

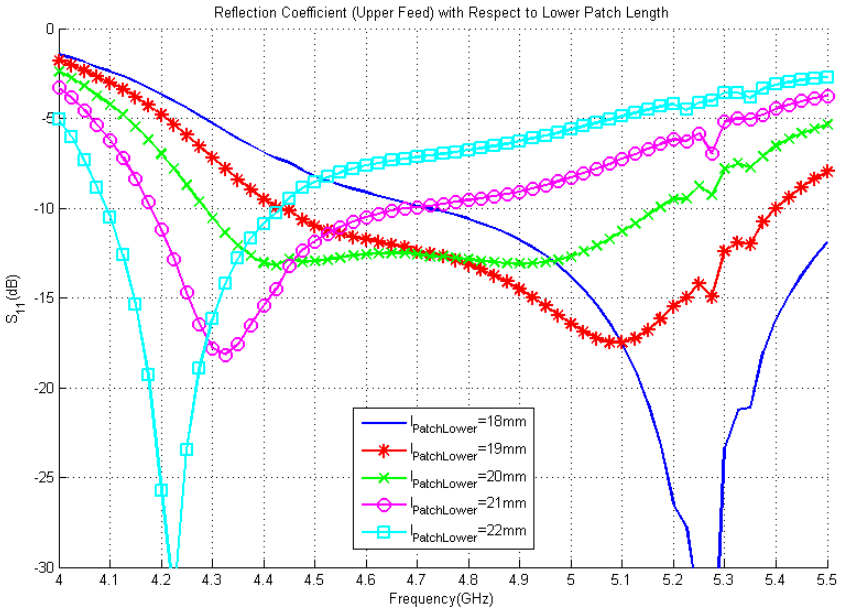

Figure 2.15: Reflection coefficient for upper feed network versus frequency for various lower patch lengths

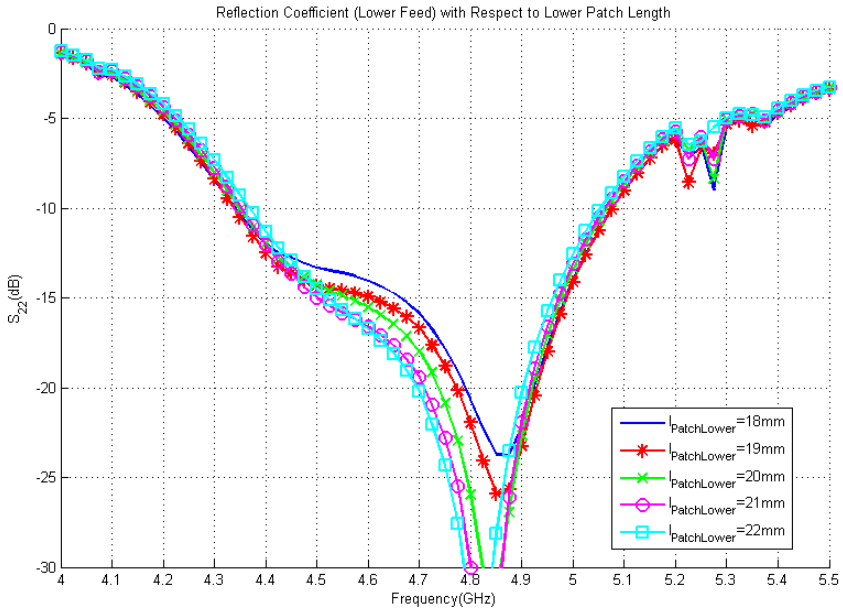

Figure 2.16: Reflection coefficient for lower feed network versus frequency for various lower patch lengths

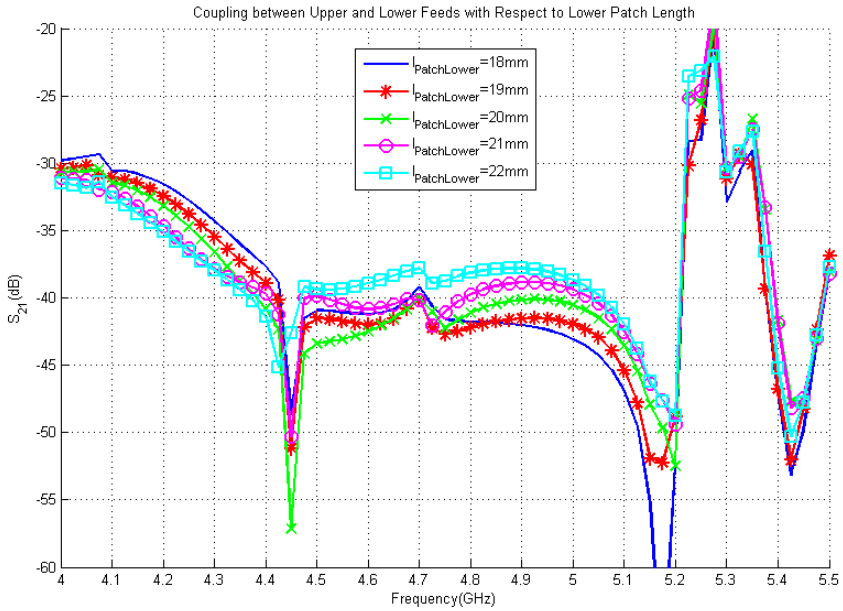

Figure 2.17: Coupling between upper and lower feed networks versus frequency for various lower patch lengths

For both lower and upper feed networks, it can be observed that an increase in the lower patch length shifts the resonance to lower frequencies. Also note that for higher values of lower patch length, the coupling between the ports increases and lower length is required for higher cross polarization isolation. It can be seen that when $l_{PatchLower}$ = 20mm, reflections coefficient of both upper and lower feed networks are better than -12.5dB and the cross polarization isolation is better than 40dB. Therefore, this value is chosen.

2.3.2 Upper Patch Length ($l_{PatchUpper}$)

Since similar patterns and impedance characteristics for both polarizations are designed, the upper patch shown in Fig. 2.3(a) is designed as square. In Fig. 2.18, Fig. 2.19 and Fig. 2.20, the effect of upper patch length on the impedance characteristics is presented.

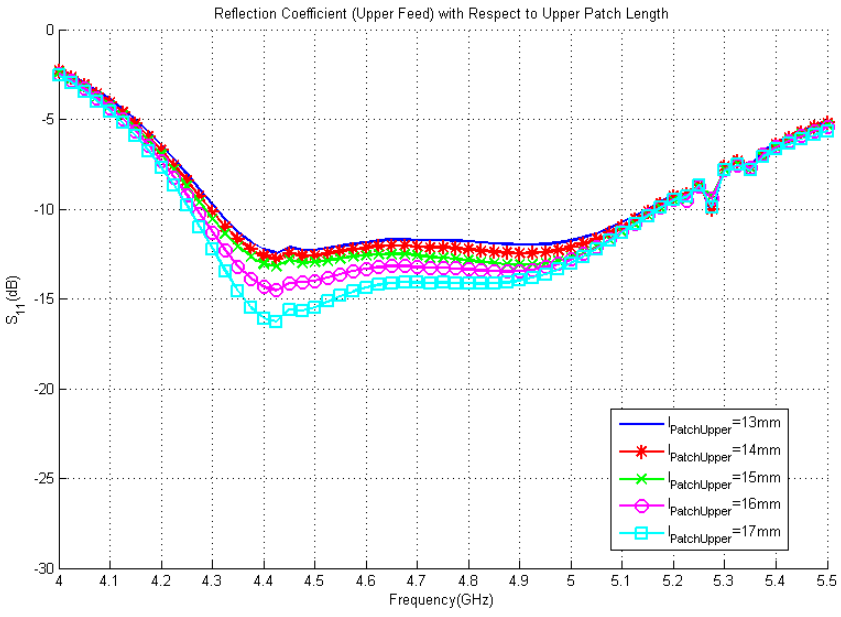

Figure 2.18: Reflection coefficient for upper feed network versus frequency for various upper patch lengths

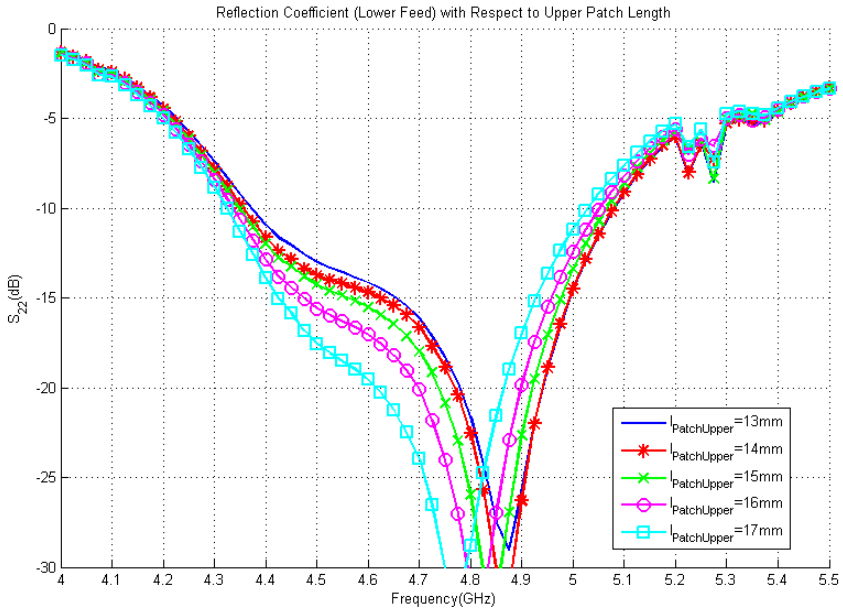

Figure 2.19: Reflection coefficient for lower feed network versus frequencies for various upper patch lengths

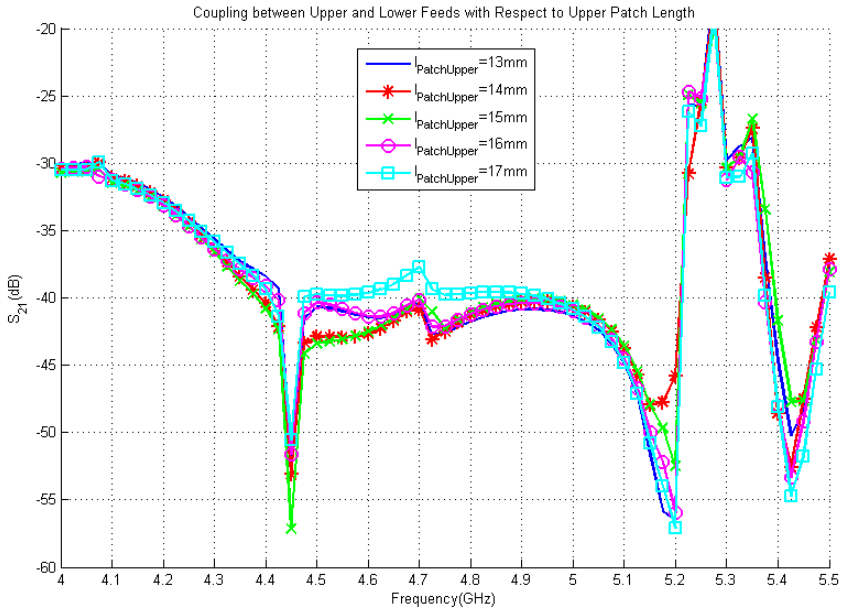

Figure 2.20: Coupling between upper and lower feed networks versus frequencies for various upper patch lengths

It can be seen from the figures that for the upper feed network, an increase in the upper patch length decreases the magnitude of the reflection coefficient. On the other hand, for the lower feed network, an increase in this parameter shifts the resonance to lower frequencies. That means, while choosing this parameter, we are limited by the lower feed. Also note that, lower length for upper patch values cause worse cross polarization isolation. It can be seen that when $l_{PatchUpper}$ = 15mm, reflection coefficients of both upper and lower feed networks are better than -12.5dB and the cross polarization isolation is better than 40dB. Therefore, this value is chosen.

2.3.3 Lower Spacer Thickness ($d_{SpacerLower}$)

Lower spacer is placed between the upper ground plane and substrate of the lower patch as shown in Fig. 2.2. In Fig. 2.21, Fig. 2.22 and Fig. 2.23, the effect of the lower spacer thickness on the impedance characteristics is presented.

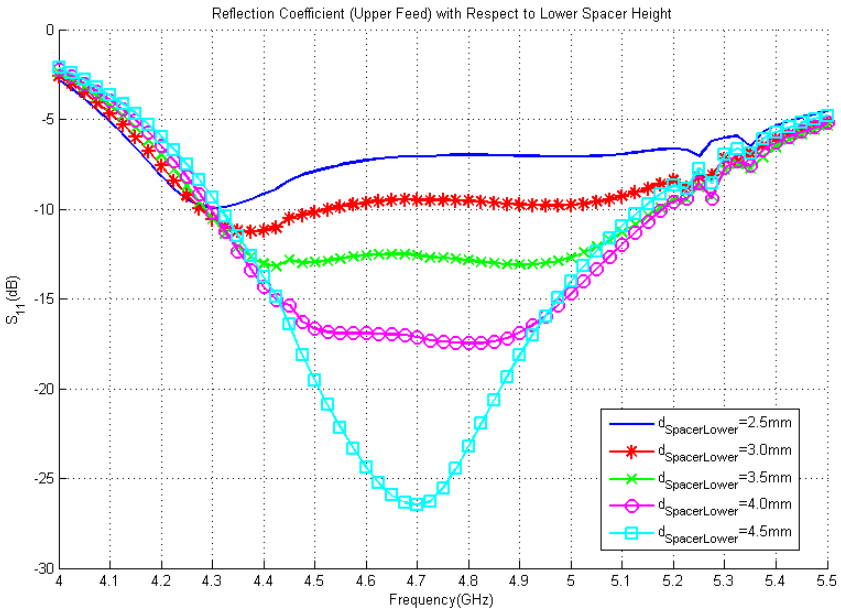

Figure 2.21: Reflection coefficient for upper feed network versus frequency for various lower spacer heights

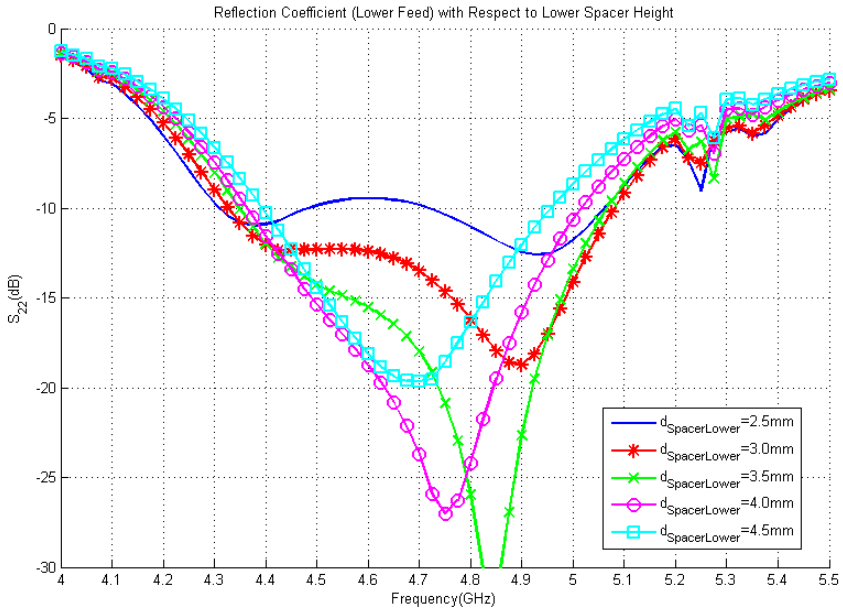

Figure 2.22: Reflection coefficient for lower feed network versus frequency for various lower spacer heights

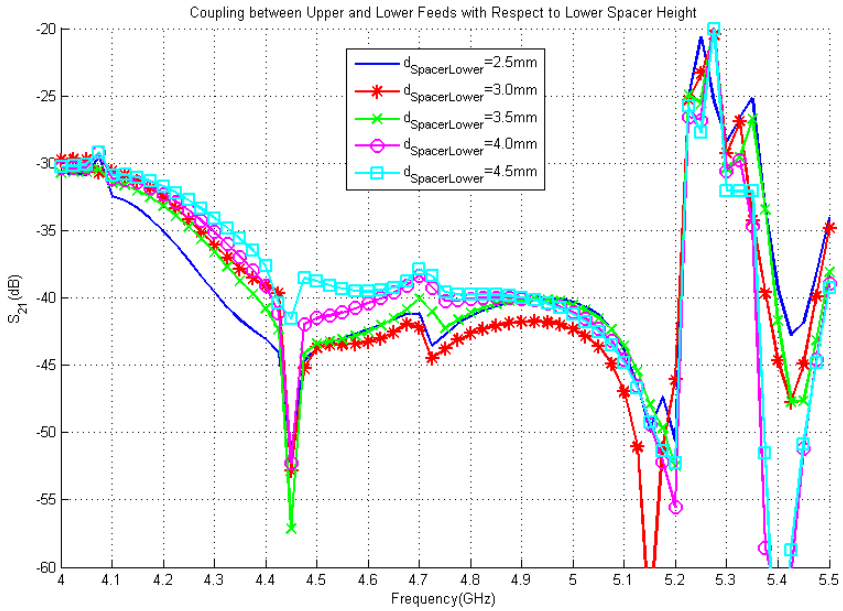

Figure 2.23: Coupling between upper and lower feed networks versus frequency for various lower spacer heights

It can be seen from the figures that for the upper feed network, an increase in lower spacer thickness decreases the magnitude of the reflection coefficient. On the other hand, for the lower feed network, an increase in this parameter shifts the resonance to lower frequencies. That means, while choosing this parameter, we are limited by the lower feed network. Also note that, higher lower spacer thickness values cause worse cross polarizations isolation. So, there is a trade-off between reflection coefficients and cross polarization isolation. It can be seen that when $d_{SpacerLower}$ = 3.5mm, reflection coefficients of both upper and lower feed network are better than -12.5dB and the cross polarization isolation is better than 40dB. Therefore, this value is chosen.

2.3.4 Upper Spacer Thickness ($d_{SpacerUpper}$)

Upper spacer is placed between the lower substrate of the patch and upper substrate of patch as spacer as shown in Fig. 2.2. In Fig. 2.24, Fig. 2.25 and Fig. 2.26, the effect of the upper spacer thickness on the impedance characteristics is presented.

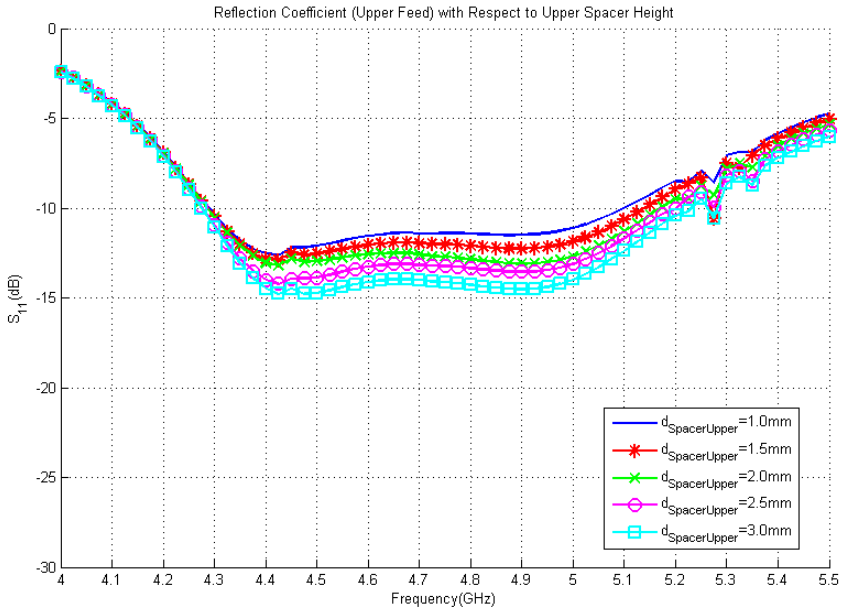

Figure 2.24: Reflection coefficient for upper feed network versus frequency for various upper spacer heights

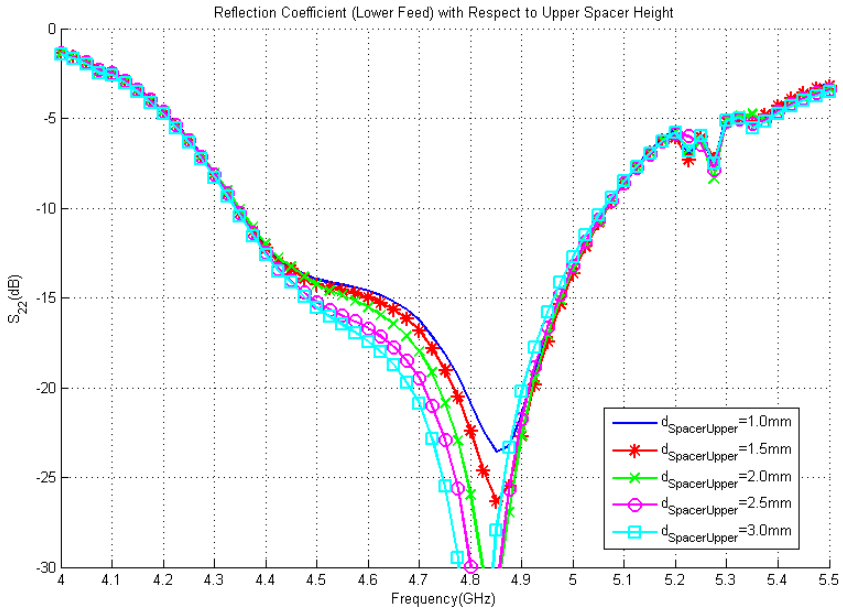

Figure 2.25: Reflection coefficient for lower feed network versus frequency for various upper spacer heights

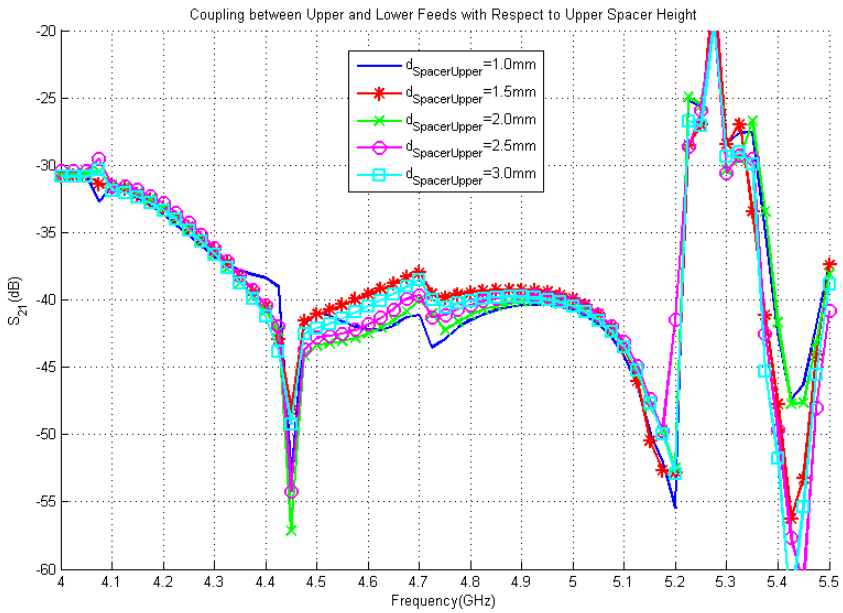

Figure 2.26: Coupling between upper and lower feed networks versus frequency for various upper spacer heights

It can be seen from the figures that for the upper feed network, an increase in the upper spacer thickness decreases the magnitude of the reflection coefficient. On the other hand, for the lower feed network, an increase in this parameter shifts the resonance to lower frequencies. That means, while choosing this parameter, we are limited by the lower feed network. Also note that, lower spacer thickness values cause worse cross polarization isolation. Hence, there is a trade-off between reflection coefficients and the cross polarization isolation. It can be seen that when $d_{SpacerUpper} = 2.0$mm, reflection coefficients of both upper and lower feed network are better than -12.5dB and the cross polarization isolation is better than 40dB. Therefore, this value is chosen.

2.3.5 Slot Length (l_{Slot})

In Fig. 2.27, Fig. 2.28 and Fig. 2.29, the effect of slot length, illustrated in Fig. 2.4 on the impedance characteristics is presented.

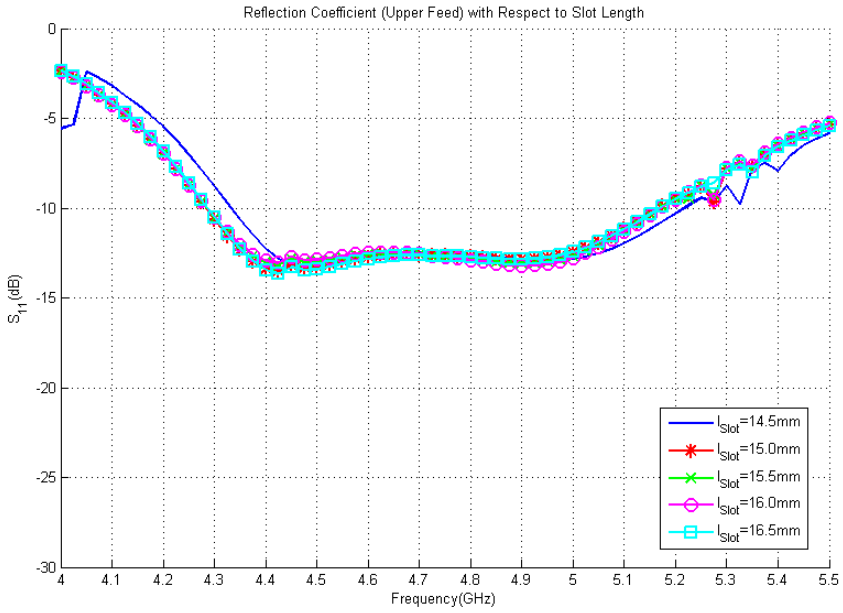

Figure 2.27: Reflection coefficient for upper feed network versus frequency for various slot lengths

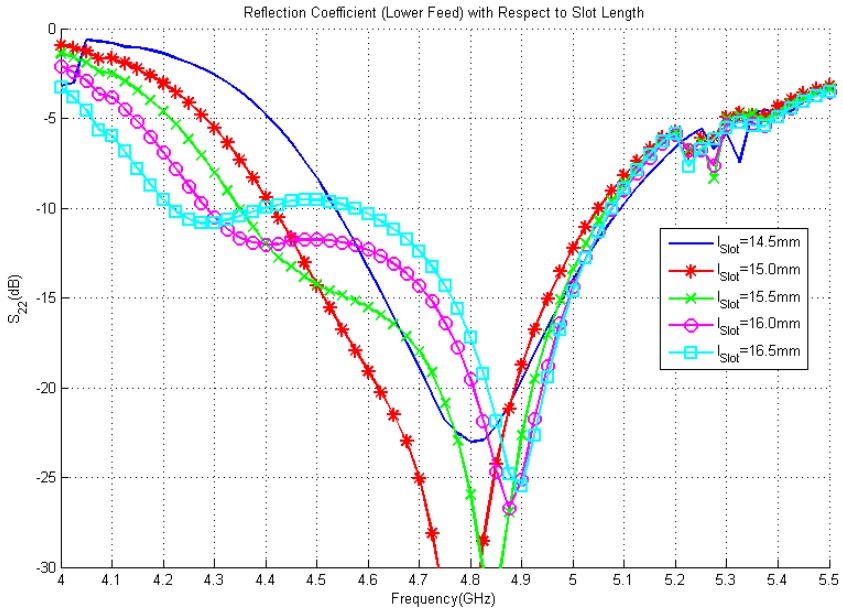

Figure 2.28: Reflection coefficient for lower feed network versus frequency for various slot lengths

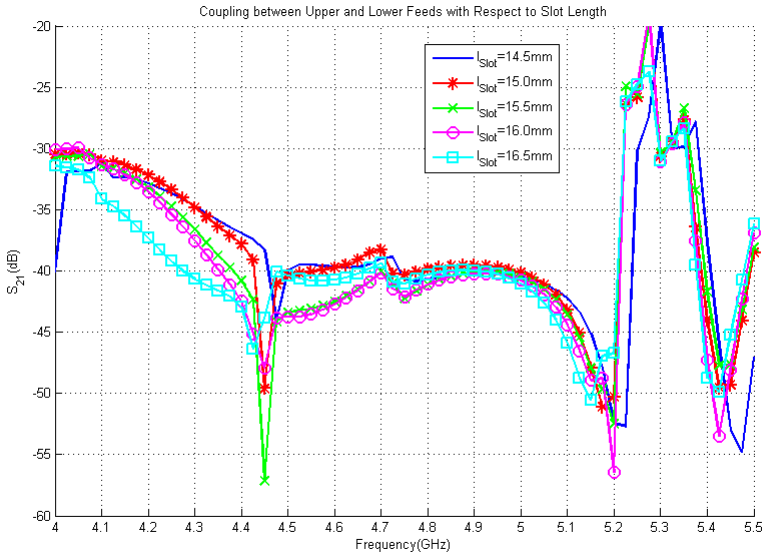

Figure 2.29: Coupling between upper and lower feed networks versus frequency for various slot lengths

As it can be seen from the figures, slot length does not change the reflection coefficient of the upper feed network significantly for the values we sweep. However, reflection coefficient of the lower feed network does change significantly, and an increase in the slot length shifts the resonance of it to higher frequencies. Also, one can observe that cross polarization isolation does not have a linear relation with the slot length and it should be optimized. Hence, there is a trade-off between reflection coefficients and the cross polarization isolation. It can be seen that when $l_{Slot} = 15.5$mm, the reflection coefficients of both upper and lower feed network are better than -12.5dB and the cross polarization isolation is better than 40dB. Therefore, this value is chosen.

2.3.6 Minimum of Slot Width (d_{Slot})

In the antenna element design, dog-bone shaped slot is chosen as shown in Fig. 2.4 due to its large bandwidth characteristics. In Fig. 2.30, Fig. 2.31 and Fig. 2.32, the effect of minimum of slot thickness, shown in Fig. 2.4, on the impedance characteristics is presented.

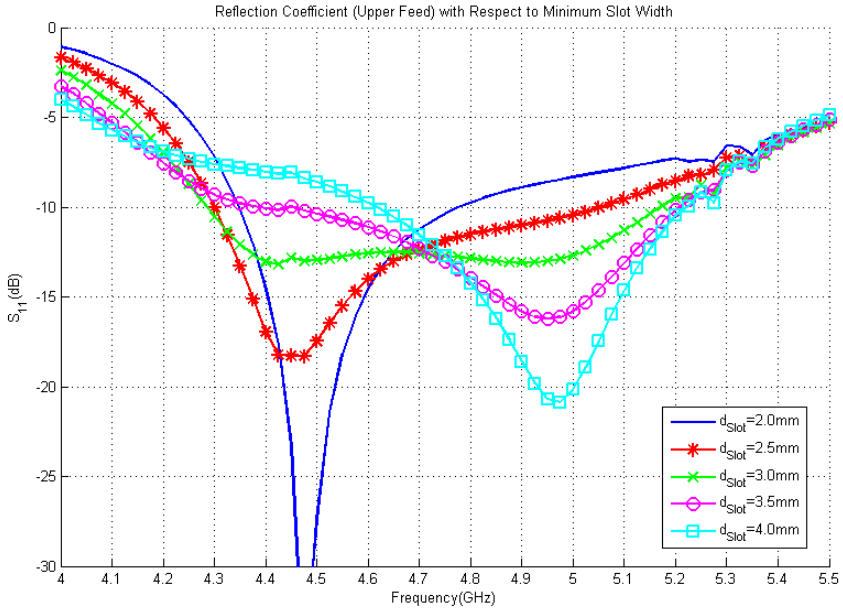

Figure 2.30: Reflection coefficient for upper feed network versus frequency for various values of minimum of slot widths

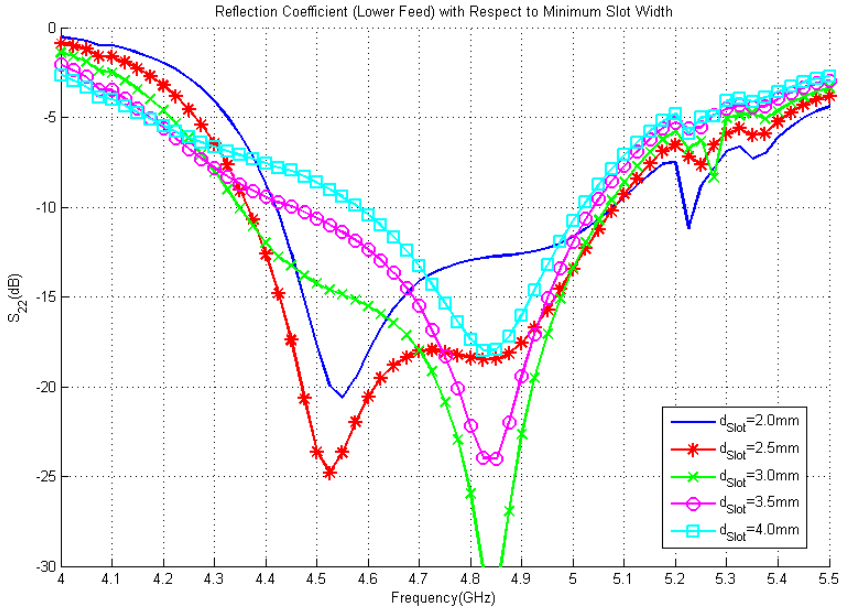

Figure 2.31: Reflection coefficient for lower feed network versus frequency for various values of minimum of slot widths

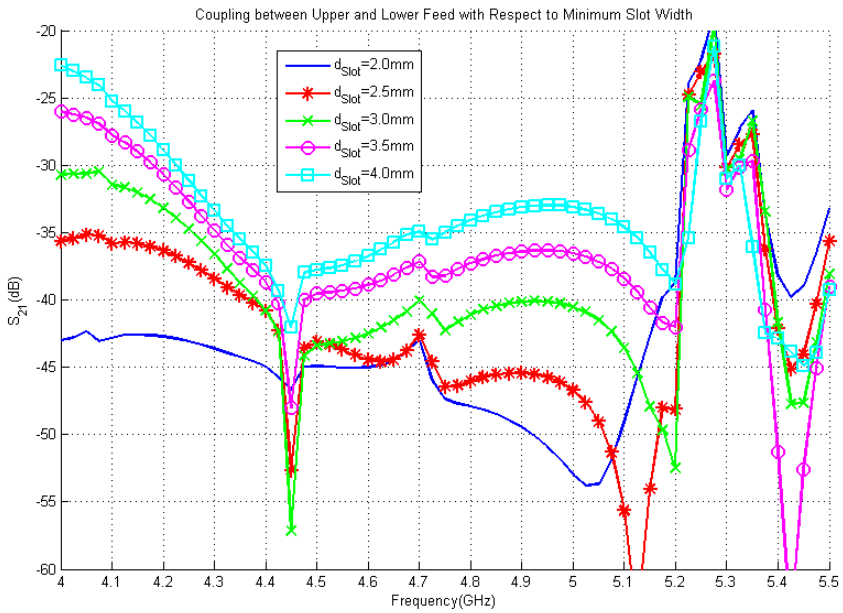

Figure 2.32: Coupling between upper and lower feed networks versus frequency for various values of minimum of slot widths

The results indicate that an increase in the minimum of slot width leads to shift in resonance to higher frequencies for both upper and lower feed networks. However, level of resonance changes significantly with this increase. An increase in minimum of slot width causes a dramatic decrease in the cross polarization isolation. So, there is a trade-off between resonance frequencies of the upper and lower feed networks and the cross polarization isolation. It can be seen that when $d_{Slot} = 3.0$mm, reflection coefficients of both upper and lower feed networks are better than -12.5dB and the cross polarization isolation is better than 40dB. Therefore, this value is chosen.

2.3.7 Maximum of Slot Width ($d_{Slot} + w_{Slot}$)

In Fig. 2.33, Fig. 2.34 and Fig. 2.35, the effect of maximum of slot thickness, shown in Fig. 2.4, on the impedance characteristics is presented.

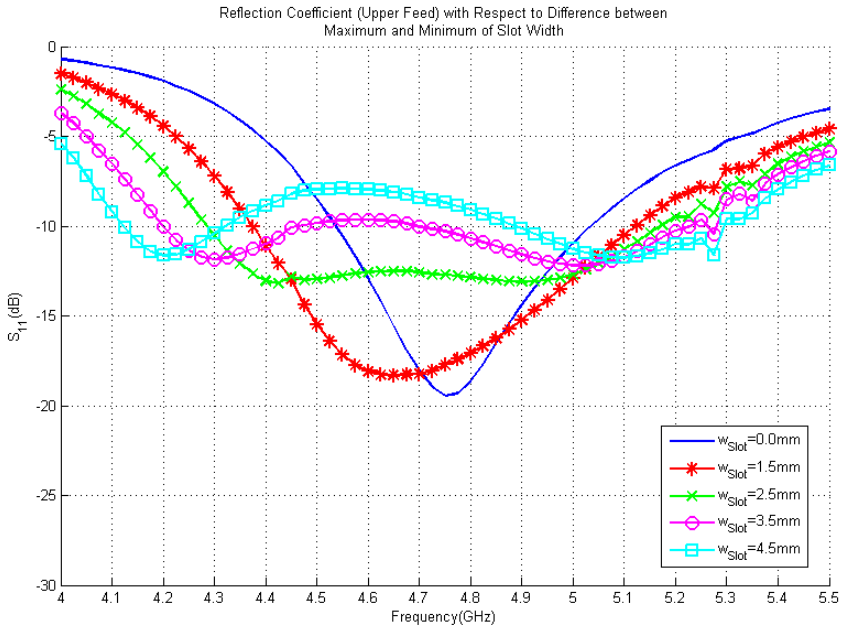

Figure 2.33: Reflection coefficient for upper feed network versus frequency for various values of maximum of slot widths

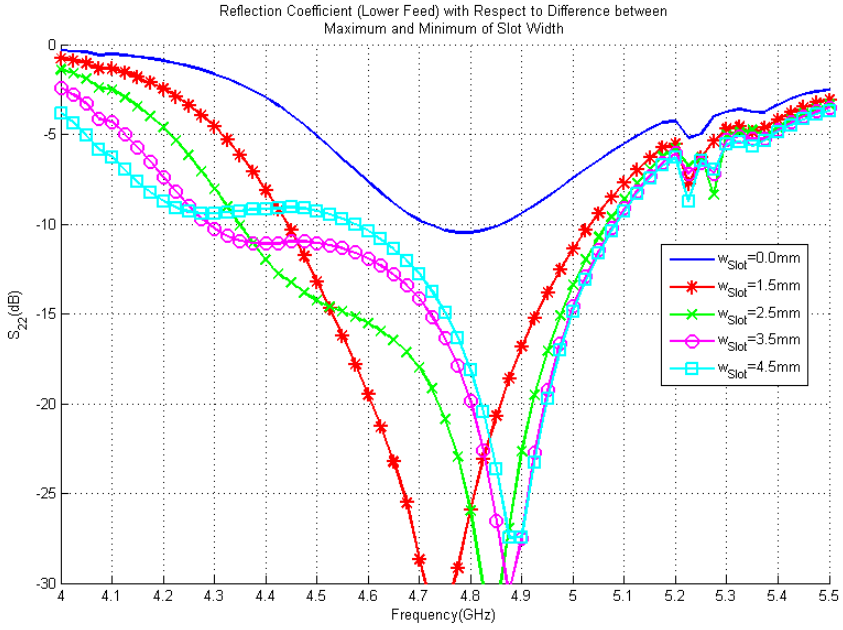

Figure 2.34: Reflection coefficient for lower feed network versus frequency for various values of maximum of slot widths

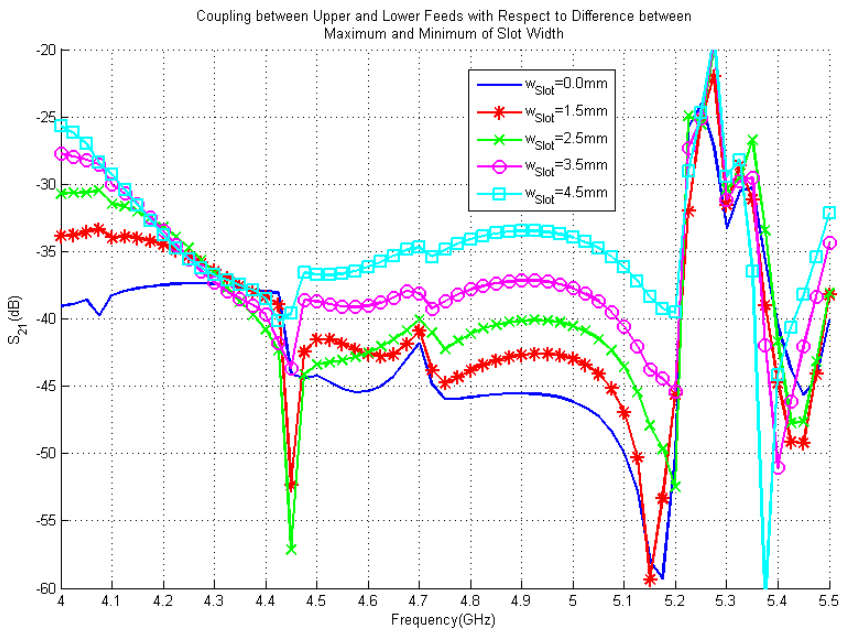

Figure 2.35: Coupling between upper and lower feed networks versus frequency for various values of maximum of slot widths

Based on Figs. 2.33 - 2.35, it can be said that an increase in maximum of slot width, the impedance bandwidth increases. On the other hand, the level of reflection coefficient can increase respectively. Additionally, note that increase in maximum of slot width causes a decrease in cross polarization isolation. So, there is a trade-off between resonance frequuencies of upper and lower feed networks and the cross polarization isolation. It can be seen that when w_{Slot} = 2.5mm, the reflection coefficient of both upper and lower feed network is better than -12.5dB and cross polarization isolation is better than 40dB. Therefore, this value is chosen.

2.3.8 Stub Length for Lower Feed ($l_{StubLower}$)

Open stubs are used in both polarizations for impedance matching as shown in Fig. 2.5 . In Fig. 2.36, Fig. 2.37 and Fig. 2.38, the effect of stub length for lower feed (see Fig. 2.5(b)) on the impedance characteristics are presented.

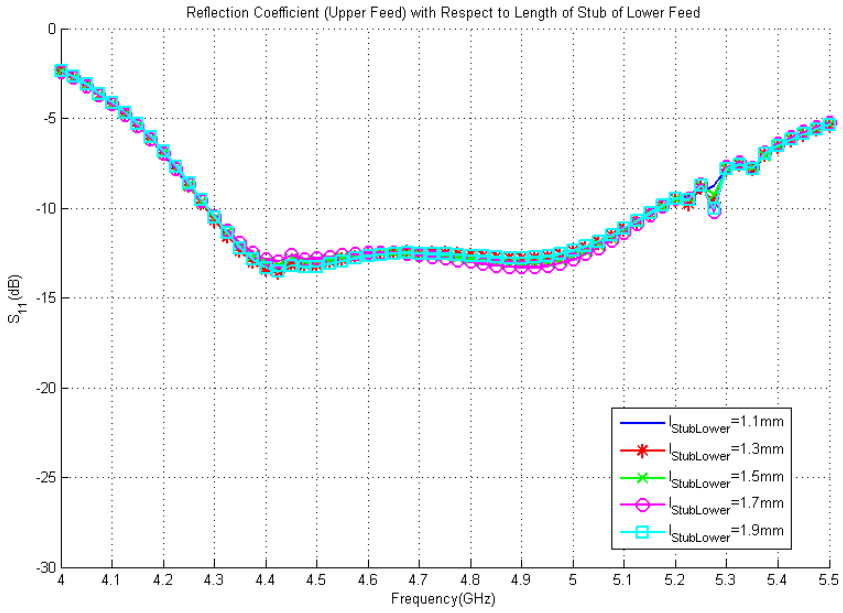

Figure 2.36: Reflection coefficient for upper feed network versus frequency for various lengths of stubs of lower feed

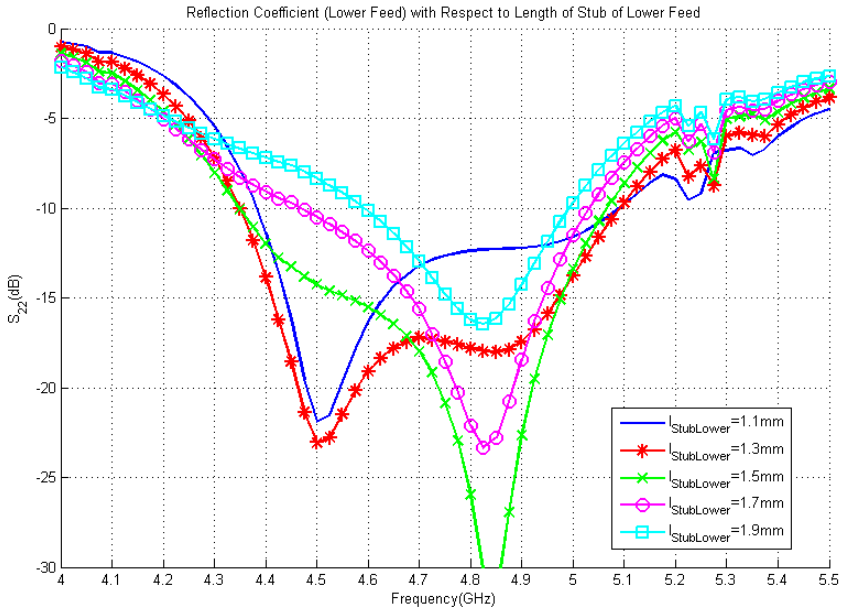

Figure 2.37: Reflection coefficient for lower feed network versus frequency for various lengths of stubs of lower feed

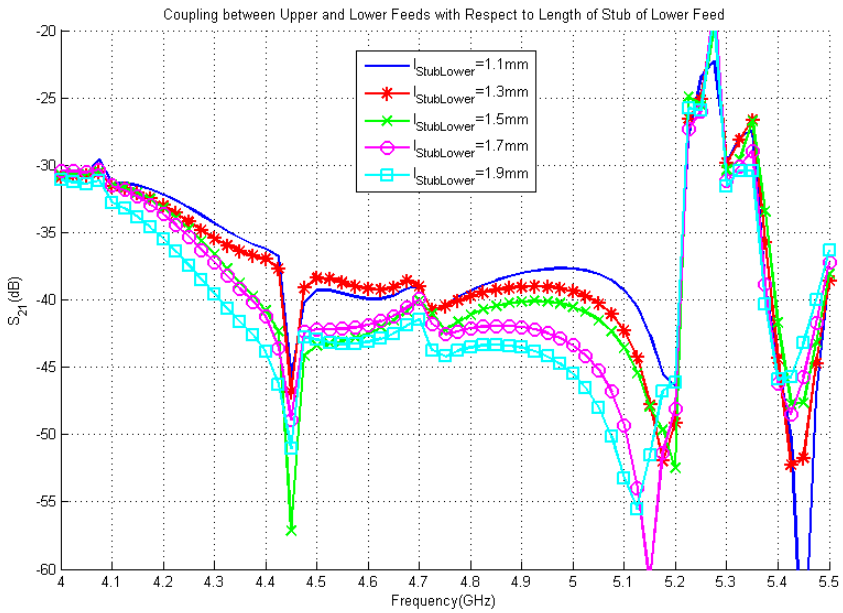

Figure 2.38: Coupling between upper and lower feed networks versus frequency for various lengths of stubs of lower feed

From these figures, one can see that an increase in the length of the open stub of the lower feed changes both the resonance frequency and the reflection level for the lower feed network. However, it has almost no effect on the upper feed network as it is expected. Another point is that, length of the open stub of the lower feed is inversely proportional to the coupling between upper and lower feed networks. Hence, there is a trade-off between the resonance frequencies of the lower feed and the cross polarization isolation. It can be seen that when $l_{StubLower} = 1.5$mm, the reflection coefficients of both upper and lower feed network are better than -12.5dB and the cross polarization isolation is better than 40dB. Therefore, this value is chosen.

2.3.9 Stub Length for Upper Feed ($l_{StubUpper}$)

In Fig. 2.39, Fig. 2.40 and Fig. 2.41, the effect of stub length for upper feed (see Fig. 2.5(a)) on the impedance characteristics is presented.

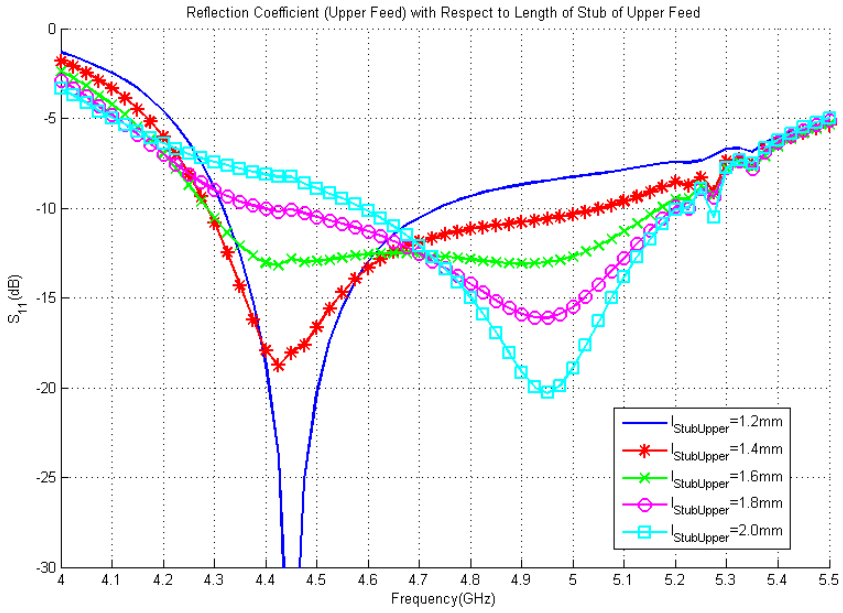

Figure 2.39: Reflection coefficient for upper feed network versus frequency for various lengths of stubs of upper feed

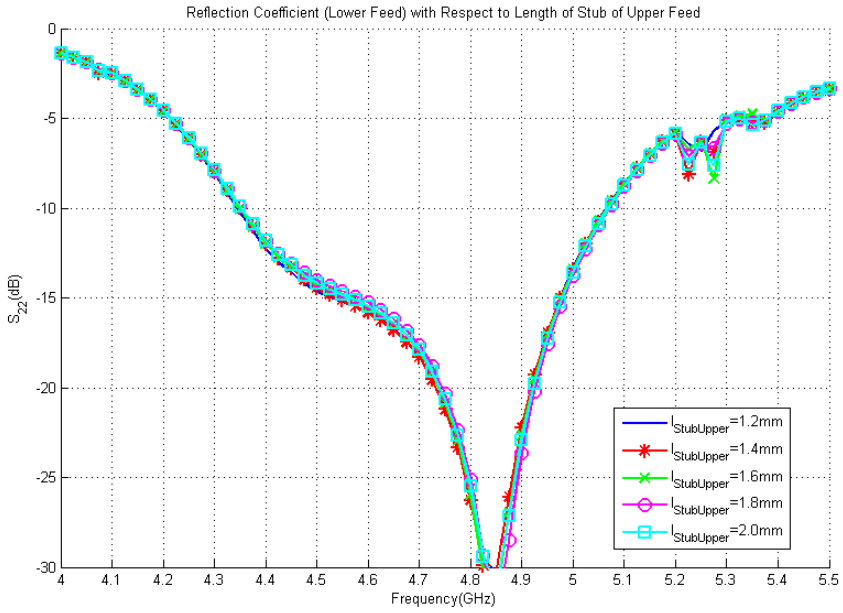

Figure 2.40: Reflection coefficient for lower feed network versus frequency for various lengths of stubs of upper feed

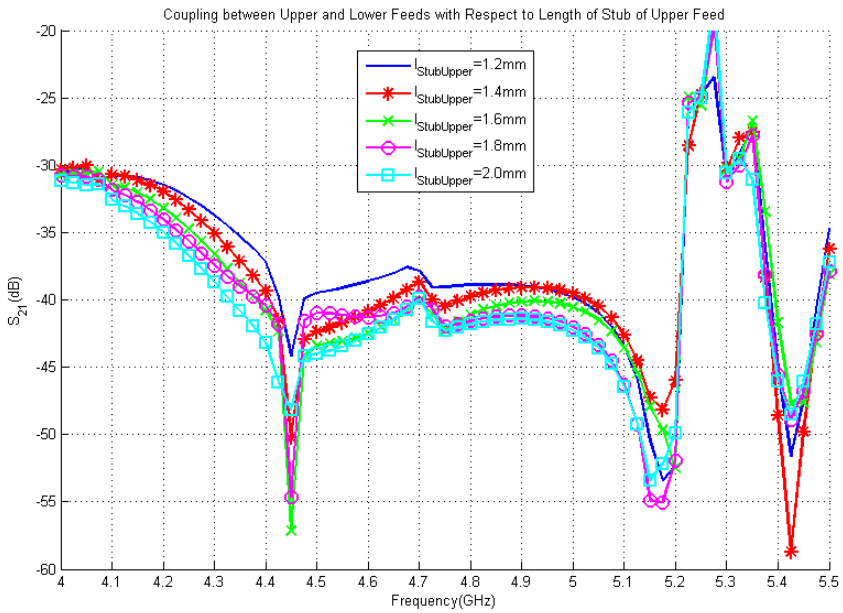

Figure 2.41: Coupling between upper and lower feed networks versus frequency for various lengths of stubs of upper feed

Based on Figs. 2.39 - 2.41, it can be said that an increase in the length of the open stub of the upper feed changes both the resonance frequency and the reflection level for the upper feed. However, it has almost no effect on the lower feed network as it is expected. Another point is that, length of the open stub of the upper feed is inversely proportional to the coupling between the upper and lower feed networks. Hence, there is a trade-off between resonance frequencies of the upper feed and the cross polarization isolation. It can be seen that when $l_{StubUpper}$ = 1.6mm, reflection coefficients of both upper and lower feed network are better than -12.5dB and the cross polarization isolation is better than 40dB. Therefore, this value is chosen.

2.3.10 Distance between Branches of Lower Feed (w_{Lower})

In Fig. 2.42, Fig. 2.43 and Fig. 2.44, the effect of the distance between branches of the lower feed network, illustrated in Fig. 2.5(b), on the impedance characteristics are presented.

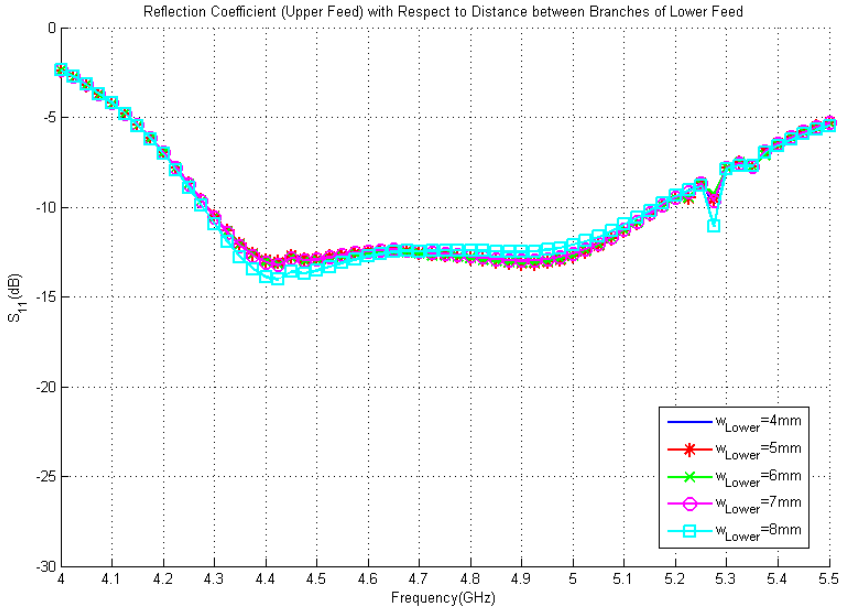

Figure 2.42: Reflection coefficient for upper feed network versus frequency for various distances between branches of lower feed

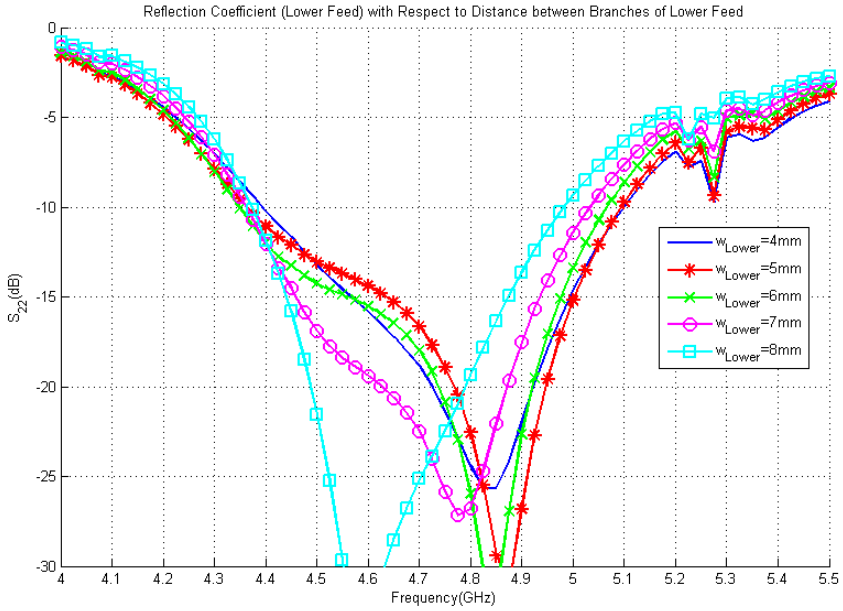

Figure 2.43: Reflection coefficient for lower feed network versus frequency for various distances between branches of lower feed

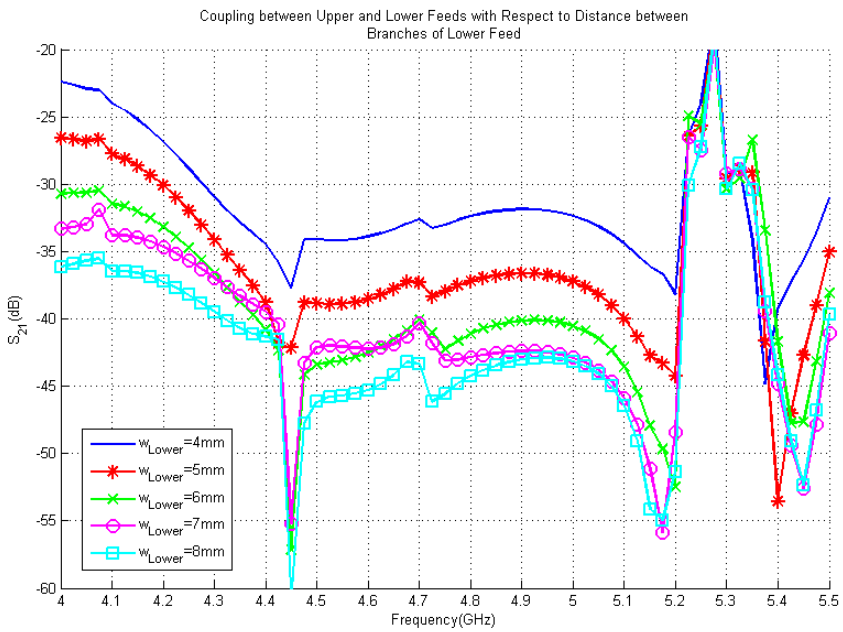

Figure 2.44: Coupling between upper and lower feed networks versus frequency for various distances between branches of lower feed

It can be observed from Figs. 2.42 - 2.44 that the distance between branches of the lower feed network has almost no effect on the reflection coefficient of the upper feed network. On the other hand, the resonance of the lower feed network is shifted to lower frequencies with an increase in this parameter. Additionally, a decrease in this parameter leads to a dramatic decrease in the cross polarization isolation. Hence, there is a trade-off between resonance frequencies of the lower feed and the cross polarization isolation. It can be seen that when w_{Lower} = 6.0mm, reflection coefficients of both upper and lower feed network are better than -12.5dB and the cross polarization isolation is better than 40dB. Therefore, this value is chosen.

2.3.11 Distance between Branches of Upper Feed (w_{Upper})

In Fig. 2.45, Fig. 2.46 and Fig. 2.47, the effect of the distance between branches of the upper feed network, illustrated in Figs. 2.5(a), on the impedance characteristics are presented.

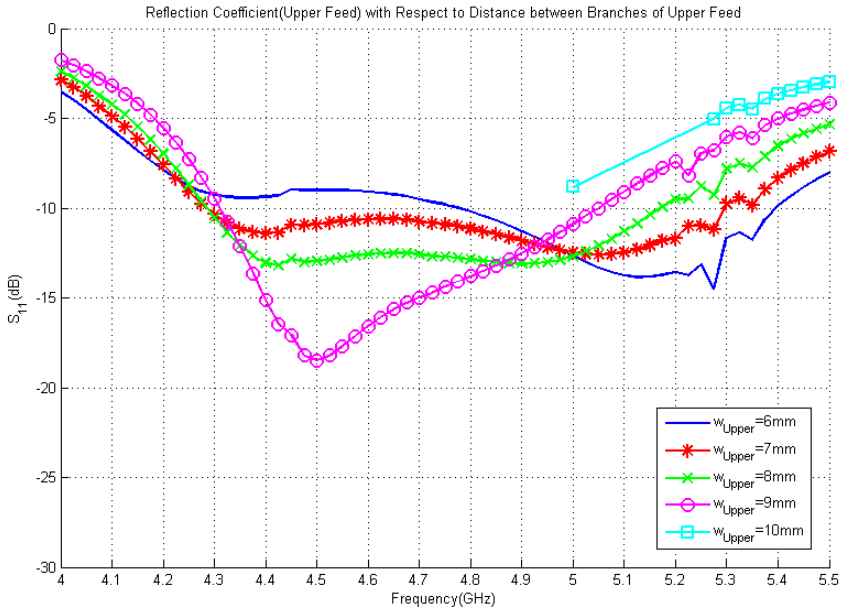

Figure 2.45: Reflection coefficient for upper feed network versus frequency for various distances between branches of upper feed

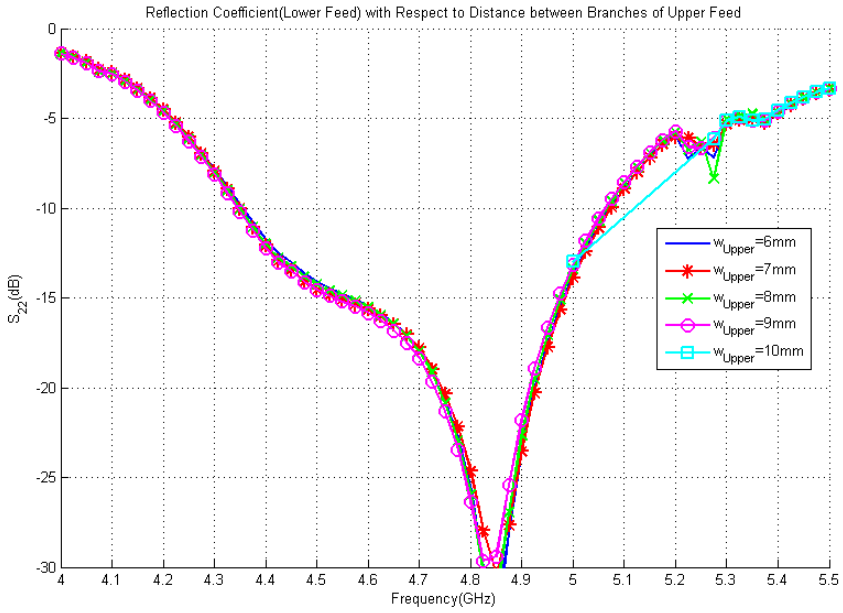

Figure 2.46: Reflection coefficient for lower feed network versus frequency for various distances between branches of upper feed

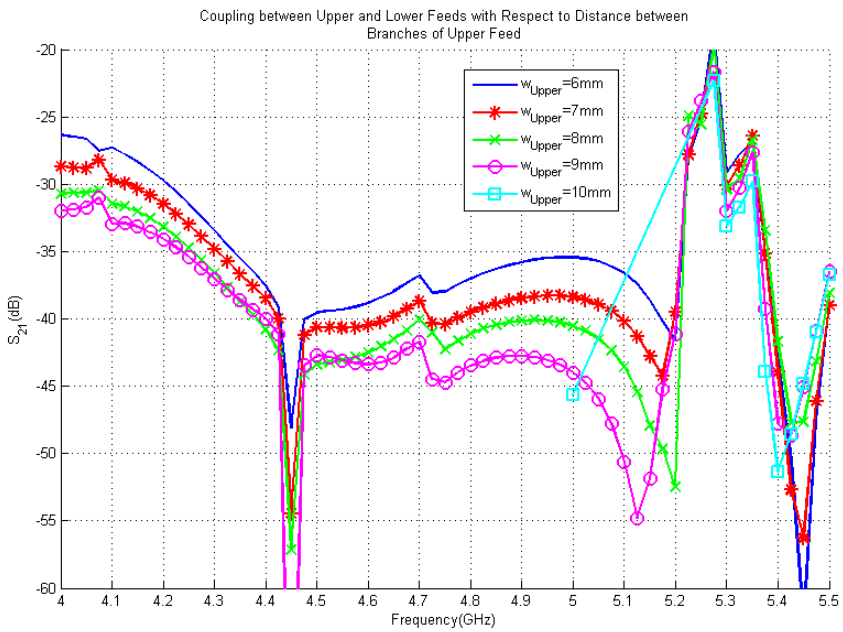

Figure 2.47: Coupling between upper and lower feed network versus frequency for various distances between branches of upper feed

It can be seen from the figures that the distance between the branches of the upper feed network has almost no effect on the reflection coefficient of the lower feed network. On the other hand, the resonance of the upper feed is shifted to lower frequencies with an increase in this parameter. Additionally, a decrease in this parameter leads to a dramatic decrease in the cross polarization isolation. Hence, there is a trade-off between resonance frequencies of the upper feed and the cross polarization isolation. It can be seen that when $w_{Upper} = 8.0$mm, reflection coefficients of both upper and lower feed networks are better than -12.5dB and the cross polarization isolation is better than 40dB. Therefore, this value is chosen.

2.3.12 Distance between Reflector and Lower Ground ($h_{Reflector}$)

In Fig. 2.48, Fig. 2.49 and Fig. 2.50, the effect of the distance between the reflector and the lower ground plane as illustrated in Fig. 2.1 and Fig. 2.2, on the impedance characteristics is presented.

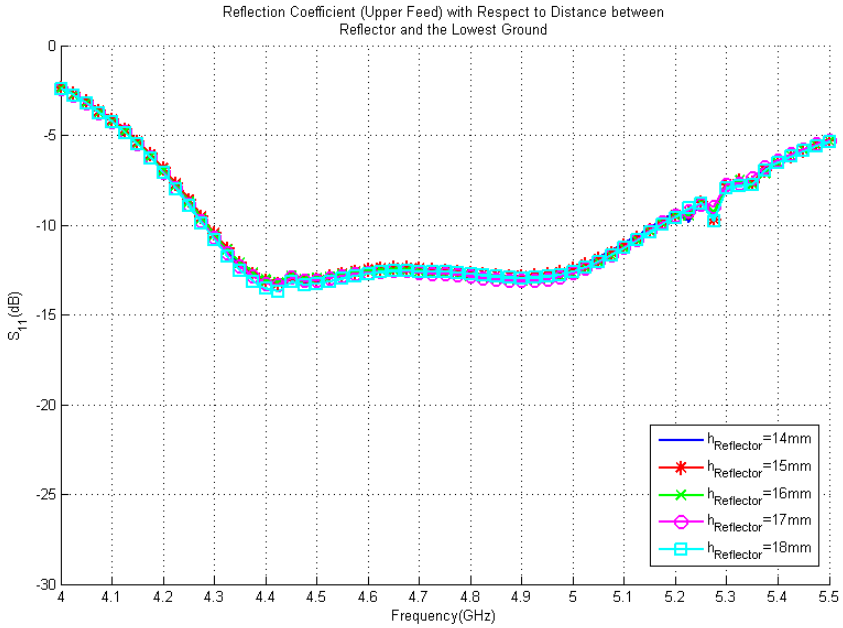

Figure 2.48: Reflection coefficient for upper feed network verus frequency for various distances between reflector and the lowest ground plane

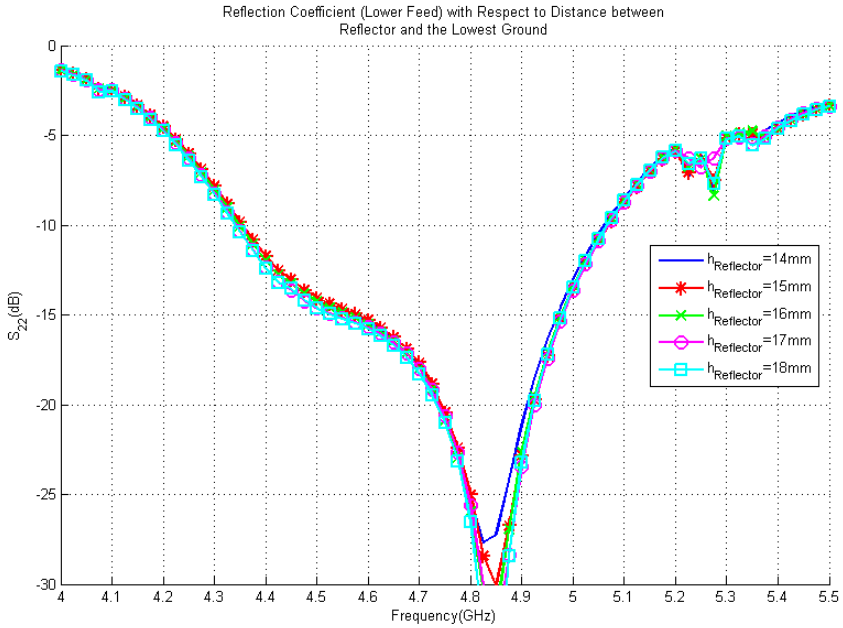

Figure 2.49: Reflection coefficient for lower feed network verus frequency for various distances between reflector and the lowest ground plane

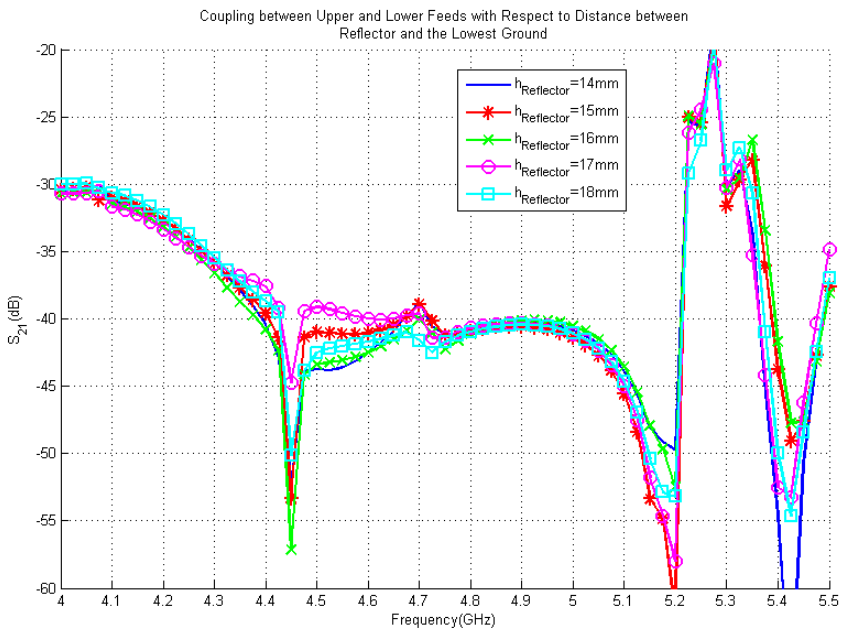

Figure 2.50: Coupling between upper and lower feed networks verus frequency for various distances between reflector and the lowest ground plane

From these figures (2.48 - 2.50), the distance between the lowest ground plane and the reflector is not very effective on the impedance behavior of the upper feed network. On the other hand, it can be observed that the level of reflection coefficient of the lower feed network changes with this parameter slightly. Moreover, the relation between cross polariztion isolation and this parameter is not linear. Therefore, it should be optimized. It can be seen that when $h_{Reflector}$ = 16mm, reflection coefficients of both upper and lower feed network are better than -12.5dB and the cross polarization isolation is better than 40dB. Therefore, this value is chosen.

Chapter 3

Feed Network Design

In this thesis, it is aimed to design an antenna array with a -15dB SLL in both cardinal and intercardinal planes. Recall that cardinal planes are the cuts for ϕ=0° and ϕ=90° when antenna elements are placed in the x- and y-directions and intercardinal planes are the cuts for other ϕ's [35]. Low SLL is desired in these planes because it results a lower interference between communication link channels and better communication quality. Additionally, vulnerability to jamming through these planes can be prevented. It is well known that the antenna pattern is the Fourier Transform of the current distribution on the antenna array. Therefore, by exciting the array elements with required amplitude and phase values, the desired array patterns can be obtained. The general practice is to feed array elements with equal amplitudes. However, this technique results in a $sinc-$shaped pattern and approximately -13dB SLL. Another possible amplitude distribution is the triangular amplitude distribution. That results a $sinc^2-$shaped pattern and -15dB SLL. Since we have a two-dimensional array, the proposed amplitude distribution should be a triangular-shaped one in both cardinal and intercardinal planes to decrease the SLL in those planes. This distribution can be called as pyramidial shape. Additionally, we require minimum 20dB gain and maximum 10° 3dB beamwidth. As a result, a 6 by 6 array with 0.96λ element spacing at 4.7GHz is chosen as the array configuration. Note that at 5GHz, this element spacing corresponds to 1.02λ and for high frequencies of the

band of the design, it causes grating lobes. However, in order to satisfy the gain and beamwidth requirements, this configuration is used and grating lobes are treated separetely. The angular positions for grating lobes are adjusted to angular positions of the single element pattern where directivity is 15dB lower than the maximum of the directivity at that point. In this way, the grating lobes can be supressed. The desired distribution is tabulated in Table 3.1, where P stands for unit power.

Antenna#1 **P**	Antenna#2 **2P**	Antenna#3 **3P**	Antenna#4 **3P**	Antenna#5 **2P**	Antenna#6 **P**
Antenna#7 **2P**	Antenna#8 **4P**	Antenna#9 **6P**	Antenna#10 **6P**	Antenna#11 **4P**	Antenna#12 **2P**
Antenna#13 **3P**	Antenna#14 **6P**	Antenna#15 **9P**	Antenna#16 **9P**	Antenna#17 **6P**	Antenna#18 **3P**
Antenna#19 **3P**	Antenna#20 **6P**	Antenna#21 **9P**	Antenna#22 **9P**	Antenna#23 **6P**	Antenna#24 **3P**
Antenna#25 **2P**	Antenna#26 **4P**	Antenna#27 **6P**	Antenna#28 **6P**	Antenna#29 **4P**	Antenna#30 **2P**
Antenna#31 **P**	Antenna#32 **2P**	Antenna#33 **3P**	Antenna#34 **3P**	Antenna#35 **2P**	Antenna#36 **P**

Table 3.1: Amplitude distribution for antenna array

Note that the desired amplitude distribution for the feed network is the matrix product of P*[1 2 3 3 2 1]^T and [1 2 3 3 2 1]. Hence, the division [1 2 3 3 2 1] should be implemented to input power at first. In this way, rows of the matrix can be obtained. Then, division [1 2 3 3 2 1] should be implemented to outputs of the first power divider separately. As a result, the matrix product can be realized. This means only one power divider [1 2 3 3 2 1] should be designed at first. Then, by combining seven of them, where one is directly connected to input power and six of them are connected between the outputs of the first divider and antenna ports, the entire feed network can be constructed. .

In the thesis, no electrical scanning is aimed and the maximum radiation is desired at boresight. Therefore, all antenna elements should be equiphase. Moreover, desired patterns are the same for both polarizations. Thus, only one 1-to-36 power divider is designed and two of them are stacked to constitute the dual-polarized feed network.

The desired amplitude and phase distributions are simulated via MATLAB®and ideal (i.e., desired) array factors are computed. The resulted array factors are presented from 4.4GHz to 5GHz with an increment of 0.1GHz in Fig. 3.1, Fig. 3.2, Fig. 3.3 and Fig. 3.4 for cardinal and intercardinal planes. Note that the upper and lower feed networks are the same to generate similar patterns for both polarizations. Therefore, expected (ideal) array factors are the same for them.

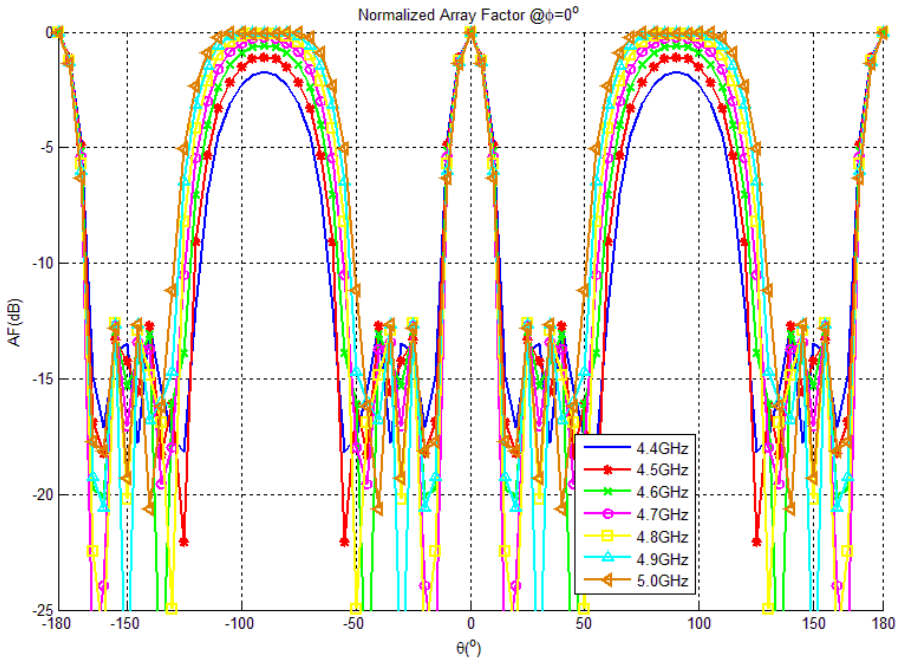

Figure 3.1: Desired array factor at $\phi = 0°$ (a cardinal plane) for various frequencies

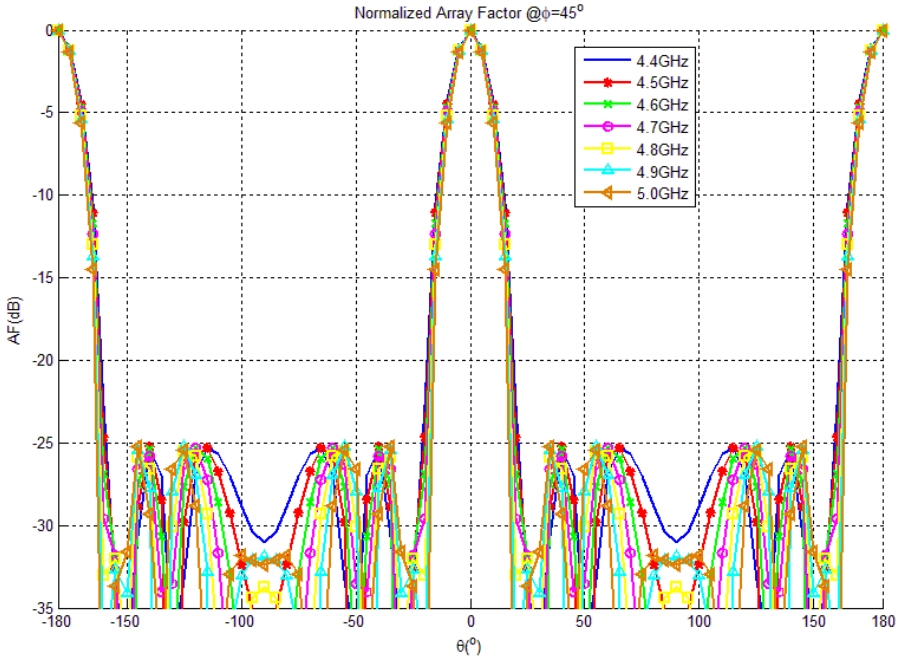

Figure 3.2: Desired array factor at ϕ =45° (an intercardinal plane) for various frequencies

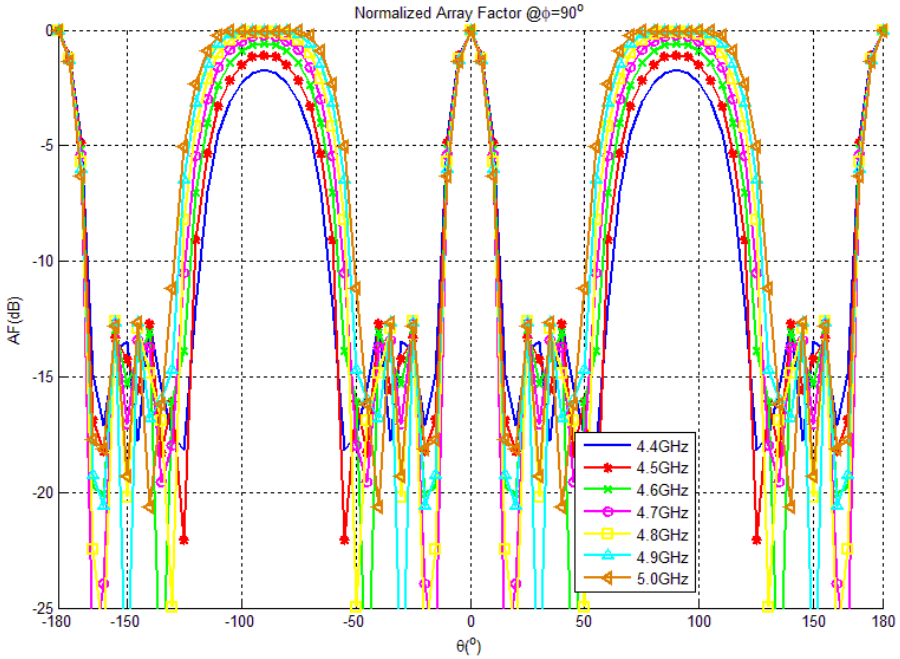

Figure 3.3: Desired array factor at ϕ =90° (a cardinal plane) for various frequencies

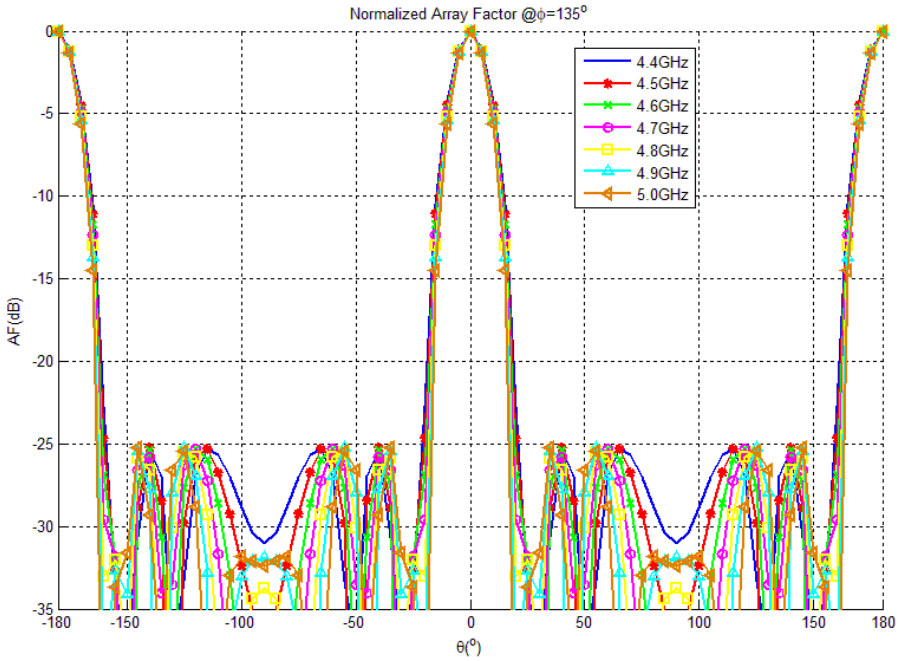

Figure 3.4: Desired array factor at ϕ =135° (an intercardinal plane) for various frequencies

It can be seen from Fig. 3.1 to Fig. 3.4 that in the desired array factors, grating lobes appear in the cardinal planes (for ϕ =0° and ϕ =90°) due to high element spacing. However, these lobes are not in the 10dB beamwidth of the single element and they can be (and will be) suppressed by the help of the element pattern in the array. In intercardinal planes (for ϕ =45° and ϕ =135°), there is no grating lobe as it is expected, because in these planes, slope of the amplitude is higher compared to cardinal planes. Thus, better SLL in ϕ =0° and ϕ =90° is expected. In Chapter 2, the antenna element patterns are obtained for both upper and lower feed networks. If the array factors are multiplied with antenna element patterns for upper and lower feed networks separetaly, the expected array patterns can be obtained. Note that, these patterns do not include effects of the coupling between antenna elements and they are modeled as perfectly isolated. In Fig. 3.5 to Fig. 3.12, the expected array gain patterns for the upper and lower feed networks in the cardinal and intercardinal planes are presented. Note that these patterns includes the effect of conduction and dielectric losses.

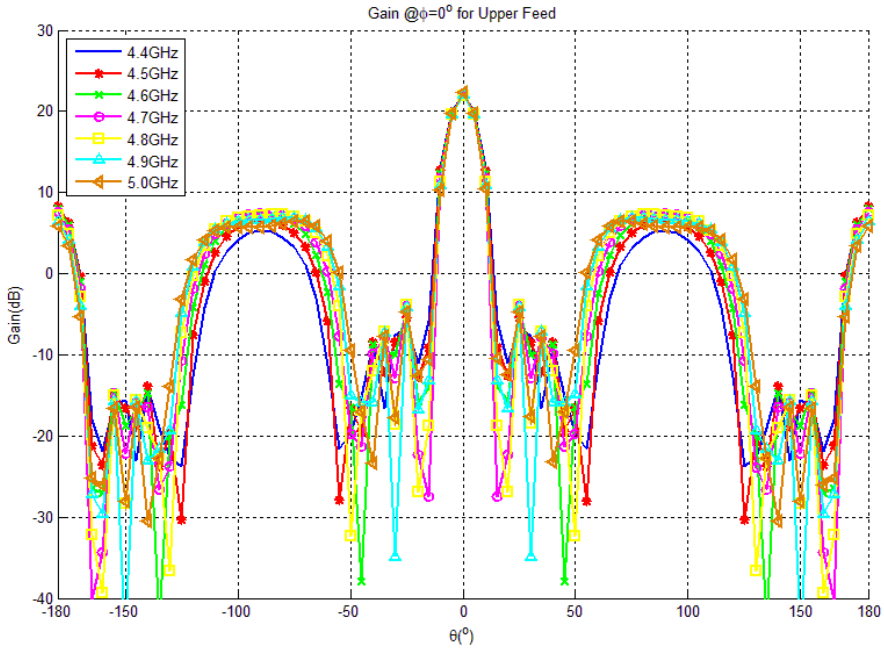

Figure 3.5: Expected antenna array gain pattern at ϕ =0° (a cardinal plane) for various frequencies for the upper feed network

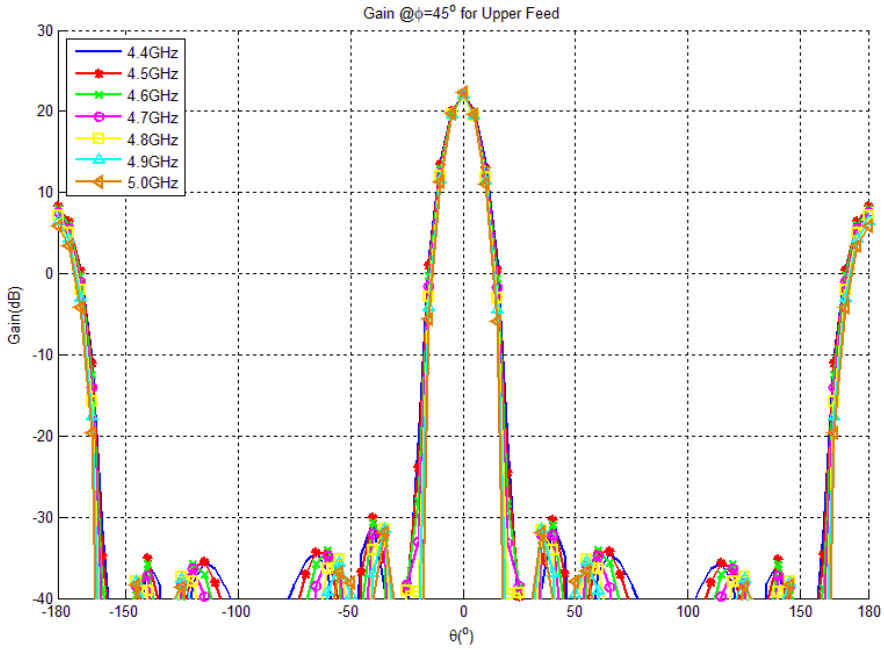

Figure 3.6: Expected antenna array gain pattern at ϕ =45° (an intercardinal plane) for various frequencies for the upper feed network

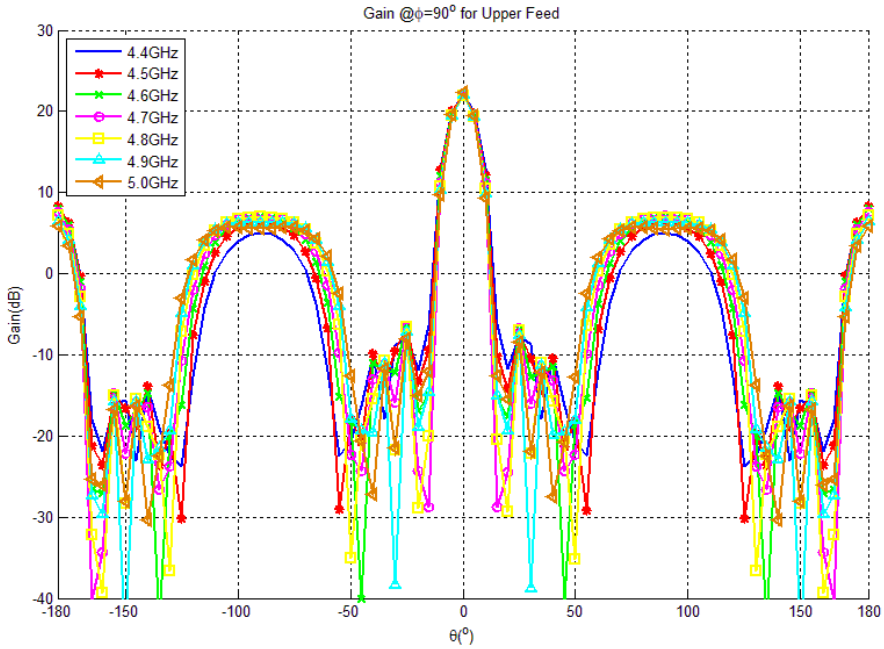

Figure 3.7: Expected antenna array gain pattern at ϕ =90° (a cardinal plane) for various frequencies for the upper feed network

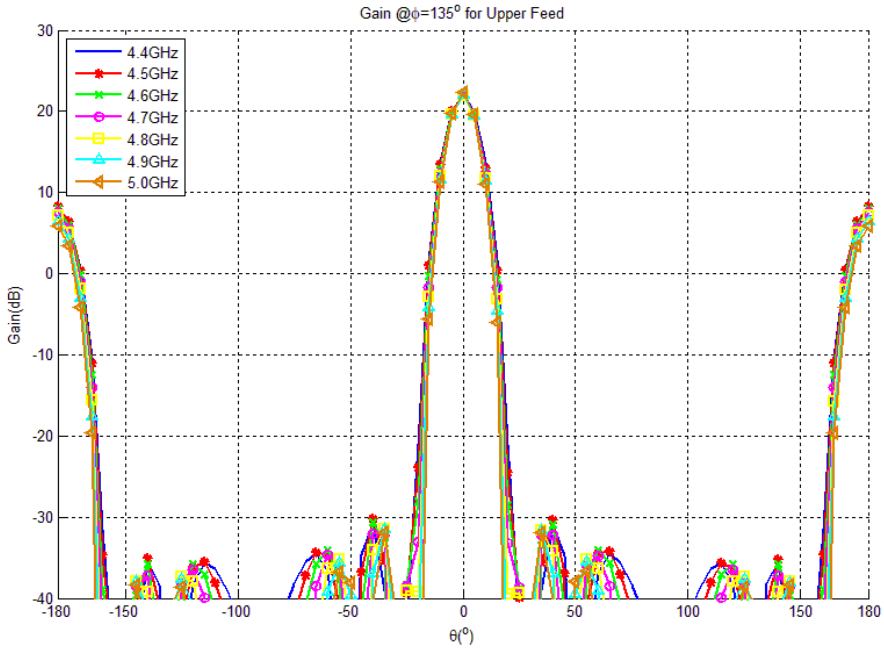

Figure 3.8: Expected antenna array gain pattern at ϕ =135° (an intercardinal plane) for various frequencies for the upper feed network

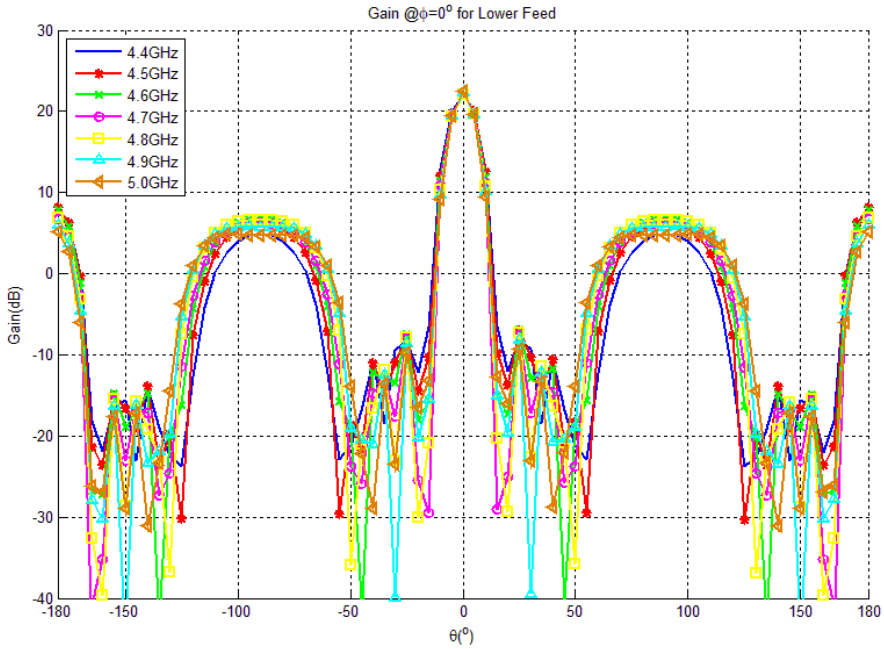

Figure 3.9: Expected antenna array gain pattern at ϕ =0° (a cardinal plane) for various frequencies for the lower feed network

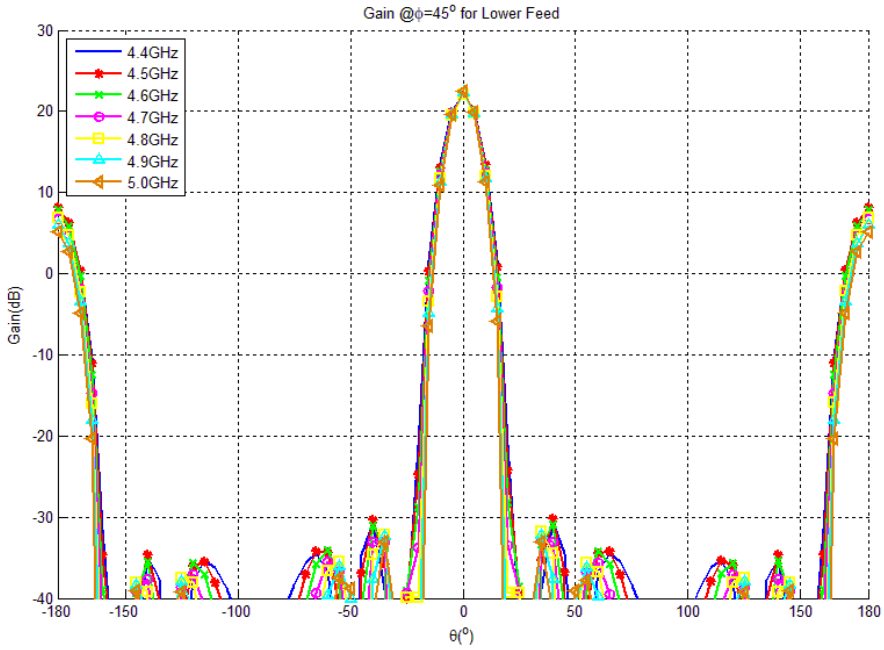

Figure 3.10: Expected antenna array gain pattern at ϕ =45° (an intercardinal plane) for various frequencies for the lower feed network

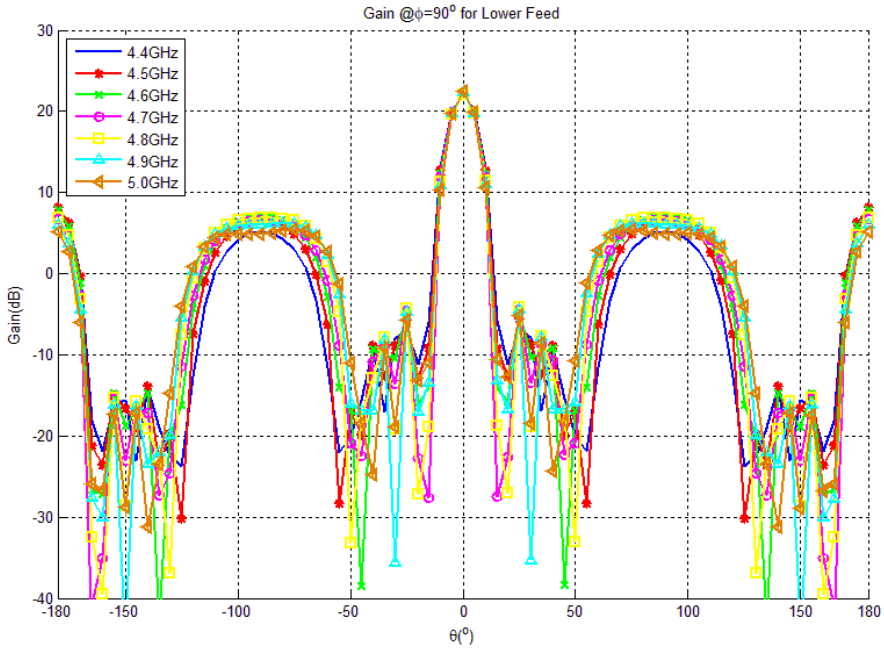

Figure 3.11: Expected antenna array gain pattern at ϕ =90° (a cardinal plane) for various frequencies for the lower feed network

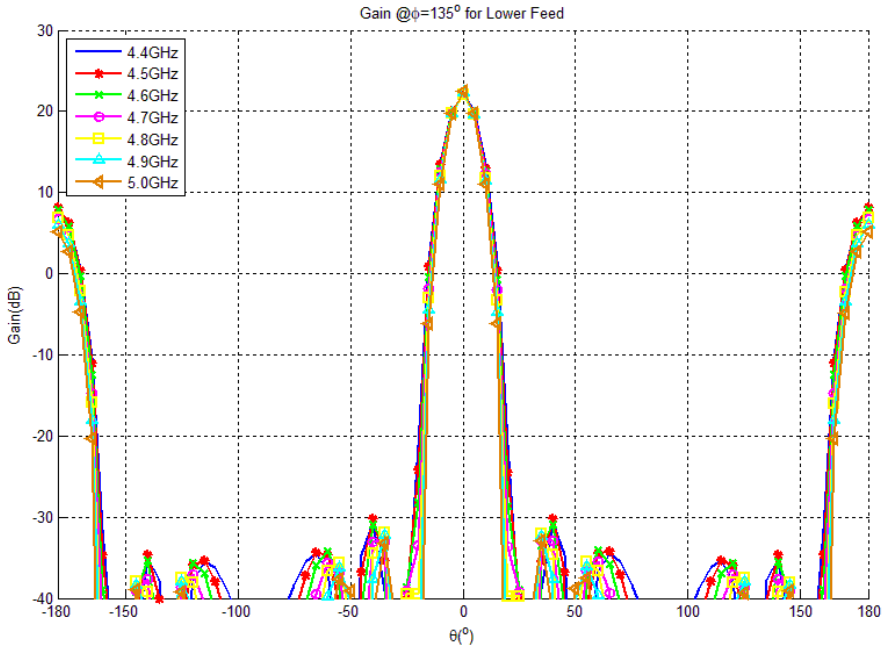

Figure 3.12: Expected antenna array gain pattern at ϕ =135° (an intercardinal plane) for various frequencies for the lower feed network

In these figures (Fig. 3.5 - Fig. 3.12), it can be seen that gain is higher than 20dB in cardinal (ϕ =0° and ϕ =90°) and intercardinal (for ϕ =45° and ϕ =135°) planes for the upper and lower feed networks as desired. Additionally, the SLL is better that -15dB in cardinal planes and better than -30dB in intercardinal planes. The SLL is better in intercardinal planes than cardinal planes because in intercardinal planes slope of the amplitude distribution is higher. With these parameters, it can be said that the proposed amplitude and phase distribution (equiphase antennas) is proper to generate the desired patterns. In the next section, the feed network design that realizes this amplitude and phase distribution is provided step by step.

3.1 Feed Network Design Steps

In order to block the coupling between the feed networks for different polarizations, the stripline technology is chosen. In this way, we can isolate the feed networks. If we use microstrip line technology, the amplitude and phase distributions on the feed networks would be distorted due to the coupling occuring on projective intersections of the feed networks for different polarizations. This would result a lower cross polarization isolation and undesired array factors and array patterns. By chosing stripline feeding, these undesired results can be prevented.

The feed network is optimized for 50Ω for antenna ports. The substrate for the feed network is chosen as 0.787mm ROGERS 5880 Duroid®, which has dielectric constant of 2.20 and tangent loss of 0.0004, for both upper and lower feed networks. The proposed entire feed network structure can be seen in Fig. 3.13.

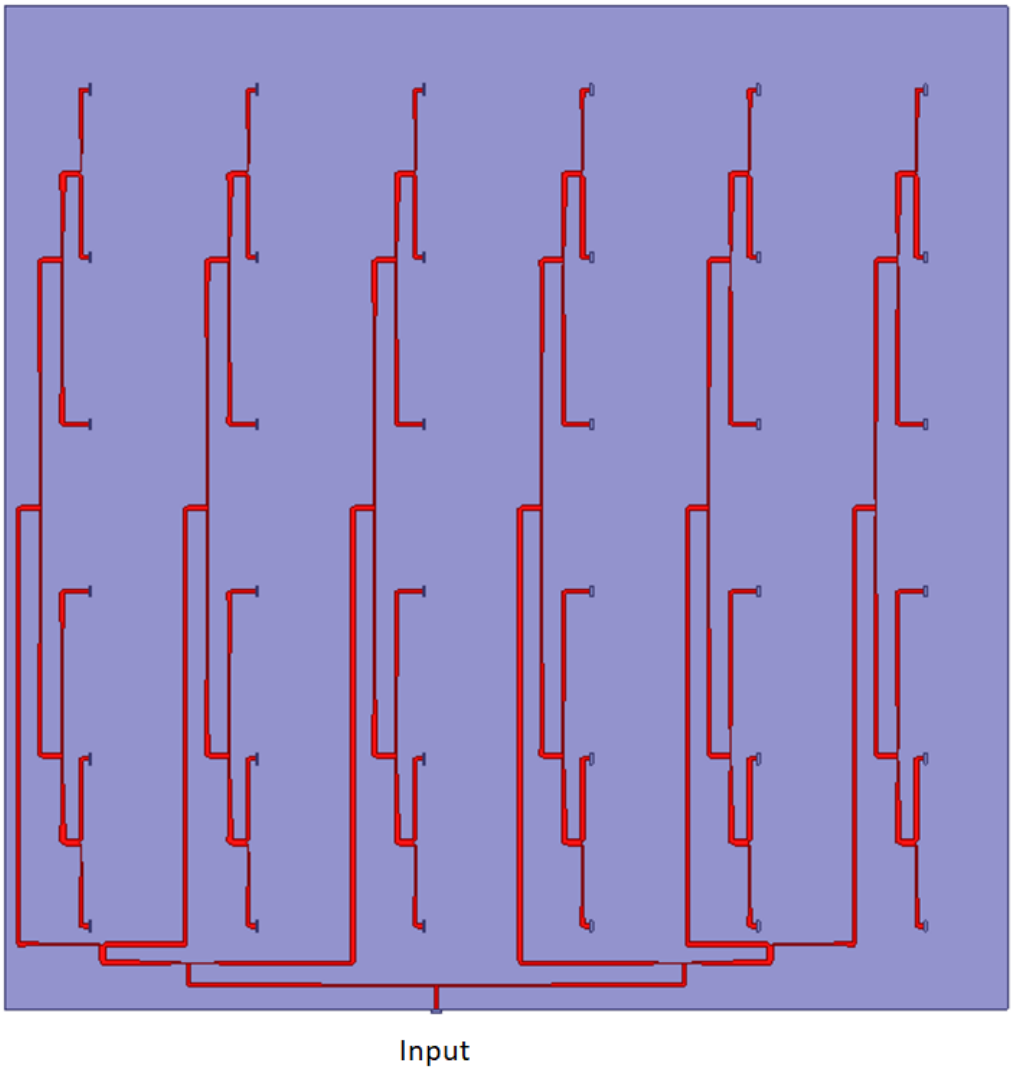

Figure 3.13: Entire feed network (both for upper and lower feed network)

As mentioned before, the feed network consists of seven power dividers [1 2 3 3 2 1] (six of them are vertical and one of them is horizontal as depicted in Fig. 3.13). The details of the design steps are provided in the following subsections. The simulations for Step 1, 2 and 3 in this chapter are performed via HFSS® in a computer having 32GB RAM and 2.8GHz Intel® i7 microprocessor. The simulation for Step 4 is performed via HFSS® in a high performance computer (HPC) having 3TB RAM and 512 cores. In the simulation model, all metallic surfaces (striplines and ground planes) are modelled as copper. The input and output ports of the feed networks are ended with waveports having 50 Ω impedance. A

vacuum box in the shape of rectangular parallelpiped is defined around the feed network. The minimum distance from the single antenna element to the vacuum box is $\lambda/4$ for the minimum frequency in the solution band. The solution frequency is chosen as the maximum frequency in the solution band. For the adaptive solution, maximum number of passes is determined as 15 and maximum of Delta S is determined as 0.02.

3.1.1 Step 1: Dividing Power 3P to Power 2P and P

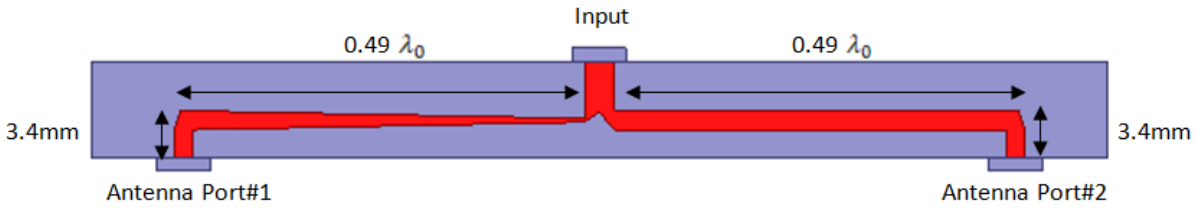

Figure 3.14: Geometry of the feed network Section#1

This section divides 3P power to 2P and P powers. Port impedances of Antenna#1 and Antenna#2 are 50Ω. In order to make power ratio of Antenna#1 to Antenna#2 one half, the impedance ratio of Antenna#1 to Antenna#2 should be made 2/1. For this reason, 50Ω stripline is used for Antenna#2, but for Antenna#1 a tapered stripline that transforms 50Ω impedance to 100Ω impedance is used. Therefore, input impedance becomes 33Ω. Line widths are 1.4mm for 50Ω, 0.4mm for 100Ω and 2.1mm for 33Ω. Also note that the total length of the lines from antenna ports to input are equal to 3.4mm + 0.49λ_0 since we desire no phase difference. Note that λ_0=63.8mm at f=f_0=4.7GHz. $|S_{Antenna\#1}|_{dB}$ should be $10log_{10}(P/3P)$= -4.77dB and $|S_{Antenna\#2}|_{dB}$ should be $10log_{10}(2P/3P)$= -1.76dB as a result of the power divider at this step.

The simulation results of this section of the divider are given in Fig. 3.15 and Fig. 3.16.

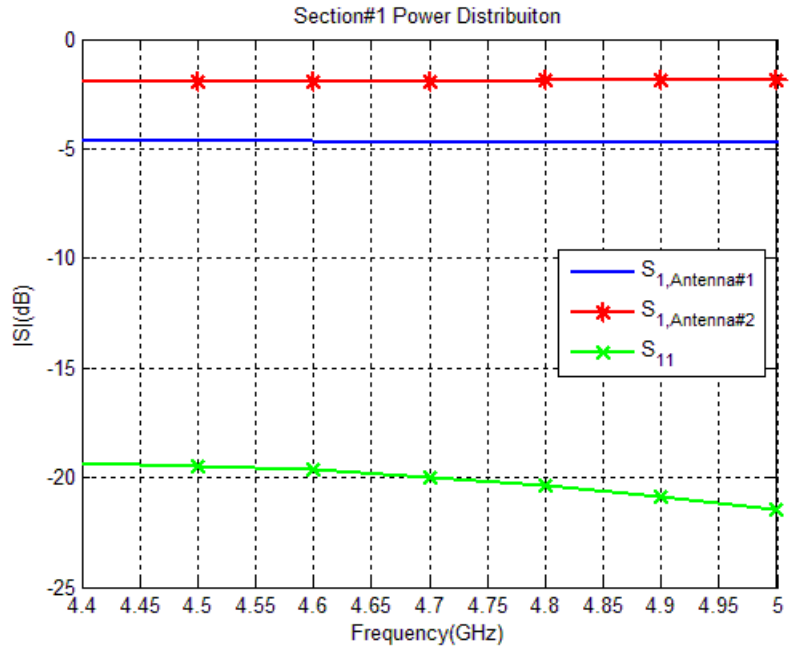

Figure 3.15: Power distribution for the feed network Section#1 through the desired frequency band

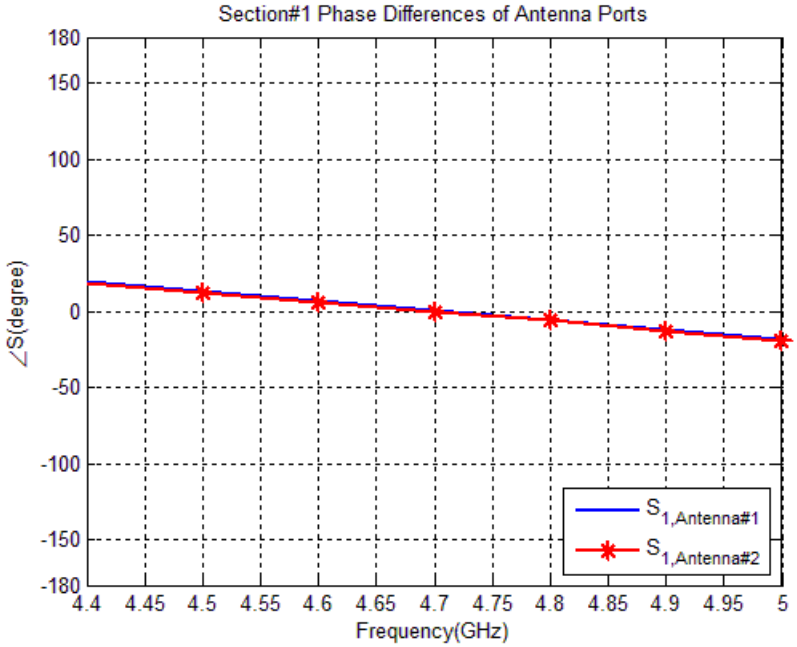

Figure 3.16: Phase differences for the feed network Section#1 through the desired frequency band

From the numerical results presented in Fig. 3.15 and Fig. 3.16 , it can be seen that $|S_{Antenna\#1}|_{dB}$=-4.7dB and $|S_{Antenna\#2}|_{dB}$=-1.9dB. Also, S_{11} is lower than -19dB, and there is almost no phase difference between the antenna ports as desired.

3.1.2 Step 2: Dividing Power 6P to Power 3P, 2P and P

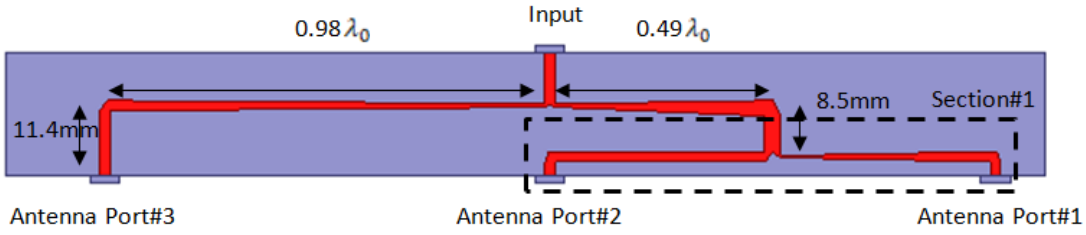

Figure 3.17: Geometry of the feed network Section#2

This section shows how 6P power is divided to 3P, 2P and P powers. In the previous step, division of 3P power to 2P and P powers is realized. Therefore, if the input port of the divider in Step 2 is connected to an output port of equal divider, the divider required for this step can be obtained. Since the sum of the powers of Antenna Port#1 and Antenna Port#2 should be equal to the power of Antenna Port#3, impedances at the intersection point of the input port of the divider in Step 2 and the Antenna Port#3 should be equal. For this reason, a tapered stripline that transforms 50Ω to 100Ω for Antenna Port#3 is used and another tapered stripline for Section#1 that transforms 33Ω to 100Ω is used. Therefore, input impedance becomes 50Ω. Also note that total length of the lines from antenna ports to input are equal to 11.4mm + 0.98λ_0 since we desire no phase difference. $|S_{Antenna\#1}|_{dB}$ should be $10log_{10}(P/6P)$= -7.78dB, $|S_{Antenna\#2}|_{dB}$ should be $10log_{10}(2P/6P)$= -4.77dB and $|S_{Antenna\#3}|_{dB}$ should be $10log_{10}(3P/6P)$= -3.01dB as a result of the power divider at this step. The simulation results of this section of the divider are presented in Fig. 3.18 and Fig. 3.19.

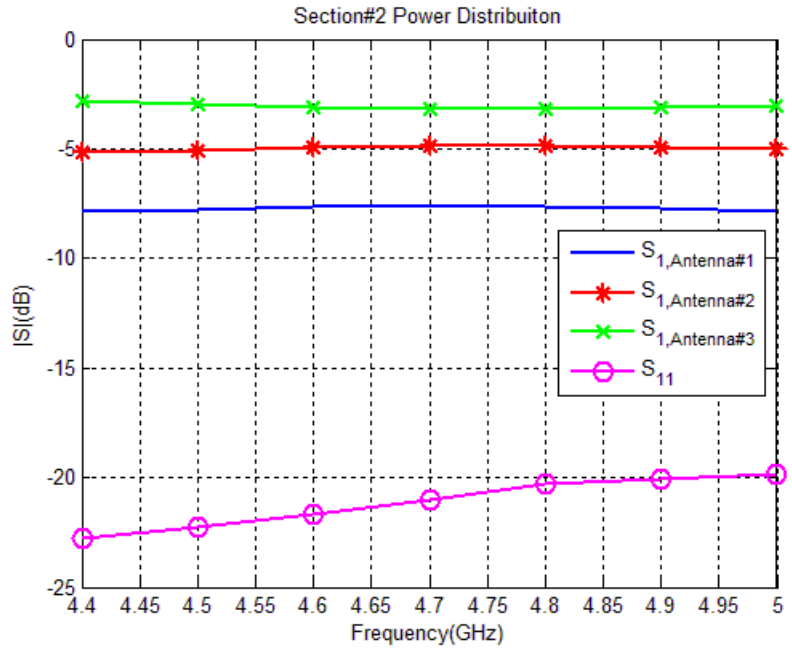

Figure 3.18: Power distribution for the feed network Section#2 through the desired frequency band

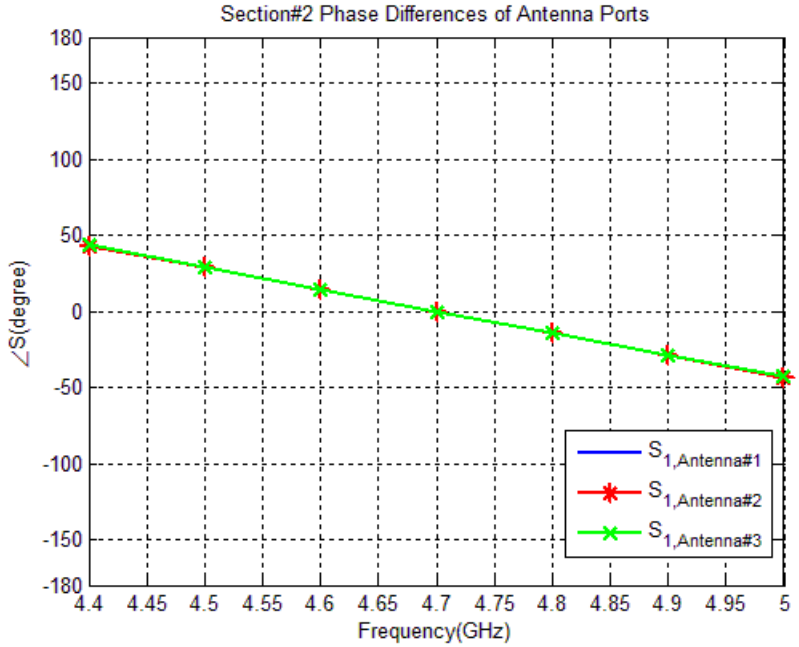

Figure 3.19: Phase differences for the feed network Section#2 through the desired frequency band

From the results presented in Fig. 3.18 and Fig. 3.19, one can see that $|S_{Antenna\#1}|_{dB}$=-7.77dB, $|S_{Antenna\#2}|_{dB}$=-4.92dB and $|S_{Antenna\#3}|_{dB}$=-3.09dB. There is almost no phase difference between the two antenna ports as desired. Besides, S_{11} is lower than -19dB.

3.1.3 Step 3: Dividing Power 12P to Power P, 2P, 3P, 3P, 2P and P

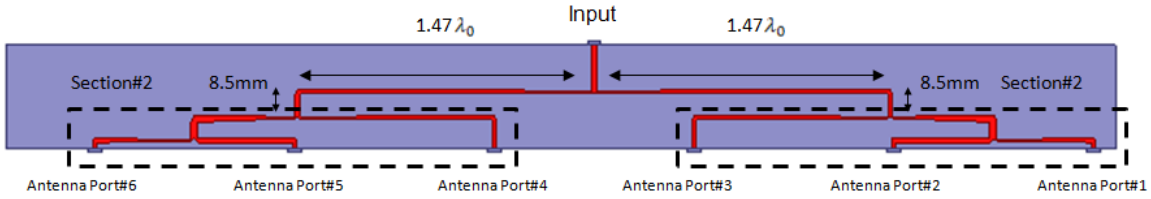

Figure 3.20: Geometry of the feed network Section#3

This subsection presents how to divide 12P power to P, 2P, 3P, 3P, 2P and P powers. For this task, two Section#2 dividers are combined. If input ports of two dividers in Step 2 are connected to output ports of an equal divider, the proposed divider can be realized. Both of them should be fed by a total of 6P powers. For this reason, at the intersection point of input ports of dividers in Step 2, impedances of them should be equal. Therefore, striplines that transform 50Ω to 100Ω are used to connect the two Section#2 dividers. As a result, input impedance becomes 50Ω. Also note that total length of the lines from the antenna ports to the input are equal to 19.9mm + $2.45\lambda_0$ since no phase difference is desired. Consequently, $|S_{Antenna\#1}|_{dB}$ and $|S_{Antenna\#6}|_{dB}$ should be $10log_{10}(P/12P)$= -10.79dB, $|S_{Antenna\#2}|_{dB}$ and $|S_{Antenna\#5}|_{dB}$ should be $10log_{10}(2P/12P)$= -7.78dB and $|S_{Antenna\#3}|_{dB}$ and $|S_{Antenna\#4}|_{dB}$ should be $10log_{10}(3P/12P)$= -6.02dB as results of the power divider at this step.

The simulation results of this section of the divider are given in Fig. 3.21 and Fig. 3.22:

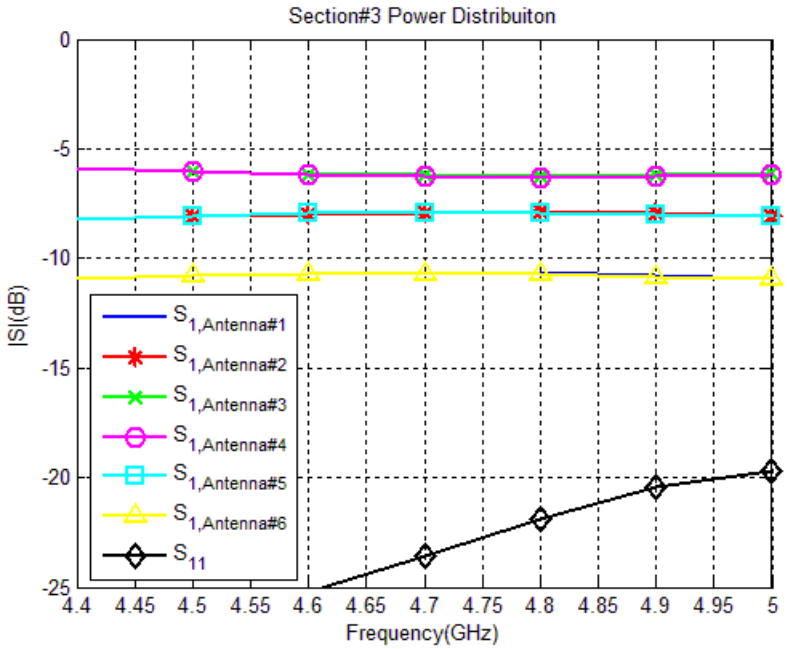

Figure 3.21: Power distribution for the feed network Section#3 through the desired frequency band

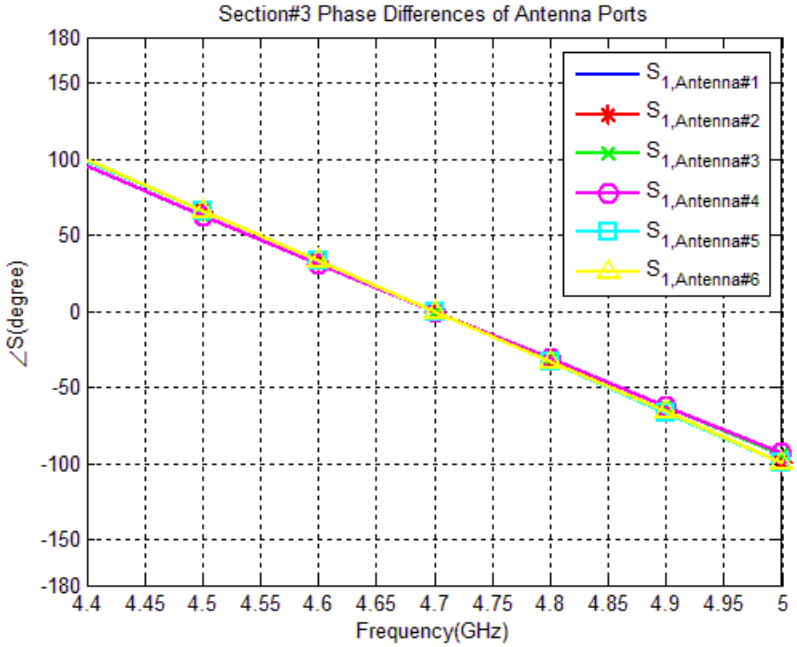

Figure 3.22: Phase differences for the feed network Section#3 through the desired frequency band

From the numerical results presented in Fig. 3.21 and Fig. 3.22, it can be seen that $|S_{Antenna\#1}|_{dB}$=$|S_{Antenna\#6}|_{dB}$=-10.72dB, $|S_{Antenna\#2}|_{dB}$=$|S_{Antenna\#5}|_{dB}$=-7.93dB and $|S_{Antenna\#3}|_{dB}$=$|S_{Antenna\#4}|_{dB}$=-6.22dB, S_{11} is lower than -19dB, and there is almost no phase difference between antenna ports as desired.

3.1.4 Step 4: Entire Feed Network

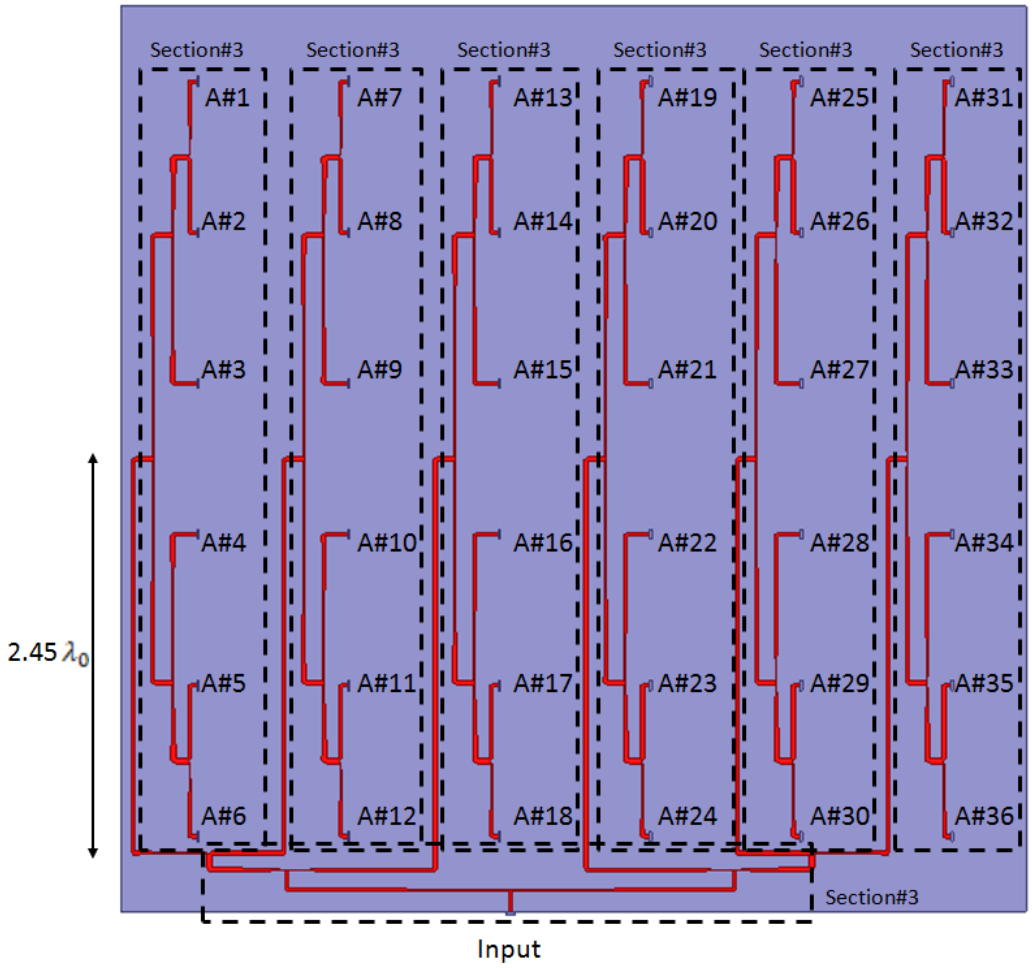

Figure 3.23: The final configuration of the entire feed network

A#i stands for the i^{th} Antenna Port in the figure. The entire feed network configuration is given in Fig. 3.23. One Section#3 divider is placed horizontally and 6 Section#3 dividers are connected to the output ports of this horizontal divider as shown in Fig. 3.23. In this way, the power distribution as the matrix product of P*[1 2 3 3 2 1]^T and [1 2 3 3 2 1] is realized. Note that there should be no phase difference between antenna ports as we want the main beam of the antenna array to be at the boresight all the time.

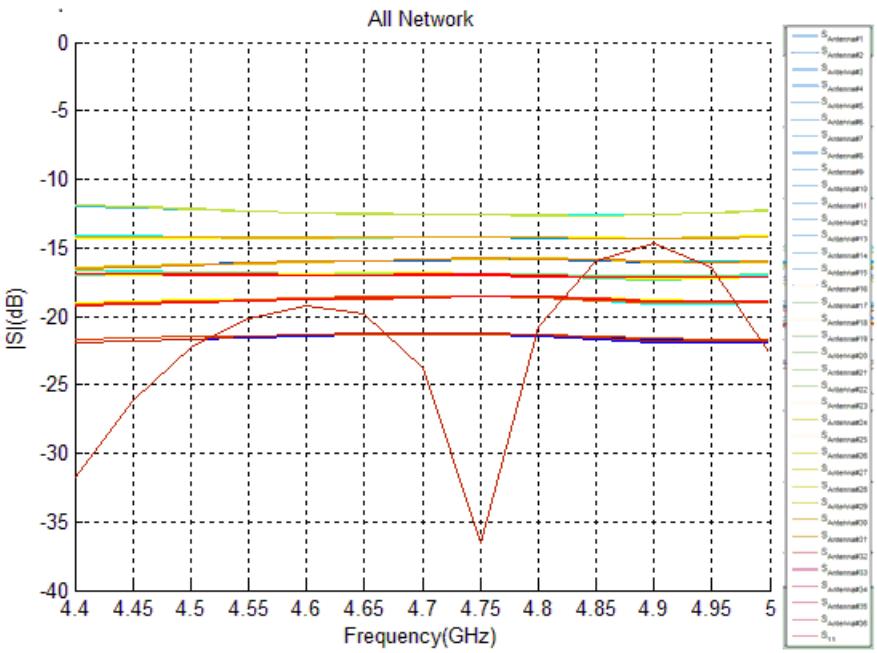

Figure 3.24: Amplitude distribution of the entire feed network through the desired frequency band

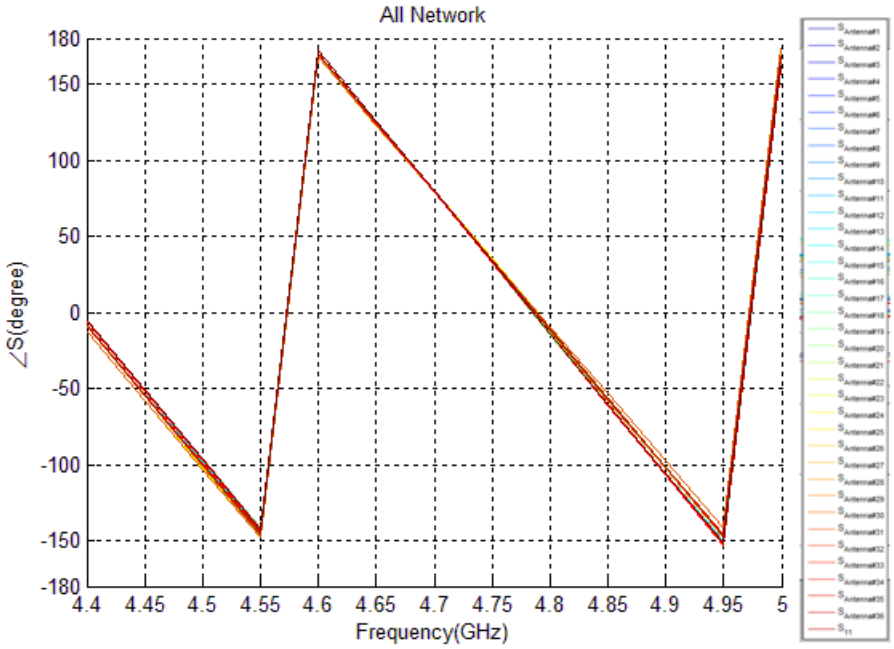

Figure 3.25: Phase distribution of the entire feed network through the desired frequency band

Table 3.2 tabulates (and compares) the desired and the numerically obtained (via HFSS) amplitude distribution (in an element by element fashion) at 4.7GHz, whereas Table 3.3 tabulates the same for the phase. Power calculation is performed using the equation $P_{dB} = 10log_{10}(P_{antenna}/P_{total})$. Percentage error rate for the power is defined as $error\% = |P_{obtained} - P_{desired}|/P_{desired} * 100$. Note that for simulations, output ports of the feed network are ended with exact 50Ω.

Antenna Index	Desired Power	Obtained Power @ 4.7GHz	Error in Power%
Antenna#1	-21.58dB	-21.36dB	5.20%
Antenna#2	-18.57dB	-18.63dB	1.37%
Antenna#3	-16.81dB	-16.97dB	3.62%
Antenna#4	-16.81dB	-16.94dB	2.95%
Antenna#5	-18.57dB	-18.58dB	0.23%
Antenna#6	-21.58dB	-21.29dB	6.91%
Antenna#7	-18.57dB	-18.58dB	0.23%
Antenna#8	-15.56dB	-15.92dB	7.96%
Antenna#9	-13.80dB	-14.21dB	9.01%
Antenna#10	-13.80dB	-14.21dB	9.01%
Antenna#11	-15.56dB	-15.84dB	6.24%
Antenna#12	-18.57dB	-18.53dB	0.93%
Antenna#13	-16.81dB	-16.91dB	2.28%
Antenna#14	-13.80dB	-14.25dB	9.84%
Antenna#15	-12.04dB	-12.53dB	10.67%
Antenna#16	-12.04dB	-12.56dB	11.28%
Antenna#17	-13.80dB	-14.19dB	8.59%
Antenna#18	-16.81dB	-16.86dB	1.14%
Antenna#19	-16.81dB	-16.96dB	3.39%
Antenna#20	-13.80dB	-14.26dB	10.05%
Antenna#21	-12.04dB	-12.55dB	11.08%
Antenna#22	-12.04dB	-12.52dB	10.46%
Antenna#23	-13.80dB	-14.22dB	9.22%
Antenna#24	-16.81dB	-16.83dB	0.46%
Antenna#25	-18.57dB	-18.61dB	0.92%
Antenna#26	-15.56dB	-15.89dB	7.32%
Antenna#27	-13.80dB	-14.22dB	9.22%
Antenna#28	-13.80dB	-14.19dB	8.59%
Antenna#29	-15.56dB	-15.85dB	6.46%
Antenna#30	-18.57dB	-18.50dB	1.62%
Antenna#31	-21.58dB	-21.36dB	5.20%
Antenna#32	-18.57dB	-18.64dB	1.60%
Antenna#33	-16.81dB	-16.99dB	4.06%
Antenna#34	-16.81dB	-16.94dB	2.95%
Antenna#35	-18.57dB	-18.62dB	1.14%
Antenna#36	-21.58dB	-21.21dB	8.89%

Table 3.2: Desired and numerically obtained (via HFSS) power distributions for the feed network

Antenna Index0	**Desired Phase**	**Obtained Phase @ 4.7GHz**
Antenna#1	0°	0°
Antenna#2	0°	0.35°
Antenna#3	0°	0.87°
Antenna#4	0°	0.70°
Antenna#5	0°	0.99°
Antenna#6	0°	0.61°
Antenna#7	0°	-0.03°
Antenna#8	0°	0°
Antenna#9	0°	0.35°
Antenna#10	0°	0.87°
Antenna#11	0°	0.70°
Antenna#12	0°	0.99°
Antenna#13	0°	0.61°
Antenna#14	0°	-0.03°
Antenna#15	0°	0.35°
Antenna#16	0°	0.80°
Antenna#17	0°	0.62°
Antenna#18	0°	1.04°
Antenna#19	0°	0.46°
Antenna#20	0°	-0.29°
Antenna#21	0°	0.51°
Antenna#22	0°	0.92°
Antenna#23	0°	0.97°
Antenna#24	0°	1.02°
Antenna#25	0°	0.58°
Antenna#26	0°	-0.21°
Antenna#27	0°	0.39°
Antenna#28	0°	0.83°
Antenna#29	0°	0.87°
Antenna#30	0°	1.09°
Antenna#31	0°	0.64°
Antenna#32	0°	-0.18°
Antenna#33	0°	0.43°
Antenna#34	0°	1.07°
Antenna#35	0°	0.85°
Antenna#36	0°	1.02°

Table 3.3: Desired and numerically obtained (via HFSS) phase distributions for the feed network

As seen from the tables, the obtained power distribution is quite close to the ideal results. Furthermore, all antenna ports have almost the same phase. To further verify that numerically obtained distributions yield patterns similar to the desired ones, array factors are generated via MATLAB®using the amplitudes and phases obtained from HFSS simulations. The resultant array factors are presented from 4.4GHz to 5GHz with an increment of 0.1GHz in Fig. 3.26 - Fig. 3.29. Note that because the upper and lower feed networks are the same, we have similar patterns for both upper and lower feed networks. Therefore, numerically obtained array factors are going to be the same for both feed networks.

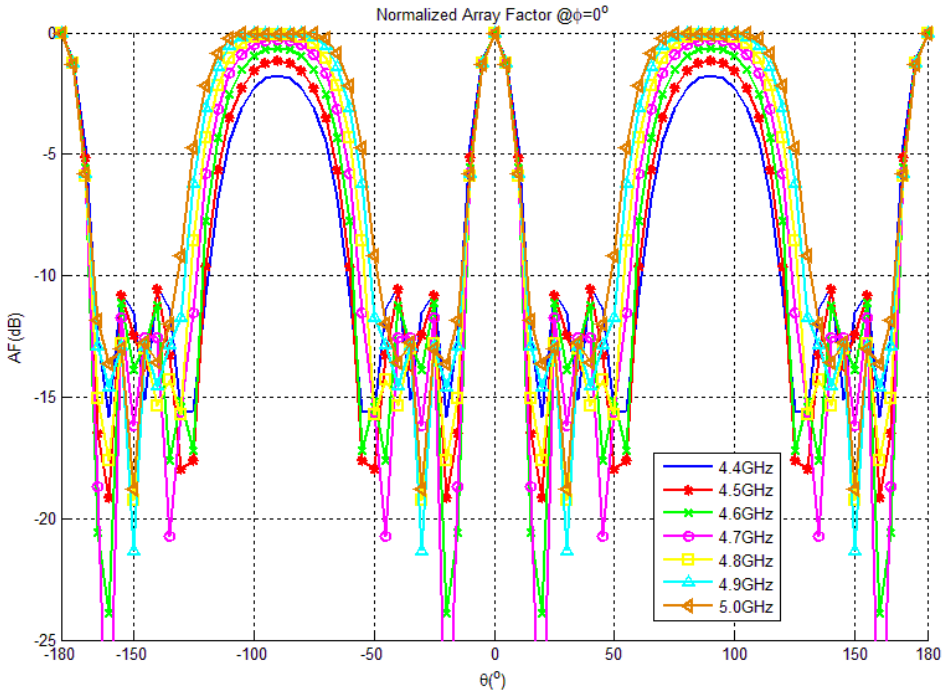

Figure 3.26: Numerically obtained array factors at ϕ =0° for various frequencies

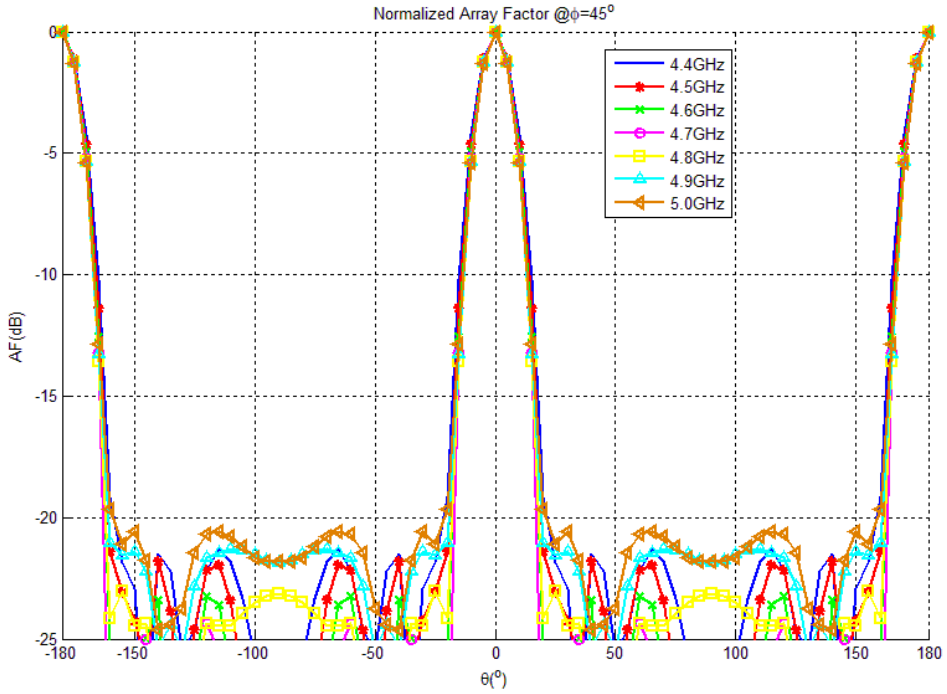

Figure 3.27: Numerically obtained array factors at ϕ =45° for various frequencies

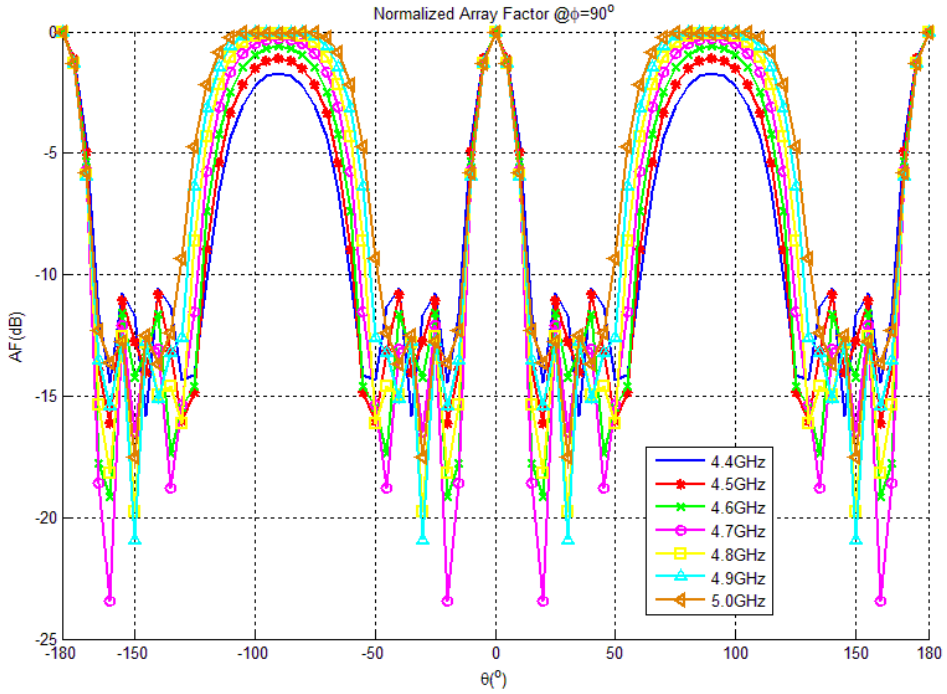

Figure 3.28: Numerically obtained array factors at ϕ =90° for various frequencies

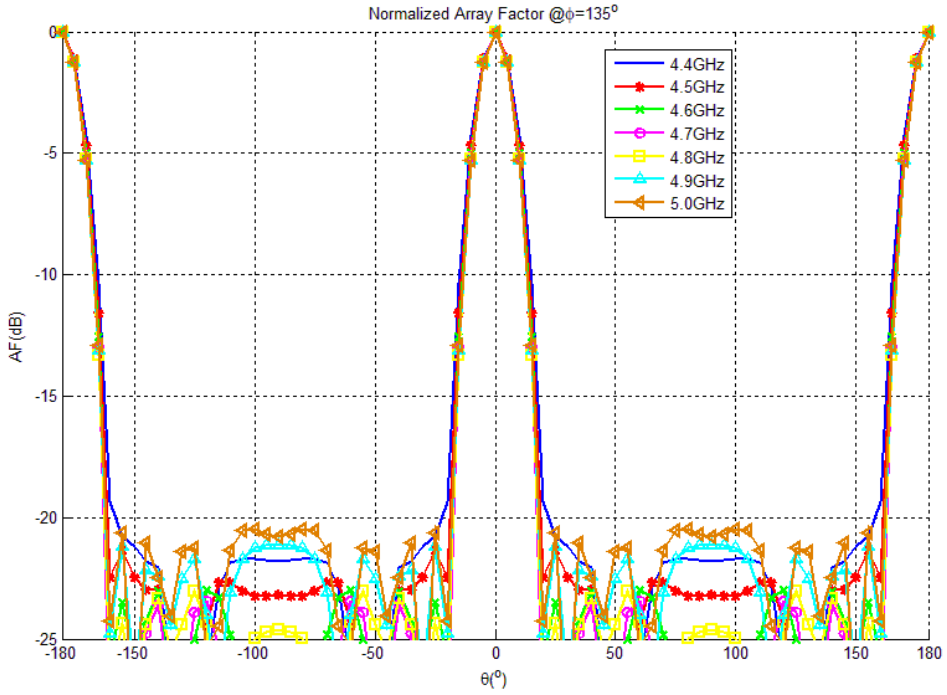

Figure 3.29: Numerically obtained array factors at ϕ =135° for various frequencies

In these figures (Fig. 3.26 - Fig. 3.29), it can be seen that grating lobes appear in the cardinal planes (for ϕ =0° and ϕ =90°). However, these lobes are not in 10dB beamwidth of the single element and they are suppressed by the element pattern in the array. In the intercardinal planes (for ϕ =45° and ϕ =135°), there is no grating lobe as it is expected, because in these planes slope of the amplitude is higher compared to the cardinal planes. In Chapter 2, the antenna element patterns are obtained for both upper and lower feed networks. If the array factors are multiplied with antenna element patterns for the upper and lower feed networks separetaly, expected array patterns can be obtained. Note that, these patterns do not include the effect of the coupling between antenna elements and they are modeled as perfectly isolated. In Fig. 3.30 to Fig. 3.37, these array patterns for upper and lower feed networks in the cardinal and intercardinal planes are presented.

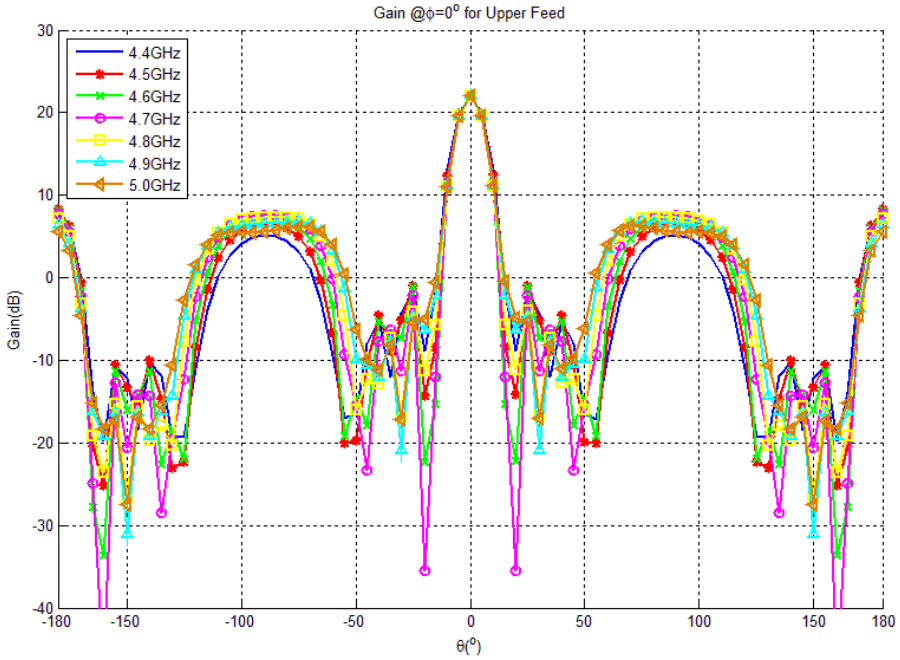

Figure 3.30: Expected antenna array pattern at ϕ =0° for the upper feed network for various frequencies

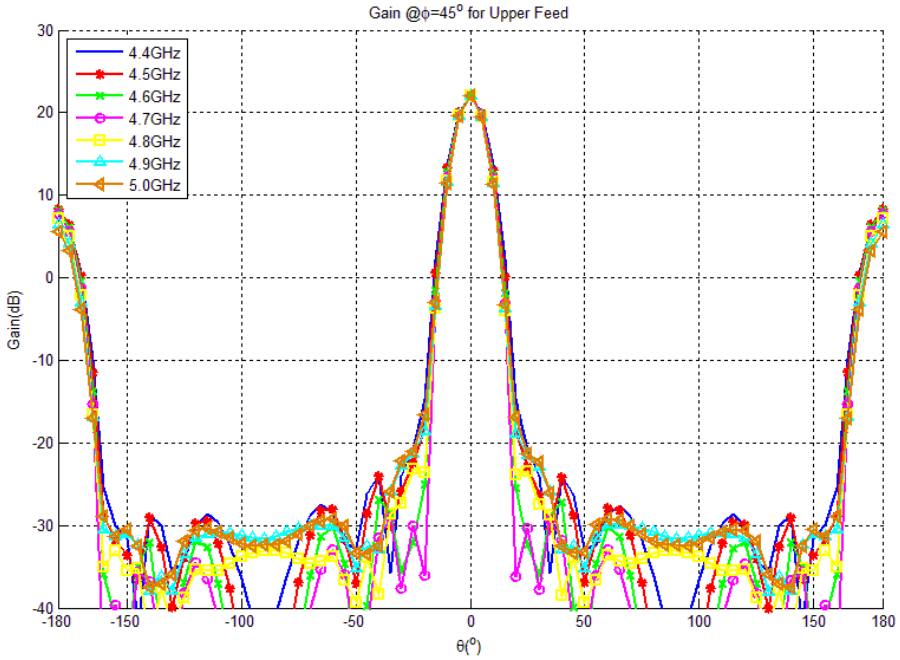

Figure 3.31: Expected antenna array pattern at ϕ =45° for the upper feed network for various frequencies

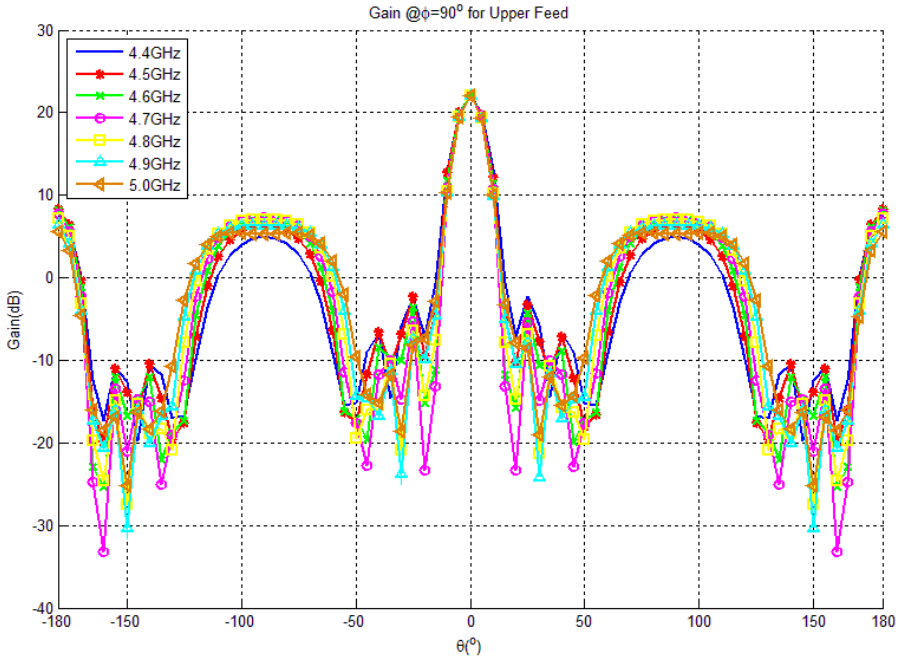

Figure 3.32: Expected antenna array pattern at ϕ =90° for the upper feed network for various frequencies

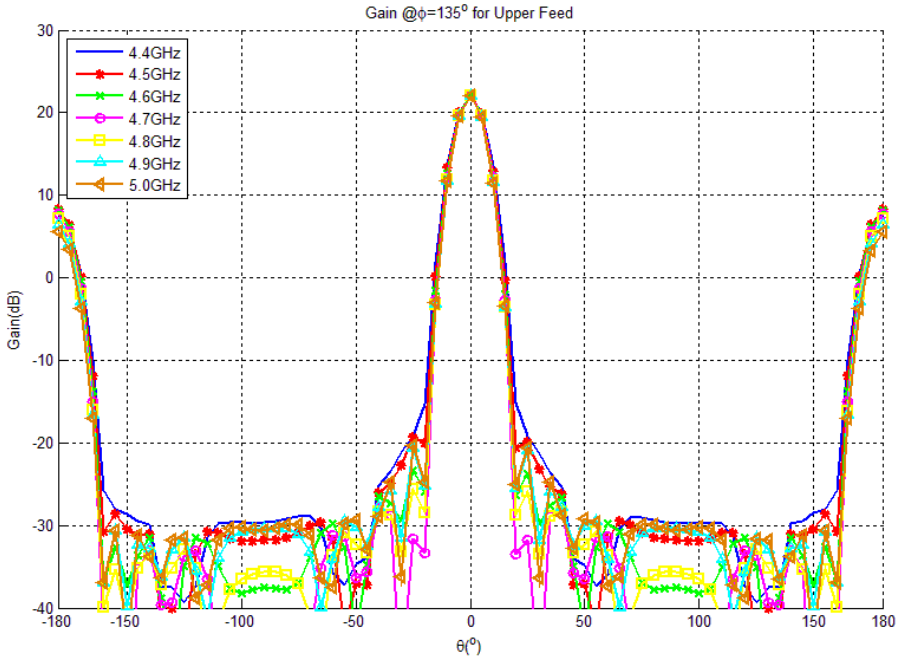

Figure 3.33: Expected antenna array pattern at ϕ =135° for the upper feed network for various frequencies

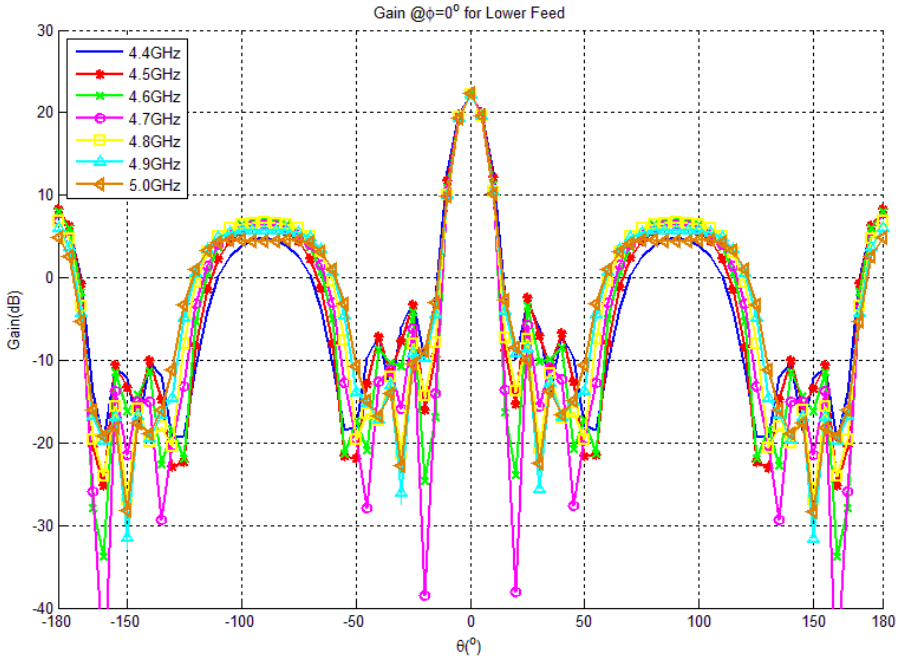

Figure 3.34: Expected antenna array pattern at ϕ =0° for the lower feed network for various frequencies

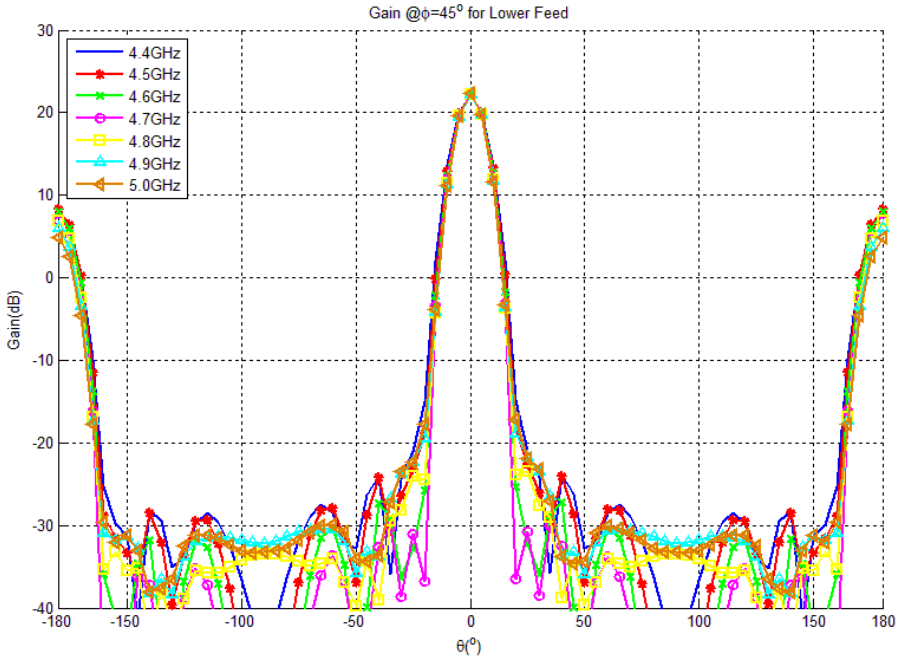

Figure 3.35: Expected antenna array pattern at ϕ =45° for the lower feed network for various frequencies

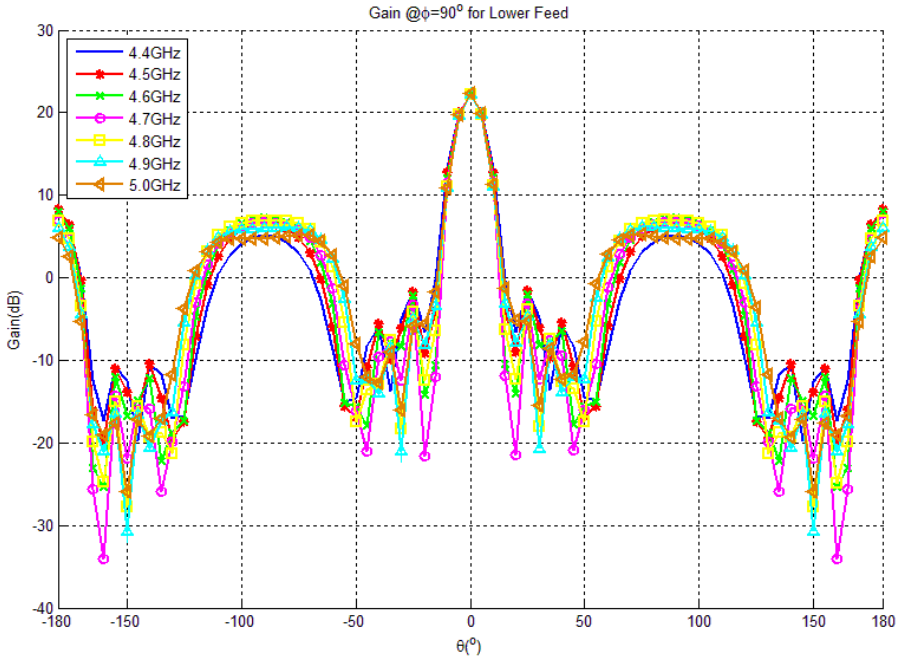

Figure 3.36: Expected antenna array pattern at ϕ =90° for the lower feed network for various frequencies

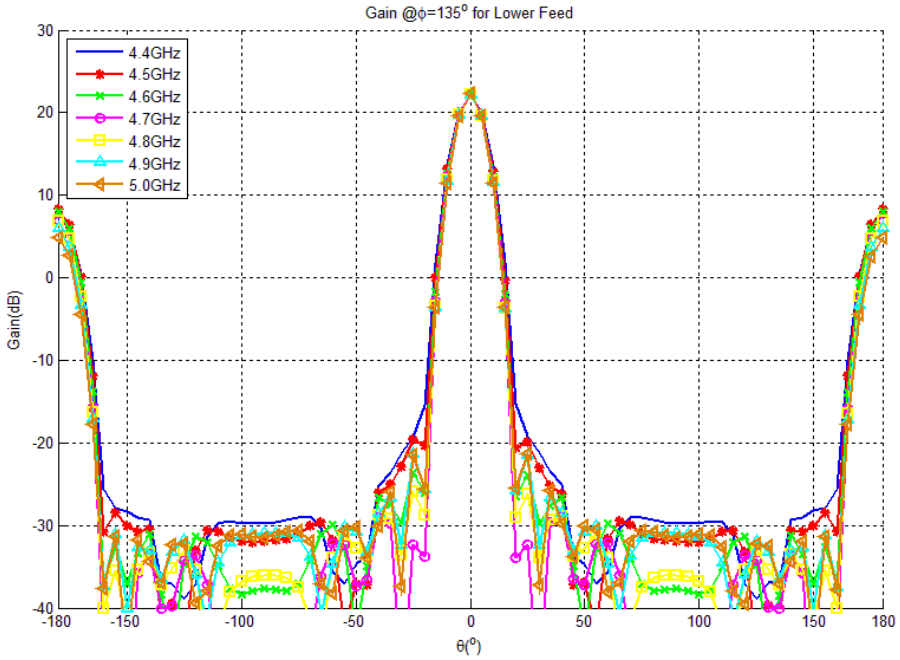

Figure 3.37: Expected antenna array pattern at ϕ =135° for the lower feed network for various frequencies

In all these figures (i.e., Fig. 3.30 to Fig. 3.37), it can be seen that the gain is higher than 20dB in both cardinal (ϕ =0° and ϕ =90°) and intercardinal (for ϕ =45° and ϕ =135°) planes for upper and lower feed networks as desired. In addition, SLL is better that -15dB in cardinal planes and it is better than -25dB in intercardinal planes. With these parameters, it can be said that the obtained amplitude and phase distribution (via HFSS) is proper to generate the desired patterns. In the next chapter, antenna elements are placed in the array environment and connected to the feed networks to constitute the entire antenna array geometry.

Chapter 4

Antenna Array Design

In previous chapters, the single element and the feed network with the required amplitude and phase distributions to synthesize the desired patterns are designed. In this chapter, 36 single elements are placed as the 6x6 array and two feed networks for different polarizations are connected to the ports of these single elements. The final array configuration is given in Fig. 4.1.

The simulations in this chapter are performed via HFSS® high performance computer (HPC) having 3TB RAM and 512 cores. In the simulation model, all metallic surfaces (patches, ground planes etc.) are modelled as copper. The antenna is fed by waveports having 50Ω impedance. A vacuum box in the shape of rectangular parallelpiped is defined around the antenna. The minimum distance from the antenna to the vacuum box is $\lambda/4$ for the minimum frequency in the solution band. The solution frequency is chosen as the maximum frequency in the solution band. For the adaptive solution, maximum number of passes is determined as 15 and maximum of Delta S is determined as 0.02. With this solution setup, 128GB RAM and 32 cores are required. Each simulation takes 38 hours, 12 hours for adaptive passes and 2 hours per each frequency solution.

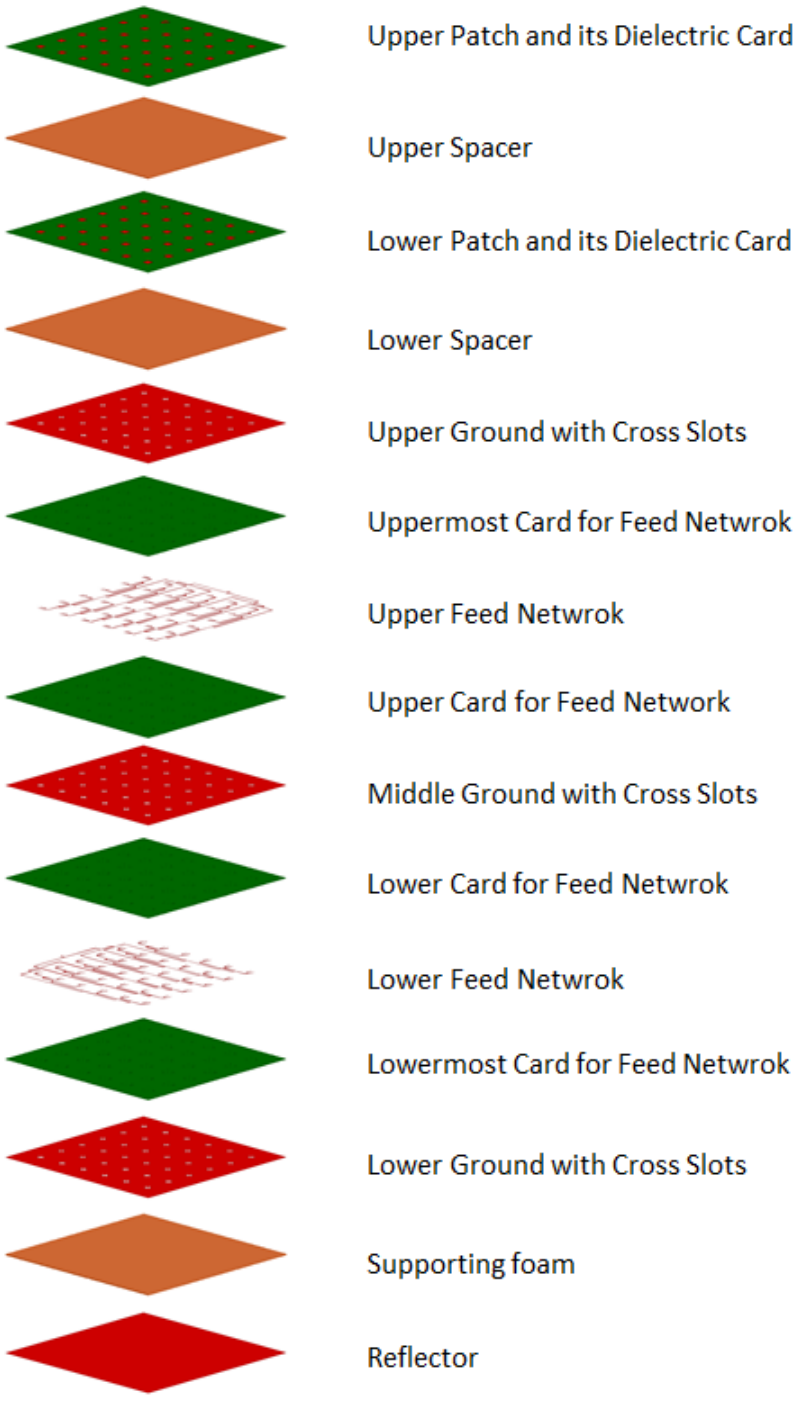

Figure 4.1: Exploded view of the proposed antenna array configuration

When this configuration is simulated fully, the results given in Fig. 4.2 to 4.10 are obtained.

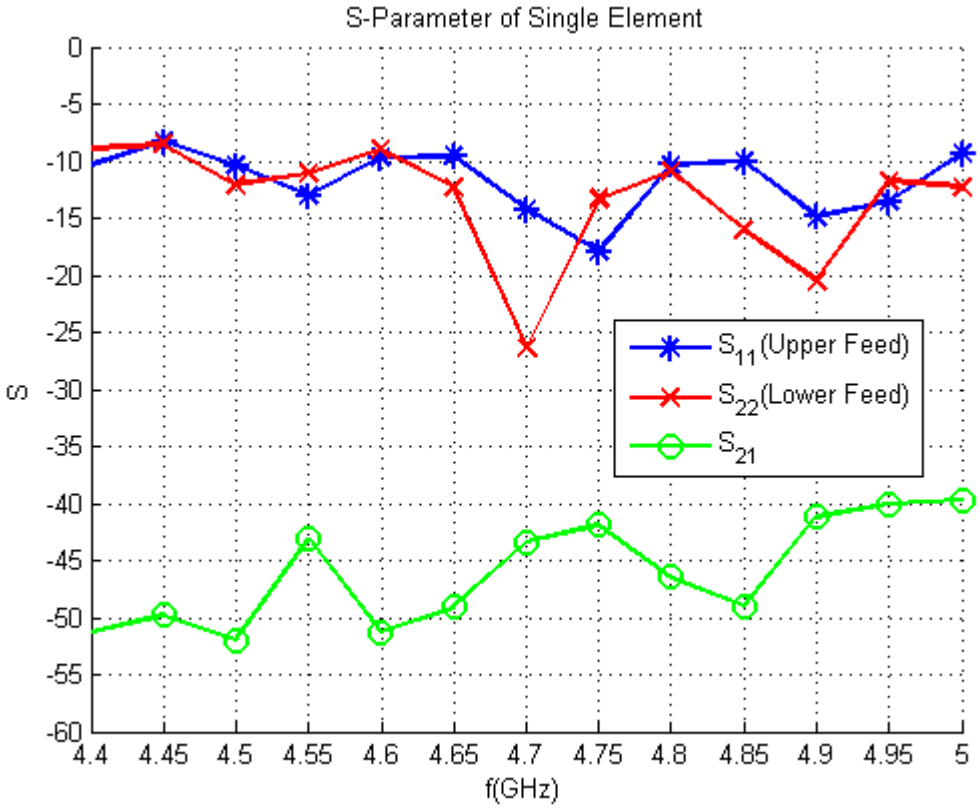

Figure 4.2: S-parameters of the entire antenna array versus frequency over the desired band

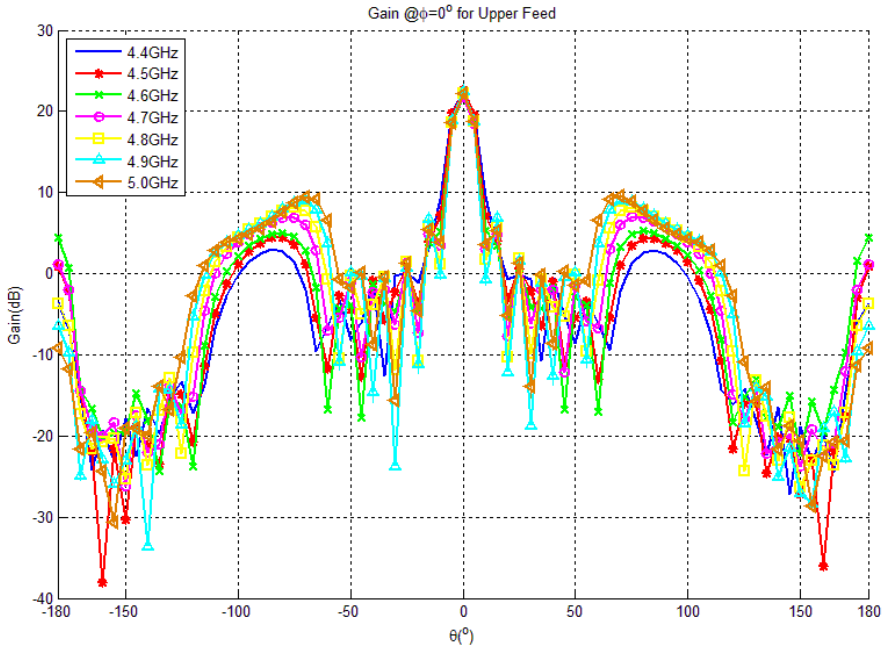

Figure 4.3: The entire array gain pattern at ϕ =0° for upper feed network for various frequencies

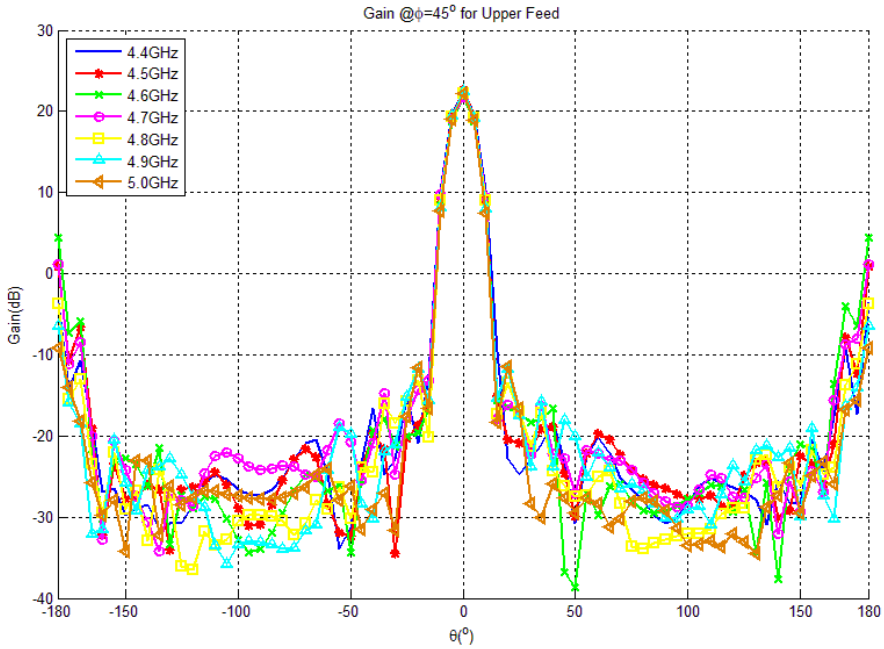

Figure 4.4: The entire array gain pattern at ϕ =45° for upper feed network for various frequencies

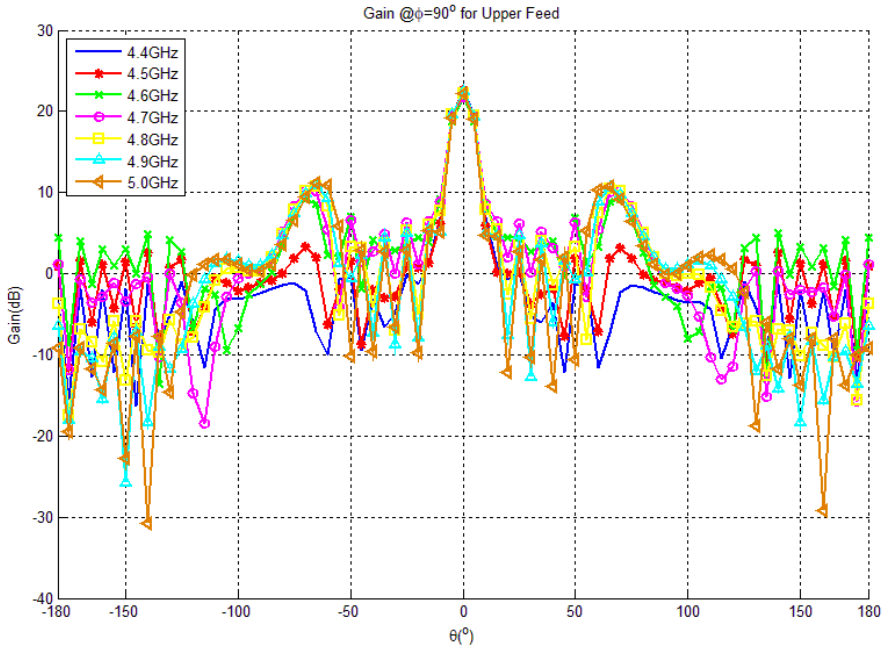

Figure 4.5: The entire array gain pattern at ϕ =90° for upper feed network for various frequencies

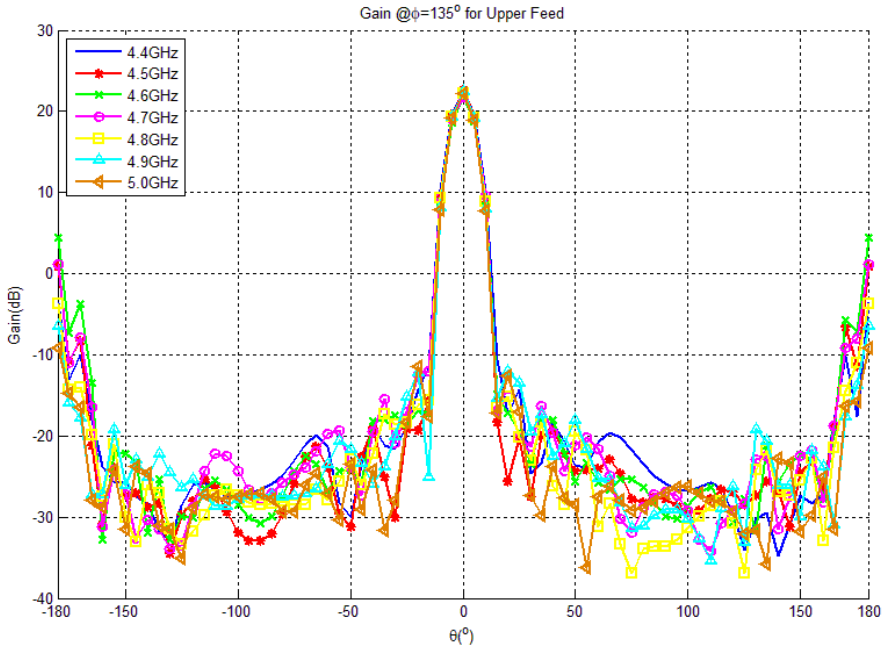

Figure 4.6: The entire array gain pattern at ϕ =135° for upper feed network for various frequencies

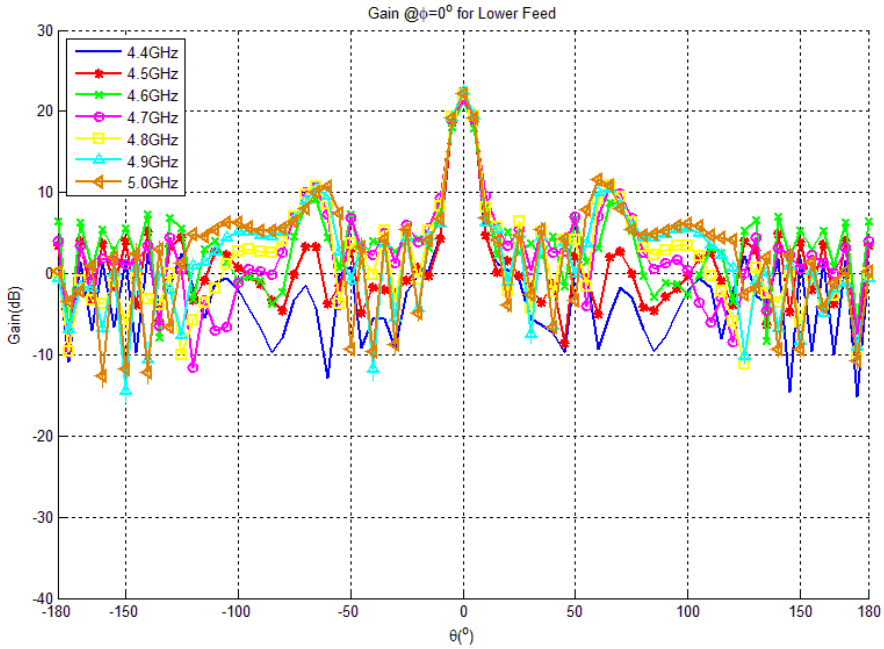

Figure 4.7: The entire array gain pattern at ϕ =0° for lower feed network for various frequencies

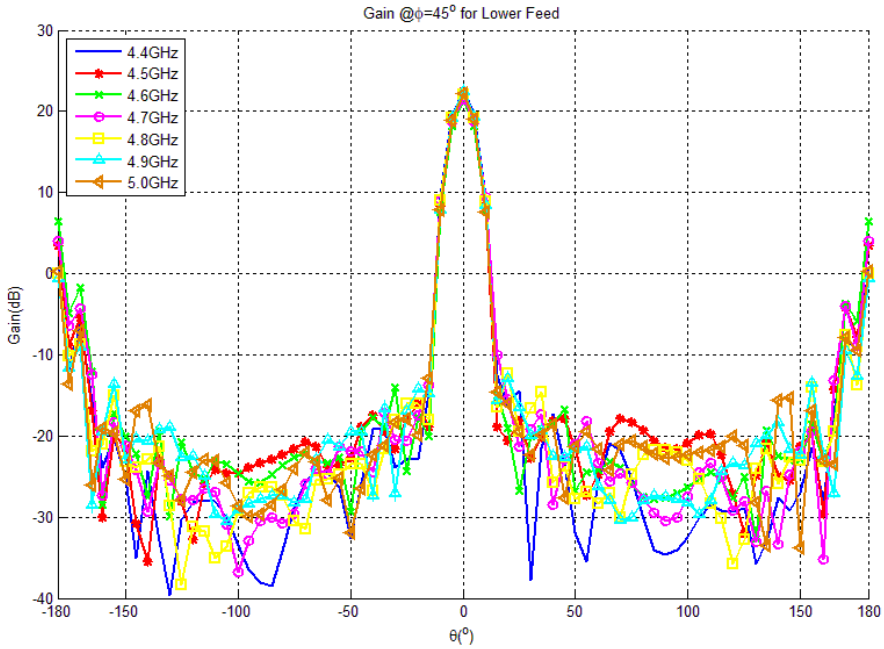

Figure 4.8: The entire array gain pattern at ϕ =45° for lower feed network for various frequencies

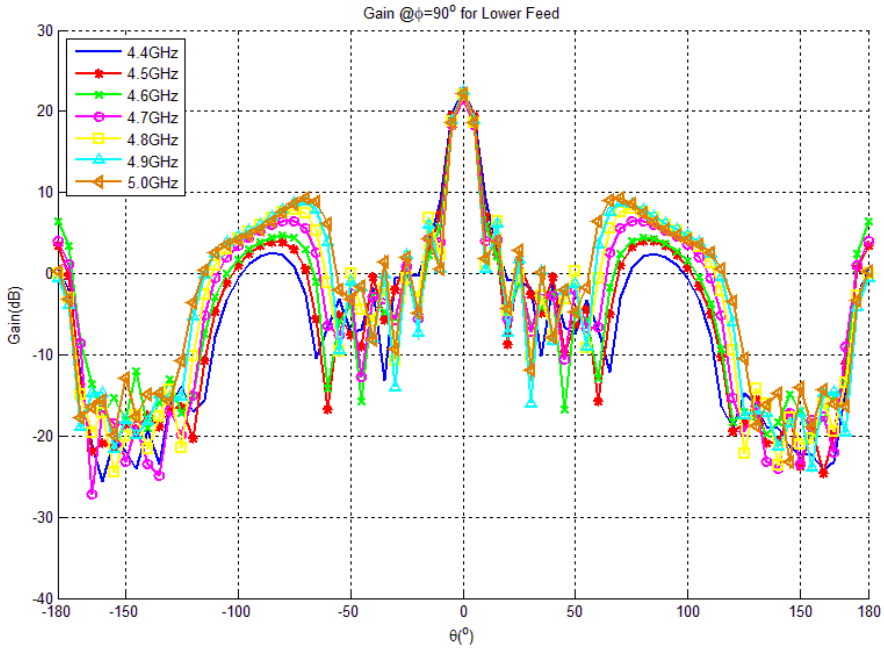

Figure 4.9: The entire array gain pattern at ϕ =90° for lower feed network for various frequencies

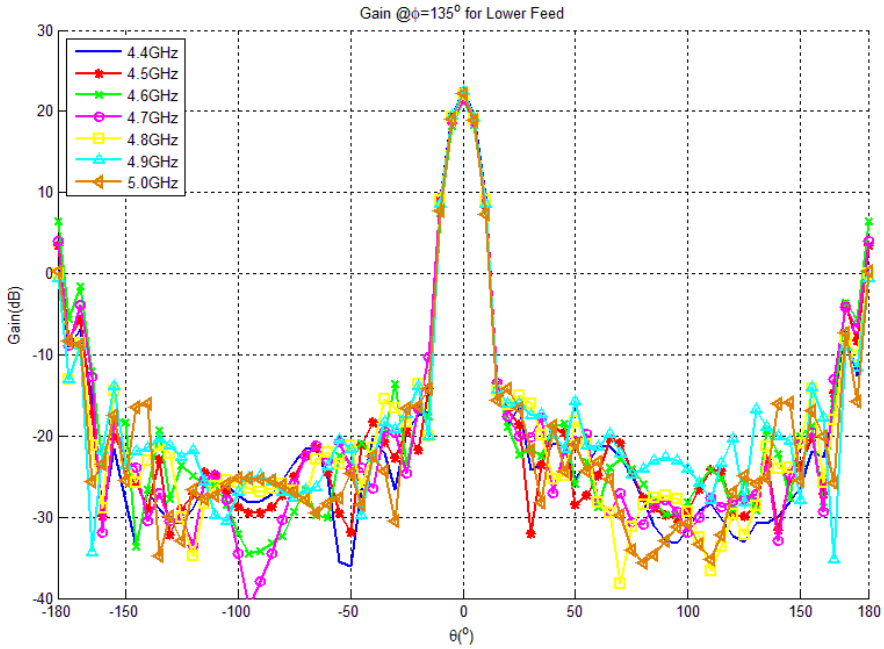

Figure 4.10: The entire array gain pattern at ϕ =135° for lower feed network for various frequencies

It can be seen from these figures that reflection coefficients for both upper and lower feed networks are higher than -10dB around 4.45GHz. Additionally, reflection coefficient becomes higher than -10dB at some frequencies in the operation band. On the other hand, the cross polarization isolation is better than 40dB and it is satisfactory for the purpose of this array. Another important point is the SLL, which is higher than -15dB for higher frequencies due to the effect of grating lobes. Moreover, 10° 3dB beamwidth is obtained. Front-to-back ratio is 10dB. This result occurs due to finite-length reflector plane. Note that patterns at ϕ =0° and ϕ =90° are different than each other although square patches are used. The reason is the direction of the feeds.

Since the reflection coefficients regarding single elements as well as the feed networks are better than -10dB, the reason why reflection coefficients regarding the entire antenna array are distorted is considered as the effect of the array environment. In order to verify this consideration, the 36 single elements are placed in the array environment without feed networks and they are fed with their own feeds separately with ideal amplitudes and phases. In this way, it is aimed to observe the behaviors of antenna elements in the array environment. The resultant S-parameters of each antenna element are given in Fig. 4.11 - Fig. 4.13. Moreover, the simulated gain patterns with ideal amplitude and phase distribution are given in Fig. 4.14 to Fig. 4.21. Besides, Table 4.1 and Table 4.2 present the minimum inter-element isolation of each antenna element for the upper and lower feed networks, respectively.

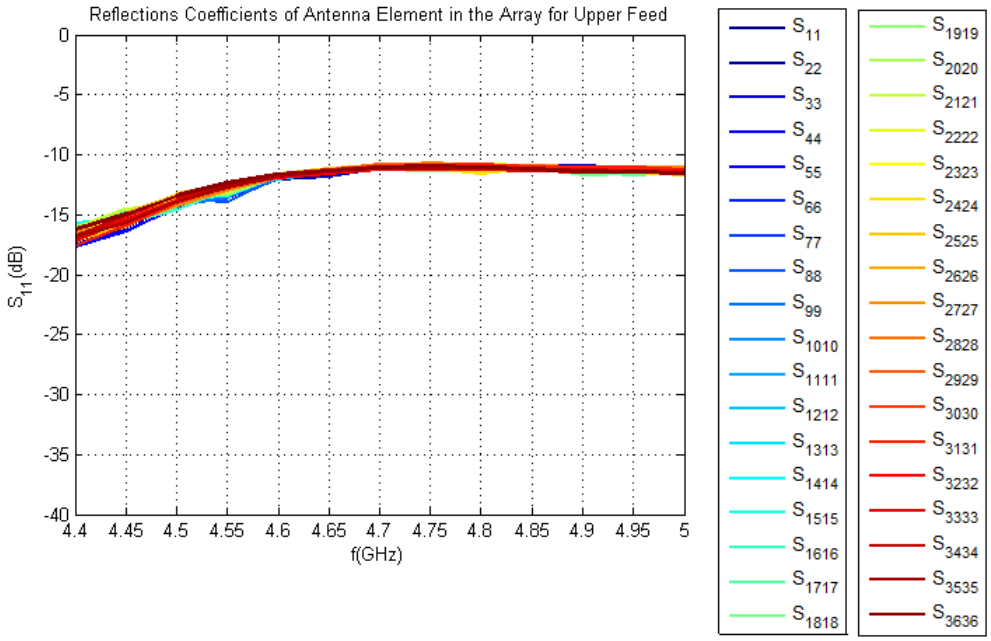

Figure 4.11: Reflection coefficients of each single element versus frequency in the antenna array for the upper feed network

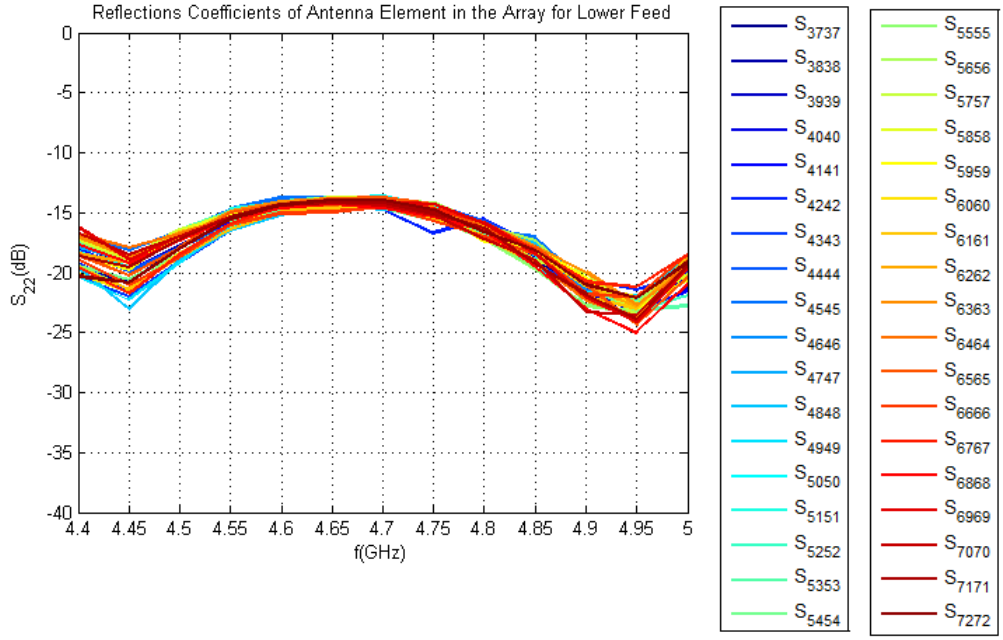

Figure 4.12: Reflection coefficients of each single element versus frequency in the antenna array for the lower feed network

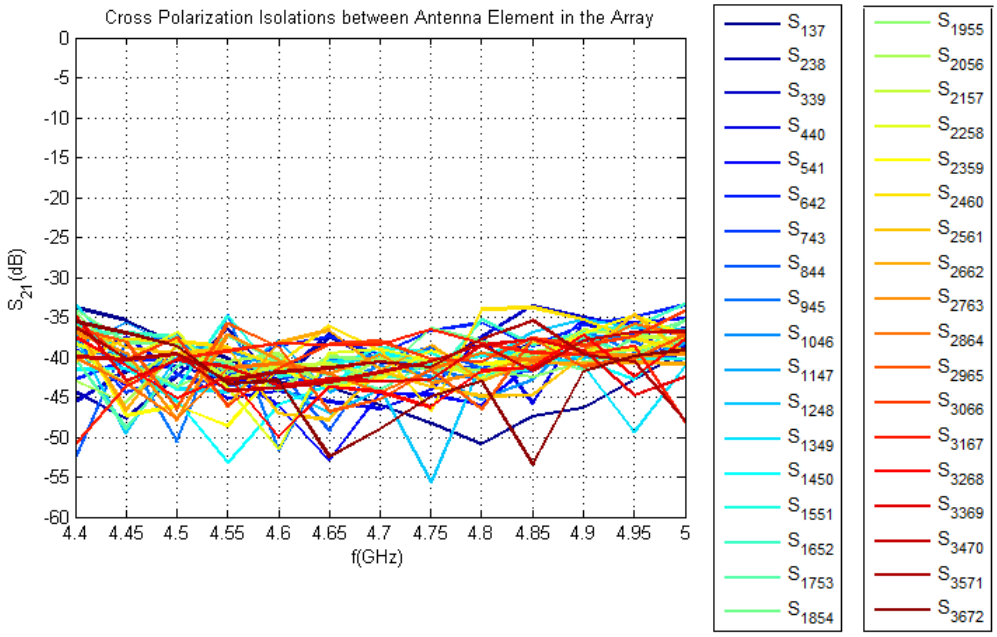

Figure 4.13: Cross polarization isolation of each single element versus frequency in the antenna array

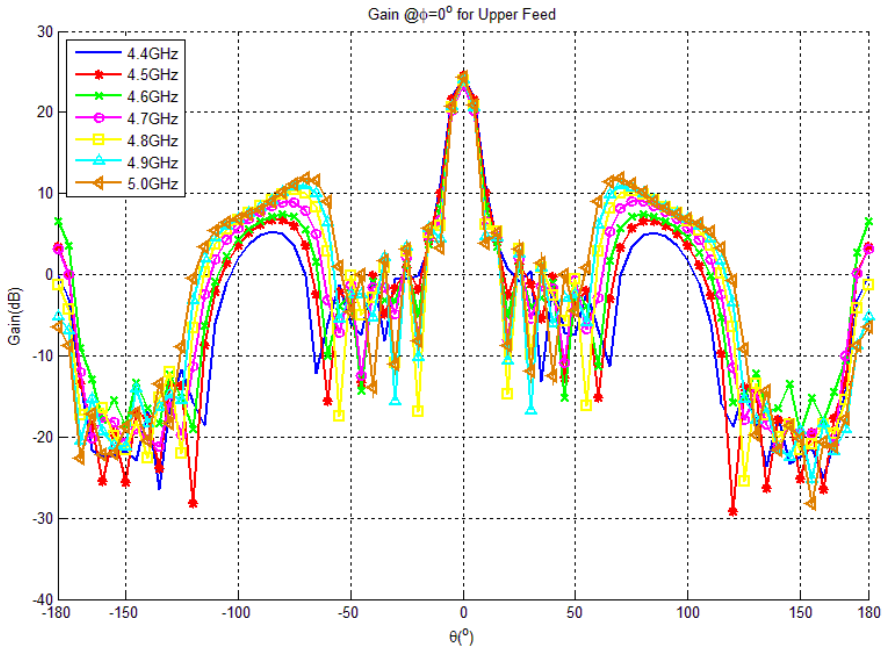

Figure 4.14: Array patterns without the feed network at ϕ =0° for the upper feed network for various frequencies

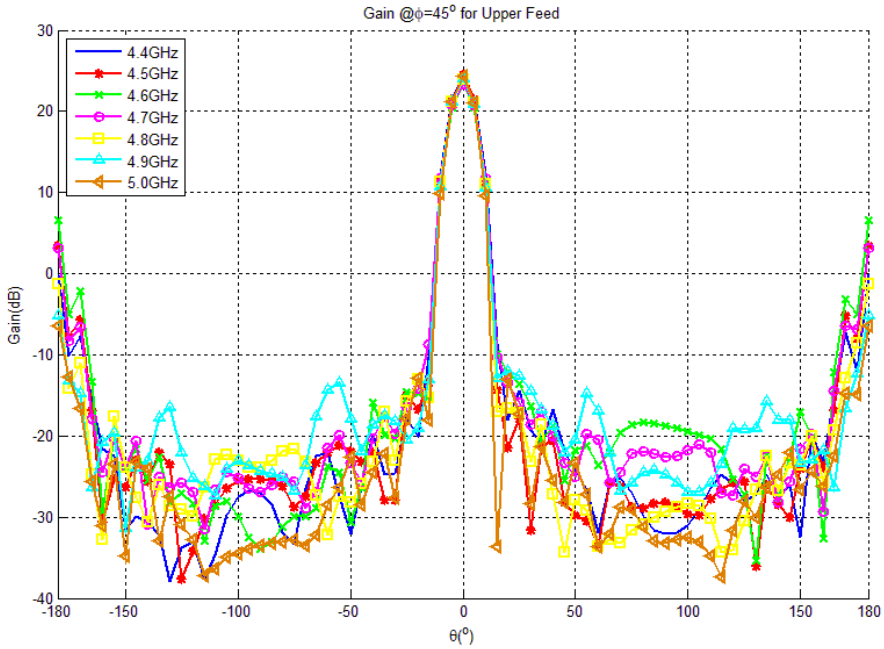

Figure 4.15: Array patterns without the feed network at ϕ =45° for the upper feed network for various frequencies

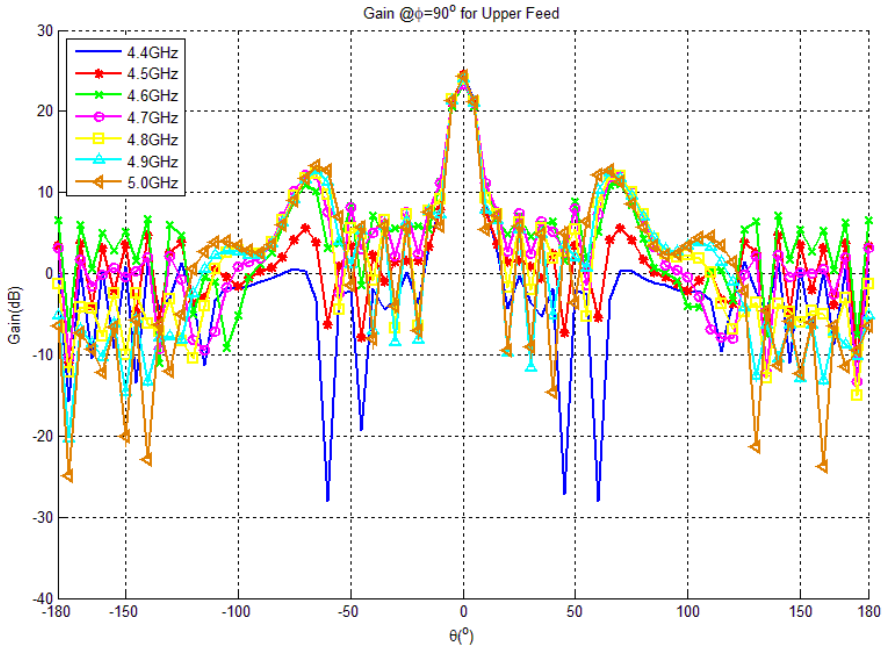

Figure 4.16: Array patterns without the feed network at ϕ =90° for the upper feed network for various frequencies

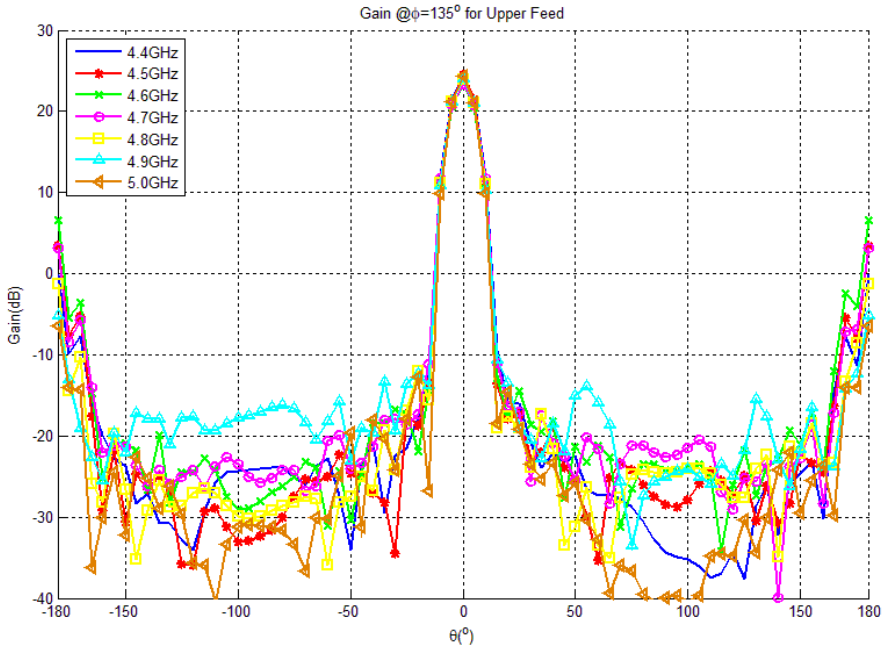

Figure 4.17: Array patterns without the feed network at ϕ =135° for the upper feed network for various frequencies

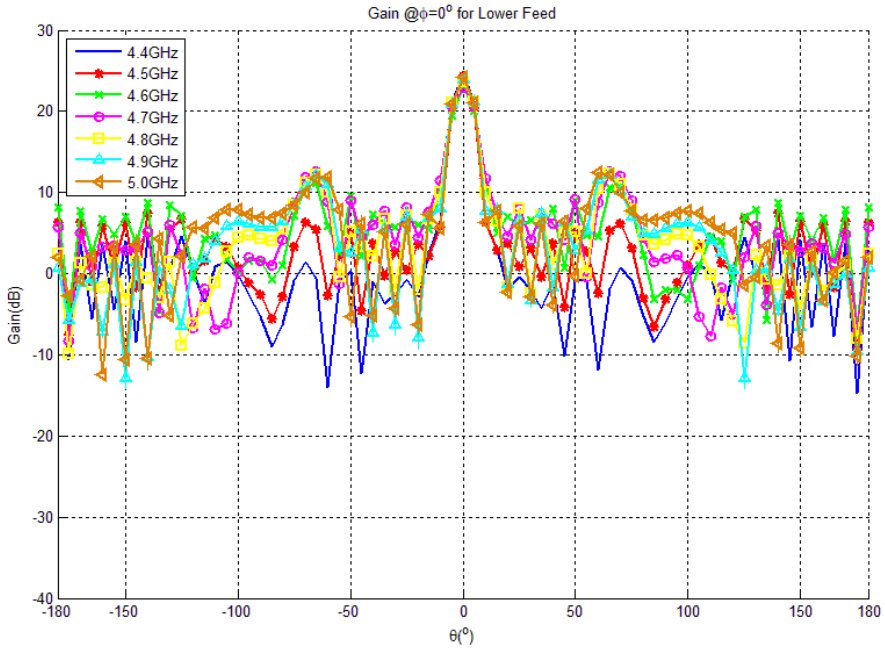

Figure 4.18: Array patterns without the feed network at ϕ =0° for the lower feed network for various frequencies

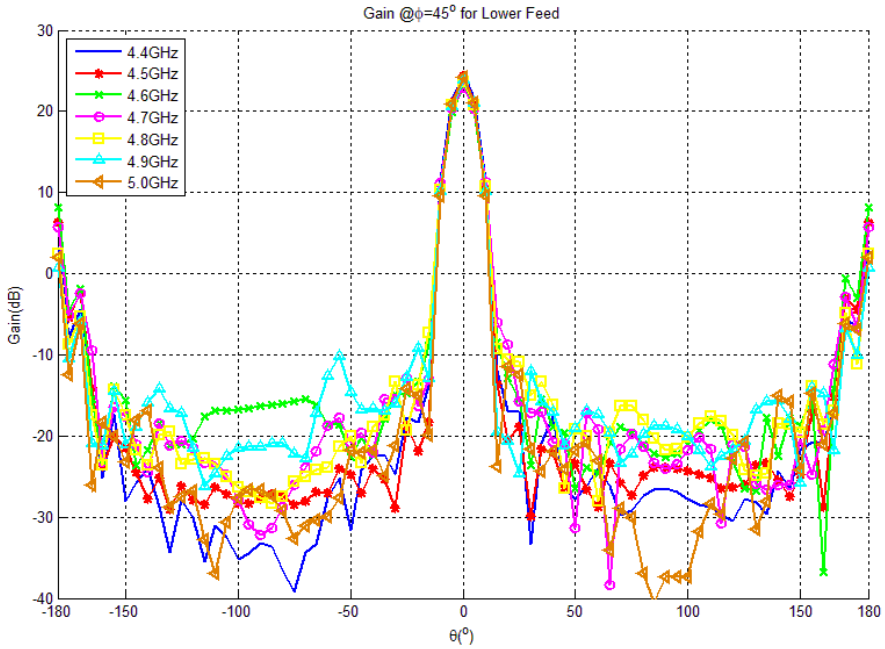

Figure 4.19: Array patterns without the feed network at ϕ =45° for the lower feed network for various frequencies

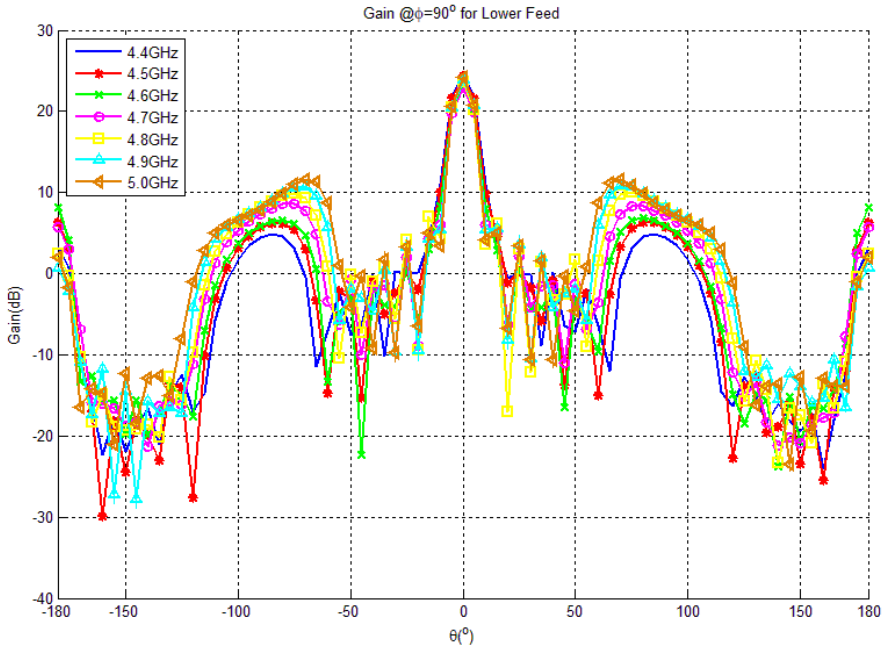

Figure 4.20: Array patterns without the feed network at ϕ =90° for the lower feed network for various frequencies

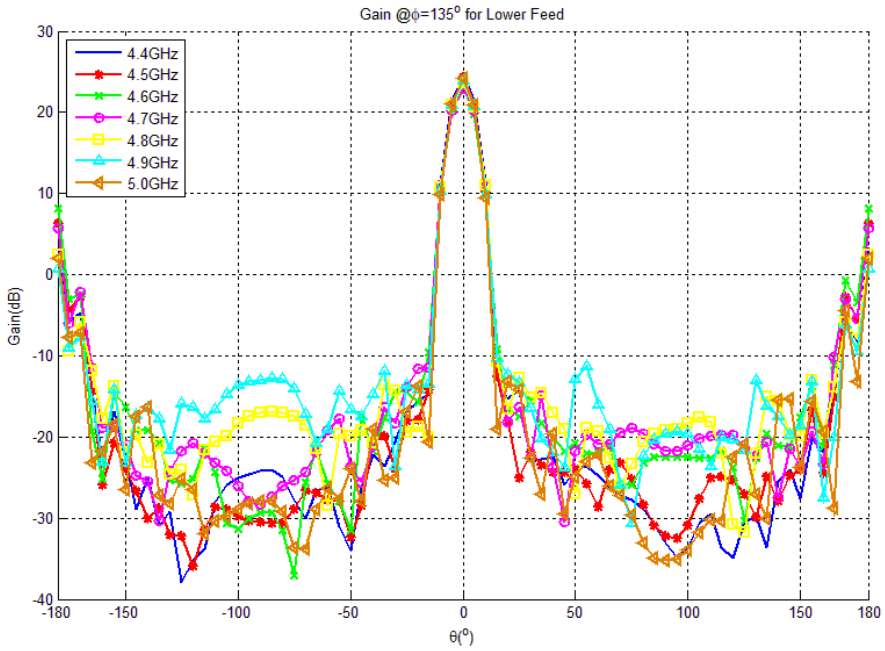

Figure 4.21: Array patterns without the feed network at ϕ =135° for the lower feed network for various frequencies

Antenna	$Coupling_{max}$ **@4.4GHz**	$Coupling_{max}$ **@4.7GHz**	$Coupling_{max}$ **@5GHz**
Antenna#1	-25.46dB	-25.90dB	-26.60dB
Antenna#2	-23.92dB	-25.91dB	-27.94dB
Antenna#3	-24.37dB	-28.63dB	-27.48dB
Antenna#4	-24.10dB	-26.04dB	-27.82dB
Antenna#5	-24.72dB	-26.27dB	-27.81dB
Antenna#6	-24.72dB	-27.36dB	-26.83dB
Antenna#7	-25.44dB	-25.90dB	-26.60dB
Antenna#8	-23.92dB	-25.91dB	-27.18dB
Antenna#9	-23.37dB	-25.88dB	-27.48dB
Antenna#10	-24.10dB	-25.78dB	-27.73dB
Antenna#11	-25.39dB	-26.27dB	-27.27dB
Antenna#12	-25.39dB	-25.81dB	-26.71dB
Antenna#13	-25.35dB	-25.65dB	-25.70dB
Antenna#14	-24.11dB	-26.12dB	-27.18dB
Antenna#15	-22.71dB	-25.88dB	-27.62dB
Antenna#16	-24.24dB	-25.78dB	-27.56dB
Antenna#17	-25.05dB	-26.63dB	-27.27dB
Antenna#18	-25.37dB	-25.81dB	-26.71dB
Antenna#19	-23.63dB	-25.59dB	-24.68dB
Antenna#20	-23.51dB	-26.02dB	-27.81dB
Antenna#21	-22.71dB	-25.79dB	-27.72dB
Antenna#22	-23.79dB	-26.10dB	-27.56dB
Antenna#23	-25.05dB	-26.08dB	-27.50dB
Antenna#24	-25.12dB	-26.64dB	-26.92dB
Antenna#25	-23.63dB	-25.47dB	-24.68dB
Antenna#26	-23.51dB	-26.02dB	-28.73dB
Antenna#27	-23.02dB	-25.79dB	-27.77dB
Antenna#28	-23.79dB	-26.10dB	-27.61dB
Antenna#29	-25.67dB	-26.05dB	-27.61dB
Antenna#30	-24.81dB	-25.56dB	-26.95dB
Antenna#31	-24.11dB	-25.47dB	-26.40dB
Antenna#32	-24.11dB	-26.72dB	-28.80dB
Antenna#33	-25.07dB	-26.49dB	-28.87dB
Antenna#34	-23.93dB	-26.05dB	-28.27dB
Antenna#35	-25.67dB	-25.56dB	-28.23dB
Antenna#36	-24.81dB	-21.21dB	-27.33dB

Table 4.1: Minimum inter-element isolation of antenna elements for the upper feed network

Antenna	$Coupling_{max}$ **@4.4GHz**	$Coupling_{max}$ **@4.7GHz**	$Coupling_{max}$ **@5GHz**
Antenna#1	-22.21dB	-23.60dB	-24.36dB
Antenna#2	-20.78dB	-23.60dB	-24.36dB
Antenna#3	-19.89dB	-23.23dB	-25.76dB
Antenna#4	-19.89dB	-23.08dB	-25.76dB
Antenna#5	-20.26dB	-23.08dB	-26.25dB
Antenna#6	-22.42dB	-24.85dB	-27.14dB
Antenna#7	-21.46dB	-23.88dB	-24.62dB
Antenna#8	-21.46dB	-23.15dB	-24.62dB
Antenna#9	-21.69dB	-23.10dB	-25.56dB
Antenna#10	-21.20dB	-23.10dB	-26.54dB
Antenna#11	-21.20dB	-22.23dB	-26.54dB
Antenna#12	-22.10dB	-22.23dB	-27.34dB
Antenna#13	-22.51dB	-24.67dB	-23.04dB
Antenna#14	-22.09dB	-23.00dB	-23.04dB
Antenna#15	-21.00dB	-23.00dB	-26.21dB
Antenna#16	-21.00dB	-23.74dB	-27.28dB
Antenna#17	-22.20dB	-23.84dB	-26.91dB
Antenna#18	-22.75dB	-23.93dB	-26.91dB
Antenna#19	-22.21dB	-24.41dB	-23.26dB
Antenna#20	-21.94dB	-23.20dB	-23.26dB
Antenna#21	-21.24dB	-23.20dB	-25.96dB
Antenna#22	-21.24dB	-23.50dB	-26.48dB
Antenna#23	-22.23dB	-23.50dB	-24.77dB
Antenna#24	-22.92dB	-23.93dB	-24.77dB
Antenna#25	-21.63dB	-23.77dB	-23.89dB
Antenna#26	-21.63dB	-23.64dB	-23.89dB
Antenna#27	-21.42dB	-23.35dB	-25.55dB
Antenna#28	-21.42dB	-23.35dB	-27.54dB
Antenna#29	-22.11dB	-23.01dB	-27.57dB
Antenna#30	-22.13dB	-23.01dB	-25.80dB
Antenna#31	-22.40dB	-22.46dB	-26.41dB
Antenna#32	-21.04dB	-22.46dB	-18.11dB
Antenna#33	-19.93dB	-22.78dB	-18.11dB
Antenna#34	-19.93dB	-22.78dB	-22.36dB
Antenna#35	-20.95dB	-23.29dB	-22.85dB
Antenna#36	-22.41dB	-23.29dB	-22.85dB

Table 4.2: Minimum inter-element isolation of antenna elements for the lower feed network

When the results are examined, it can be seen that reflection coefficients for both upper and lower feed networks are lower than -10dB. On the other hand, inter-element isolations have some values around -20dB for both feeds. Since the feed networks are not output matched, it can be the reason for higher reflection coefficients in the antenna array in the presence of the feed network. Also, the effect of grating lobes in SLL still remains. When the source of low inter-element isolation is investigated, it is observed that the source is the radiation between antenna elements. In order to prevent the effect of radiation among the antenna elements, a 6x6 grid structure with a 10mm wall height and 61.2mm cell size is introduced to the overall array as shown in Fig. 4.33. In this way, it is expected that the inter-element isolations among the antenna elements can be increased and the effect of grating lobes on SLL can be reduced. In this structure, each antenna element is fed by its own feeds with an ideal amplitude and phase, again. Fig. 4.11 to Fig. 4.21 as well as Table 4.1 and Table 4.2 are repeated for this situation (i.e., in the presence of the grid) and presented in Fig. 4.22 to Fig. 4.24 for the S-parameters, Fig. 4.25 to Fig. 4.32 for the gain patterns and Table 4.3 and Table 4.4 for the minimum inter-element isolation.

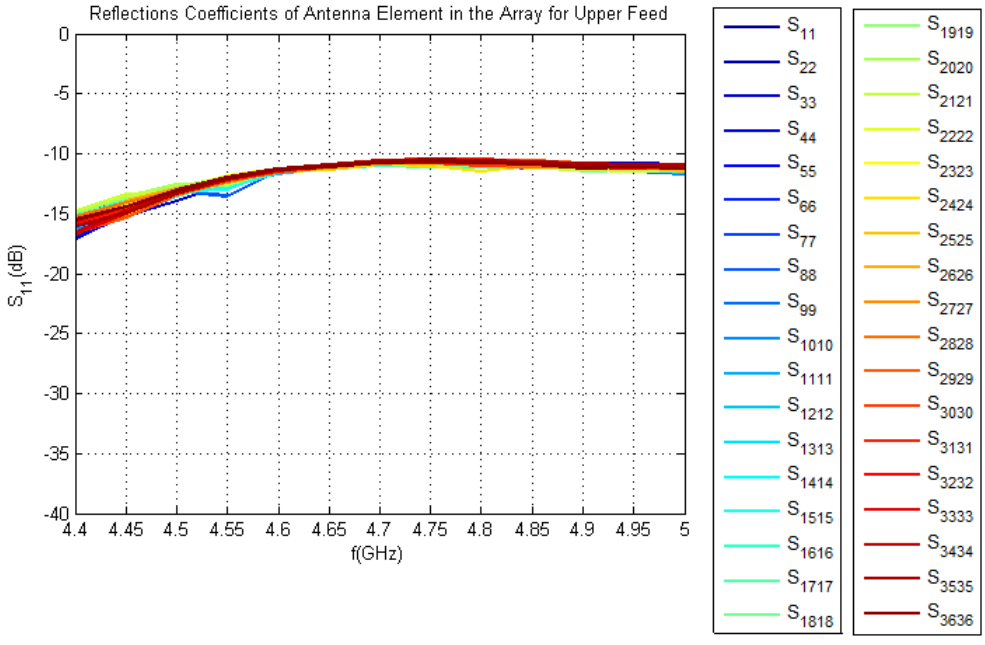

Figure 4.22: Reflection coefficients of each single element versus frequency in the antenna array for the upper feed network in the presence of the grid

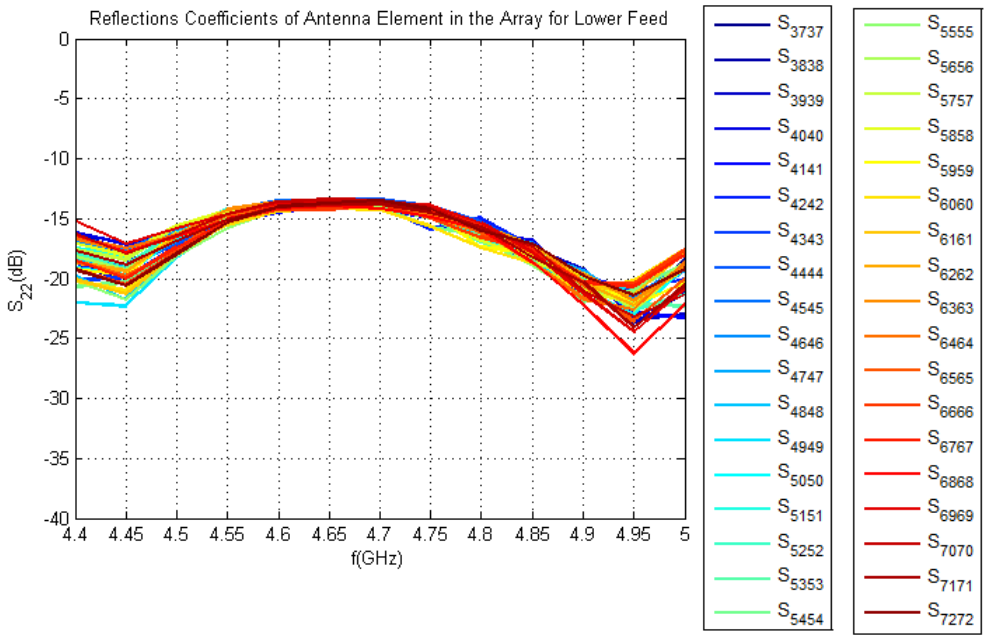

Figure 4.23: Reflection coefficients of each single element versus frequency in the antenna array for the lower feed network in the presence of the grid

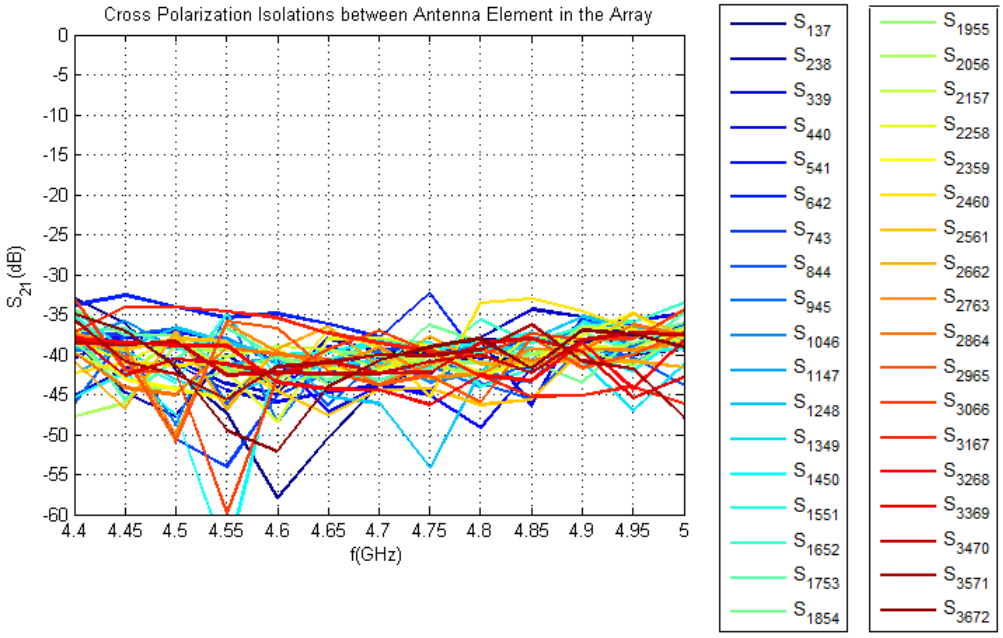

Figure 4.24: Cross polarization isolation of each single element versus frequency in the antenna array in the presence of the grid

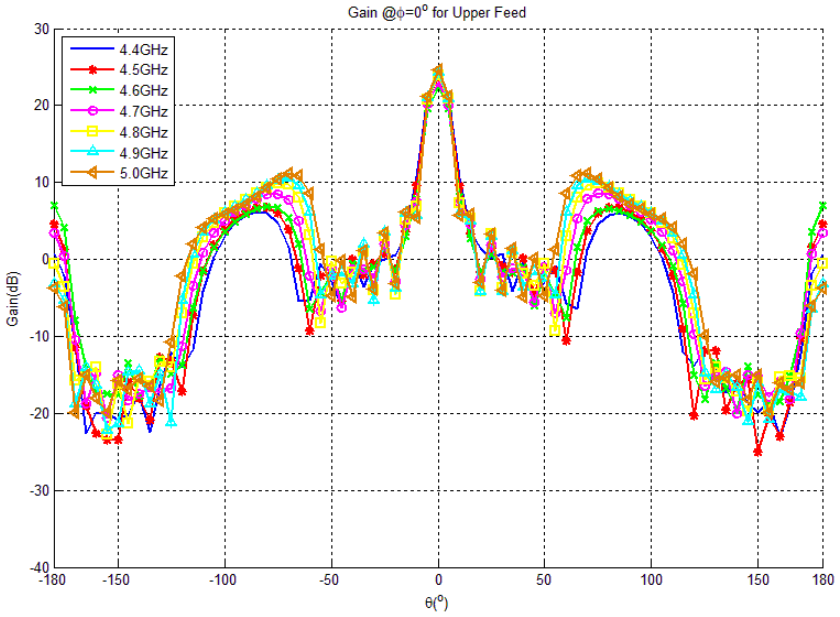

Figure 4.25: Array pattern in the presence of the grid without the feed network at ϕ =0° for the upper feed network for various frequencies

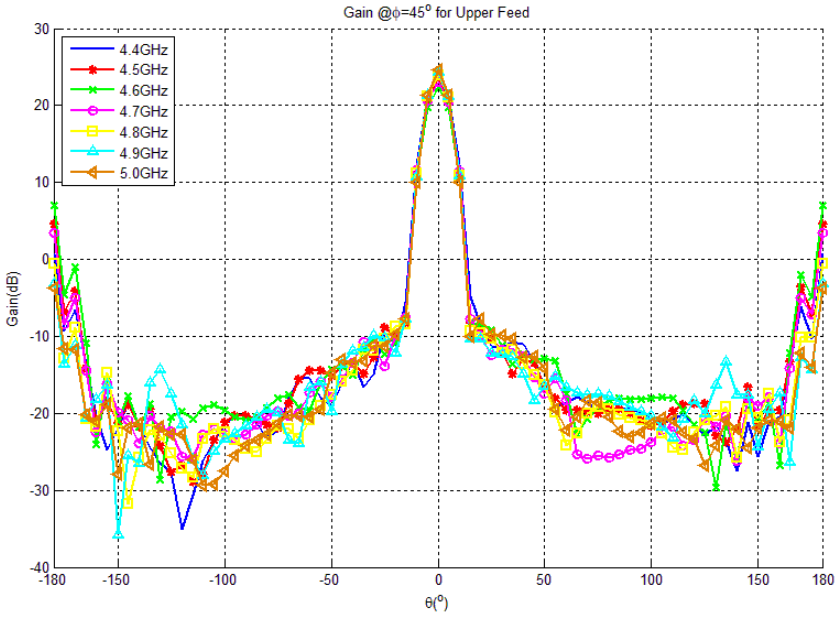

Figure 4.26: Array pattern in the presence of the grid without the feed network at ϕ =45° for the upper feed network for various frequencies

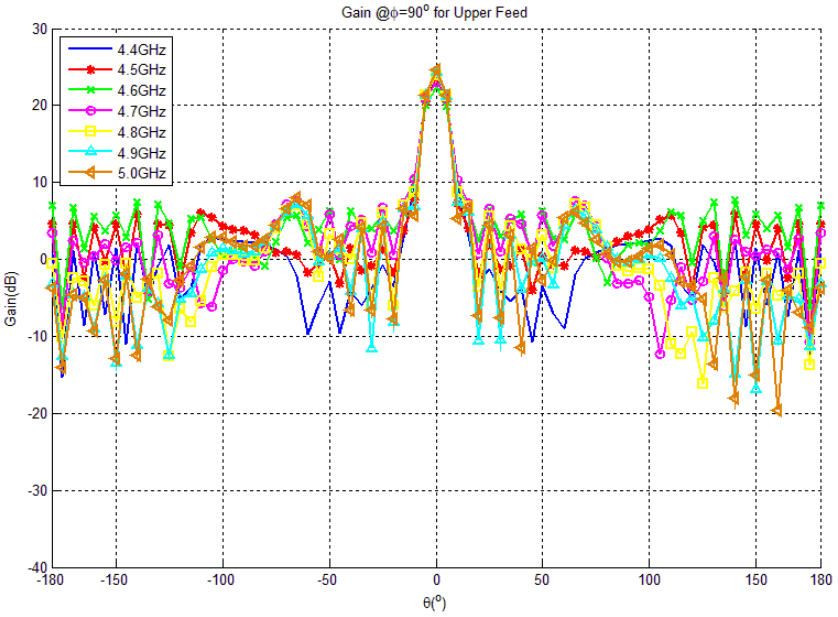

Figure 4.27: Array pattern in the presence of the grid without the feed network at ϕ =90° for the upper feed network for various frequencies

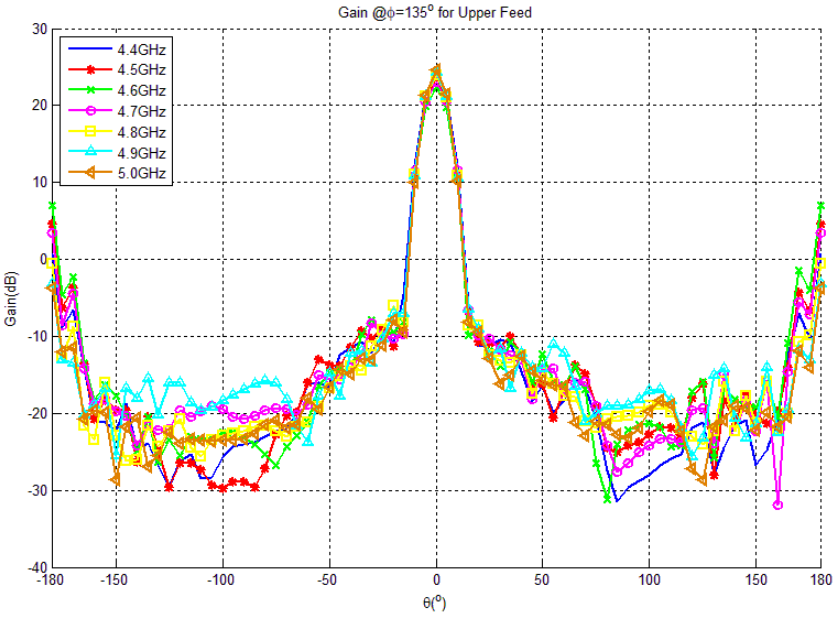

Figure 4.28: Array pattern in the presence of the grid without the feed network at ϕ =135° for the upper feed network for various frequencies

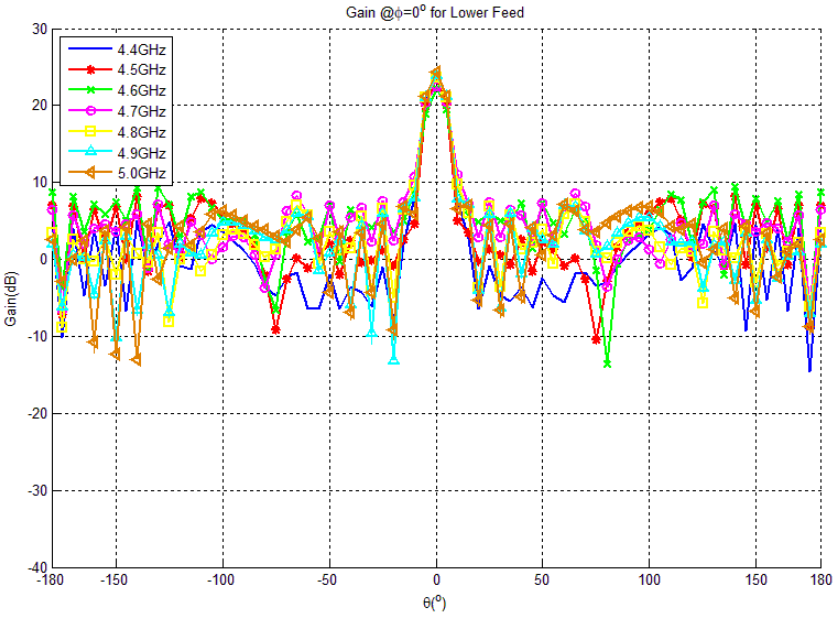

Figure 4.29: Array pattern in the presence of the grid without the feed network at ϕ =0° for the lower feed network for various frequencies

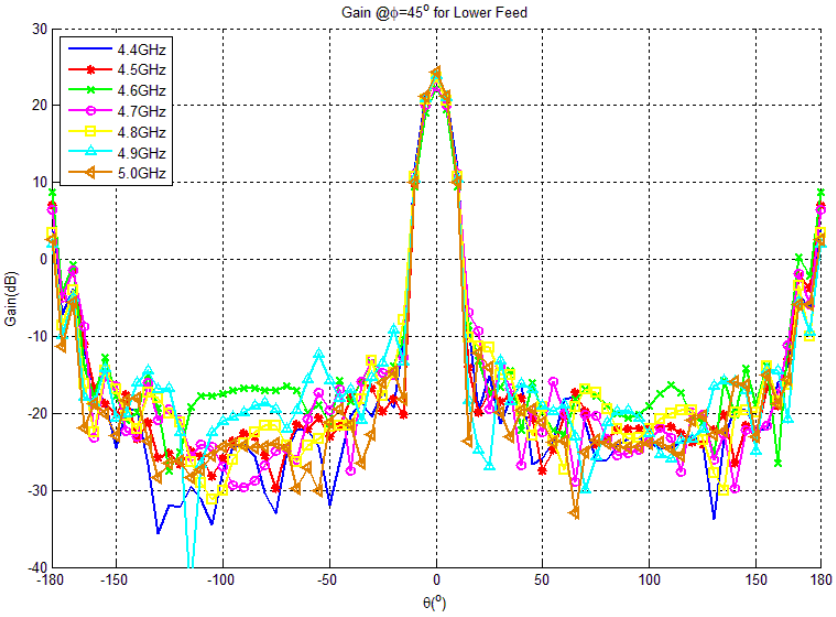

Figure 4.30: Array pattern in the presence of the grid without the feed network at ϕ =45° for the lower feed network for various frequencies

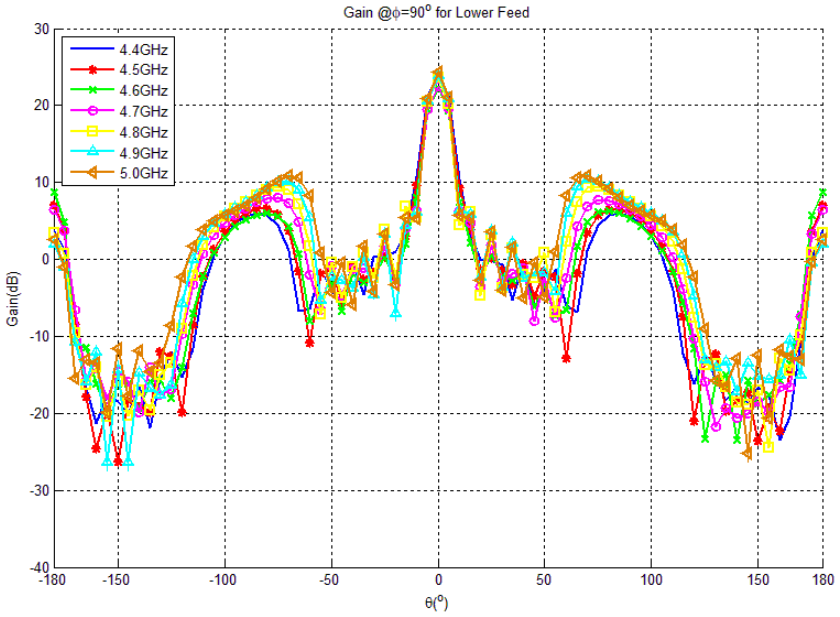

Figure 4.31: Array pattern in the presence of the grid without the feed network at ϕ =90° for the lower feed network for various frequencies

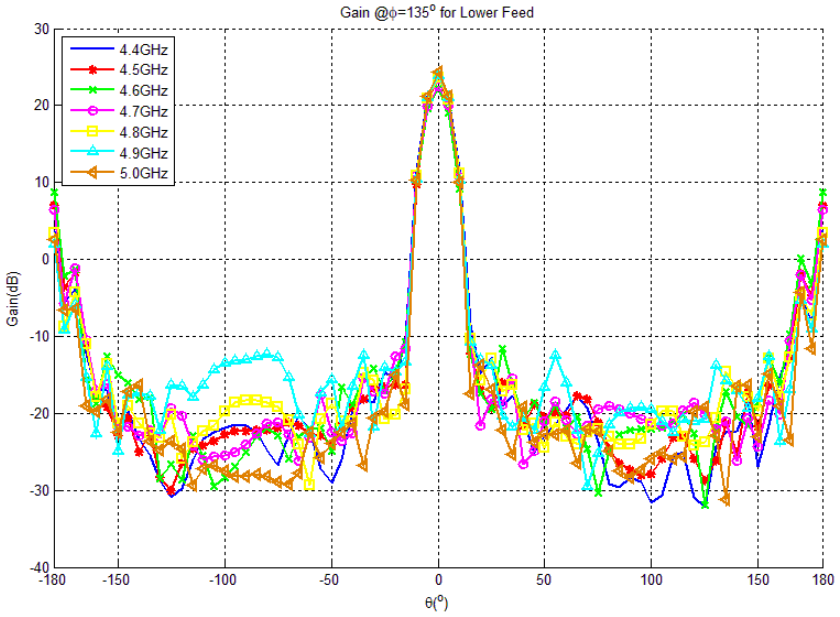

Figure 4.32: Array pattern in the presence of the grid without the feed network at ϕ =135° for the lower feed network for various frequencies

Antenna	$Coupling_{max}$ **@4.4GHz**	$Coupling_{max}$ **@4.7GHz**	$Coupling_{max}$ **@5GHz**
Antenna#1	-32.98dB	-31.24dB	-32.88dB
Antenna#2	-32.21dB	-33.14dB	-33.51dB
Antenna#3	-33.36dB	-34.45dB	-32.27dB
Antenna#4	-31.98dB	-32.62dB	-31.59dB
Antenna#5	-33.02dB	-33.14dB	-32.95dB
Antenna#6	-30.34dB	-31.16dB	-31.38dB
Antenna#7	-30.56dB	-31.24dB	-32.43dB
Antenna#8	-32.13dB	-33.14dB	-32.62dB
Antenna#9	-31.86dB	-33.49dB	-32.21dB
Antenna#10	-31.39dB	-32.62dB	-31.46dB
Antenna#11	-30.49dB	-33.14dB	-32.66dB
Antenna#12	-29.33dB	-31.16dB	-31.19dB
Antenna#13	-29.75dB	-32.20dB	-32.16dB
Antenna#14	-29.72dB	-34.94dB	-32.62dB
Antenna#15	-30.35dB	-33.28dB	-32.21dB
Antenna#16	-29.19dB	-33.13dB	-31.46dB
Antenna#17	-29.57dB	-33.86dB	-32.53dB
Antenna#18	-28.70dB	-32.48dB	-31.19dB
Antenna#19	-29.47dB	-32.66dB	-31.19dB
Antenna#20	-29.72dB	-33.37dB	-32.39dB
Antenna#21	-30.35dB	-33.28dB	-32.43dB
Antenna#22	-29.19dB	-32.30dB	-33.11dB
Antenna#23	-29.57dB	-33.22dB	-32.23dB
Antenna#24	-28.70dB	-32.23dB	-31.52dB
Antenna#25	-29.47dB	-30.99dB	-31.19dB
Antenna#26	-31.31dB	-33.28dB	-32.39dB
Antenna#27	-31.54dB	-33.07dB	-32.43dB
Antenna#28	-30.84dB	-32.30dB	-32.68dB
Antenna#29	-32.00dB	-32.75dB	-32.23dB
Antenna#30	-30.49dB	-31.11dB	-31.52dB
Antenna#31	-31.95dB	-30.99dB	-33.40dB
Antenna#32	-33.99dB	-33.28dB	-32.49dB
Antenna#33	-32.64dB	-33.07dB	-33.67dB
Antenna#34	-34.07dB	-32.67dB	-32.68dB
Antenna#35	-33.85dB	-32.75dB	-32.53dB
Antenna#36	-30.71dB	-31.11dB	-32.97dB

Table 4.3: Minimum inter-element isolation of antenna elements for the upper feed network in the presence of the grid

Antenna	$Coupling_{max}$ **@4.4GHz**	$Coupling_{max}$ **@4.7GHz**	$Coupling_{max}$ **@5GHz**
Antenna#1	-26.93dB	-27.90dB	-28.12dB
Antenna#2	-25.32dB	-27.90dB	-28.12dB
Antenna#3	-23.64dB	-28.11dB	-29.25dB
Antenna#4	-23.64dB	-28.11dB	-31.20dB
Antenna#5	-25.67dB	-28.37dB	-29.96dB
Antenna#6	-27.67dB	-28.37dB	-29.96dB
Antenna#7	-28.11dB	-29.63dB	-27.28dB
Antenna#8	-27.96dB	-29.09dB	-27.28dB
Antenna#9	-27.22dB	-28.96dB	-29.96dB
Antenna#10	-27.22dB	-28.96dB	-30.02dB
Antenna#11	-28.42dB	-29.43dB	-30.02dB
Antenna#12	-29.00dB	-29.43dB	-30.07dB
Antenna#13	-29.01dB	-29.00dB	-27.82dB
Antenna#14	-28.29dB	-28.31dB	-27.82dB
Antenna#15	-26.57dB	-28.31dB	-28.60dB
Antenna#16	-26.57dB	-28.98dB	-29.15dB
Antenna#17	-27.93dB	-28.98dB	-29.15dB
Antenna#18	-28.70dB	-29.52dB	-30.03dB
Antenna#19	-28.55dB	-29.07dB	-26.76dB
Antenna#20	-28.62dB	-29.07dB	-26.76dB
Antenna#21	-26.46dB	-28.55dB	-29.10dB
Antenna#22	-26.46dB	-28.55dB	-30.49dB
Antenna#23	-28.46dB	-28.80dB	-30.49dB
Antenna#24	-29.11dB	-28.80dB	-32.01dB
Antenna#25	-28.36dB	-29.11dB	-26.90dB
Antenna#26	-27.89dB	-28.99dB	-26.90dB
Antenna#27	-26.88dB	-27.83dB	-30.91dB
Antenna#28	-26.88dB	-27.83dB	-30.55dB
Antenna#29	-28.00dB	-28.26dB	-29.85dB
Antenna#30	-28.89dB	-28.26dB	-29.85dB
Antenna#31	-26.84dB	-27.75dB	-29.00dB
Antenna#32	-25.47dB	-27.75dB	-26.52dB
Antenna#33	-24.14dB	-28.52dB	-26.52dB
Antenna#34	-24.14dB	-28.52dB	-28.85dB
Antenna#35	-24.98dB	-27.55dB	-28.85dB
Antenna#36	-27.64dB	-27.55dB	-30.76dB

Table 4.4: Minimum inter-element isolation of antenna elements for the lower feed network in the presence of the grid

As it can be seen from these results, there is no significant change in reflection coefficients for the upper and lower feed networks as well as cross polarization isolations. On the other hand, the maximum inter-element isolations are increased approximately by 5dB. The final configuration for the proposed antenna array in the presence of the grid structure is illustrated in Fig. 4.33. The feed networks now can be connected to antenna elements.

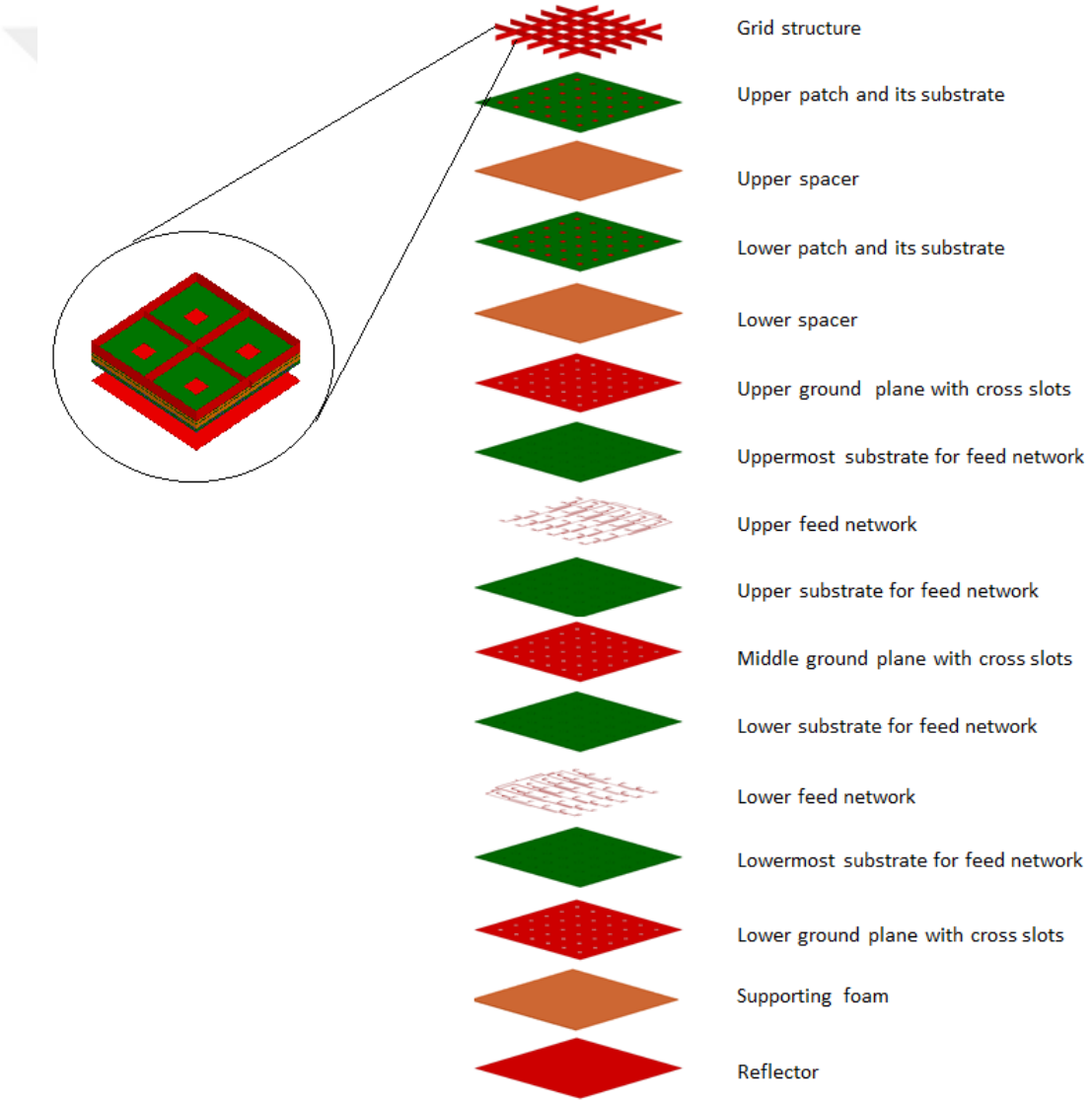

Figure 4.33: Exploded view of the proposed antenna array configuration in the presence of the grid structure

When the entire array is simulated in the presence of the grid structure, the following S-parameters results (Fig. 4.34) and the gain pattern results (see Fig. 4.35 - Fig. 4.42) are obtained:

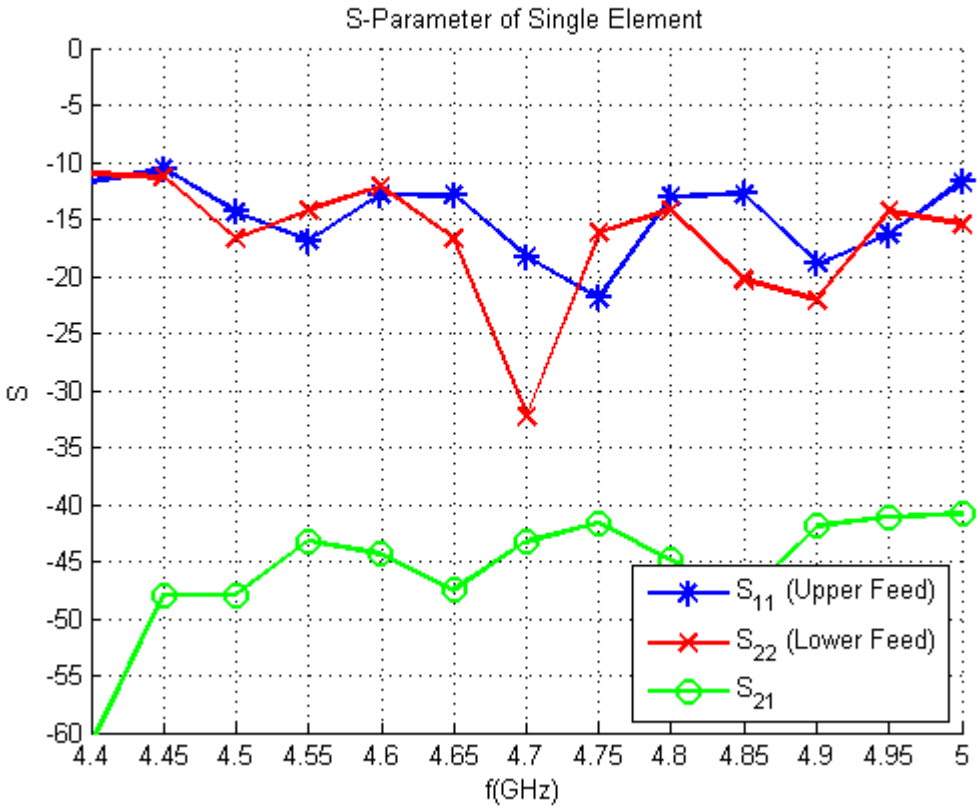

Figure 4.34: S-parameters of the entire antenna array in the presence of the grid versus frequency over the desired band

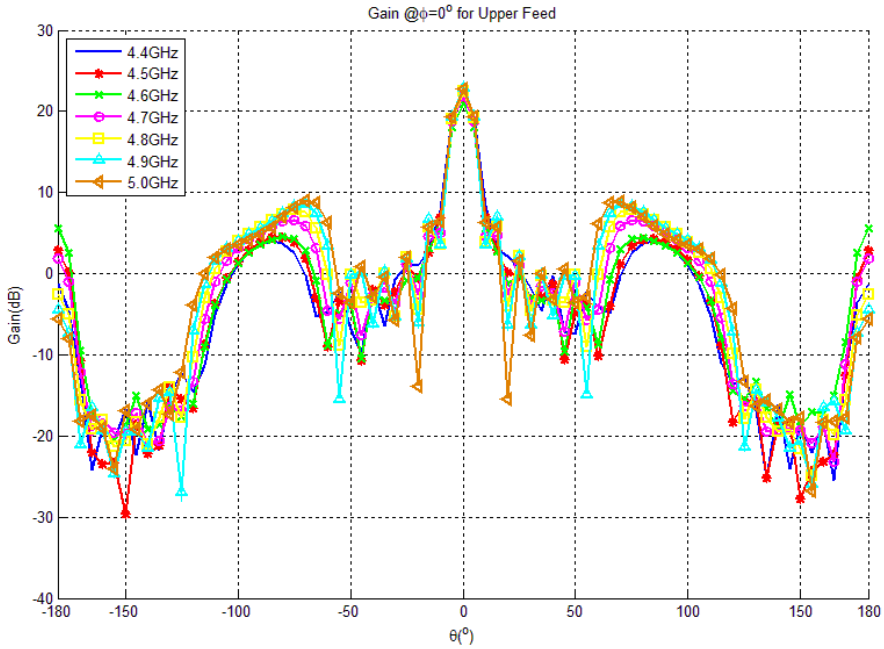

Figure 4.35: The entire array gain pattern at ϕ =0° for the upper feed network in the presence of the grid for various frequencies

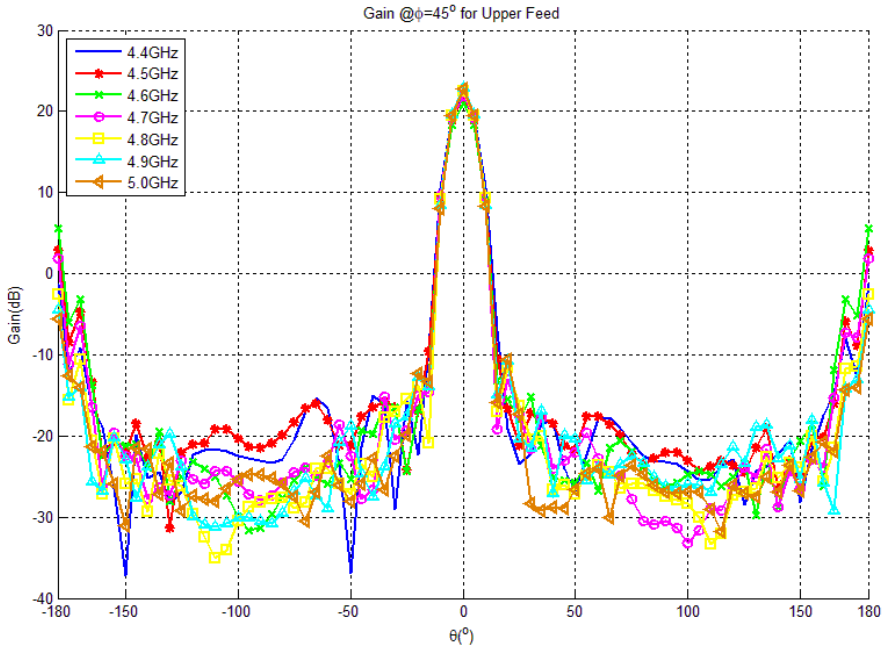

Figure 4.36: The entire array gain pattern at ϕ =45° for the upper feed network in the presence of the grid for various frequencies

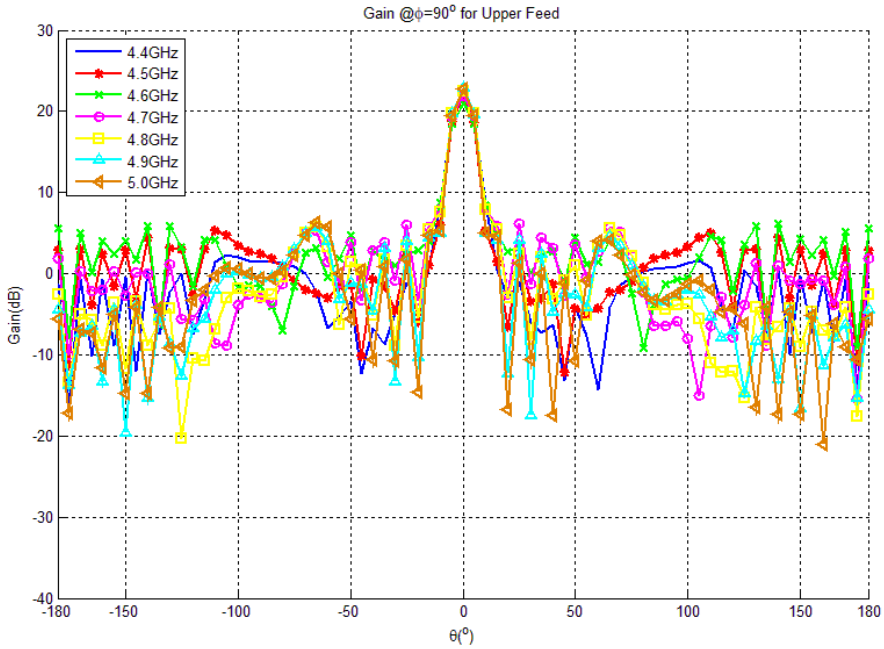

Figure 4.37: The entire array gain pattern at ϕ =90° for the upper feed network in the presence of the grid for various frequencies

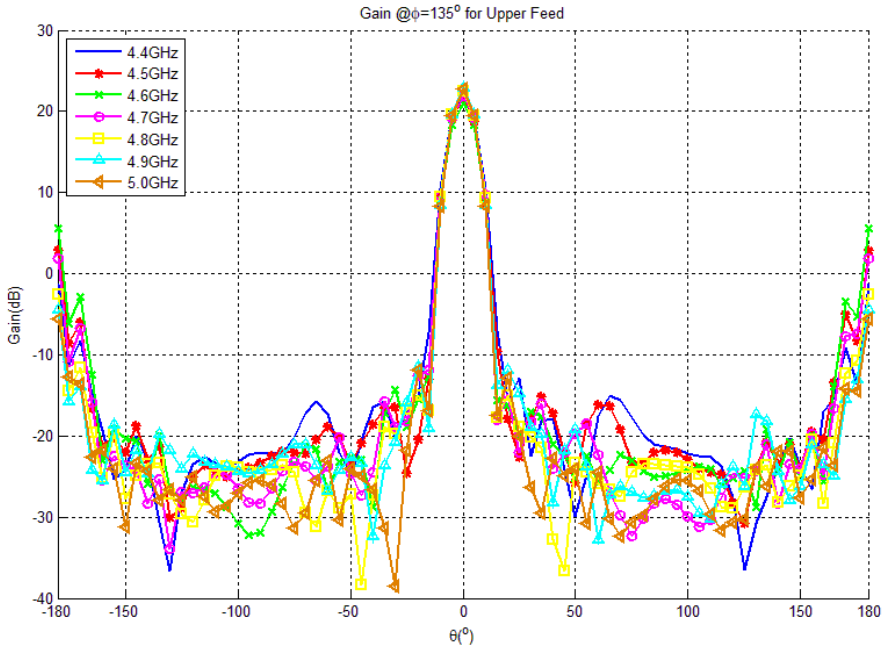

Figure 4.38: The entire array gain pattern at ϕ =135° for the upper feed network in the presence of the grid for various frequencies

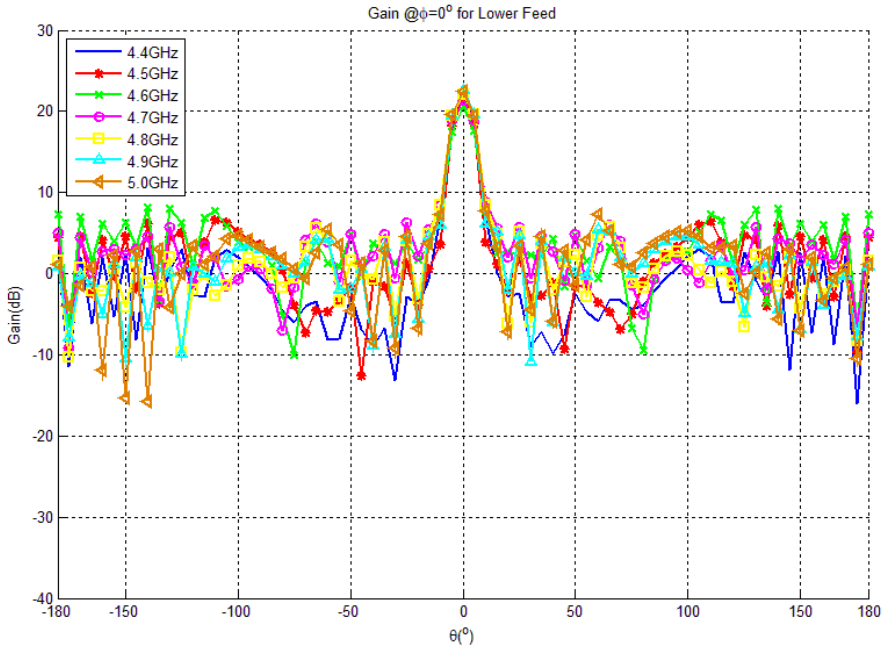

Figure 4.39: The entire array gain pattern at ϕ =0° for the lower feed network in the presence of the grid for various frequencies

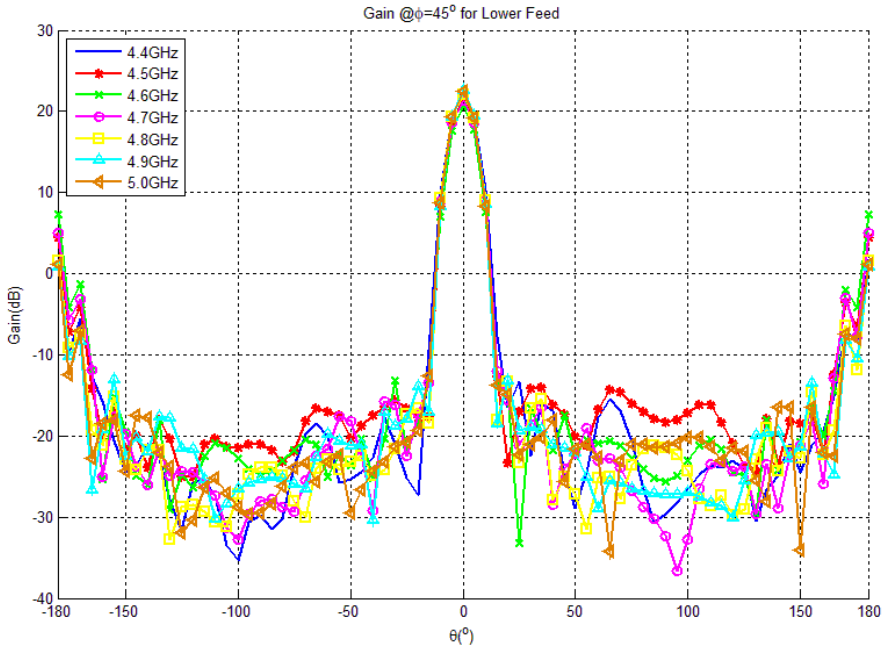

Figure 4.40: The entire array gain pattern at ϕ =45° for the upper feed network in the presence of the grid for various frequencies

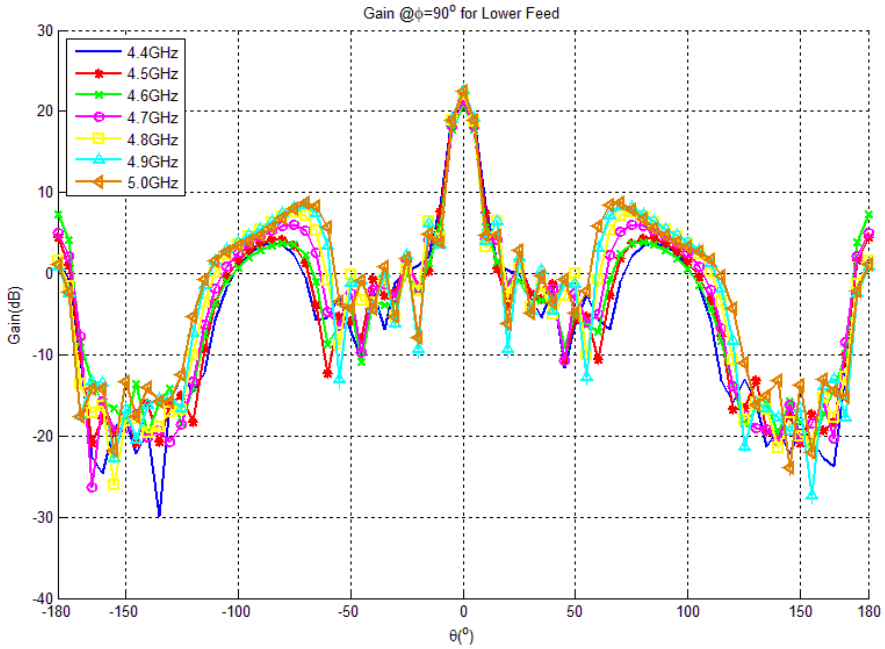

Figure 4.41: The entire array gain pattern at ϕ =90° for the upper feed network in the presence of the grid for various frequencies

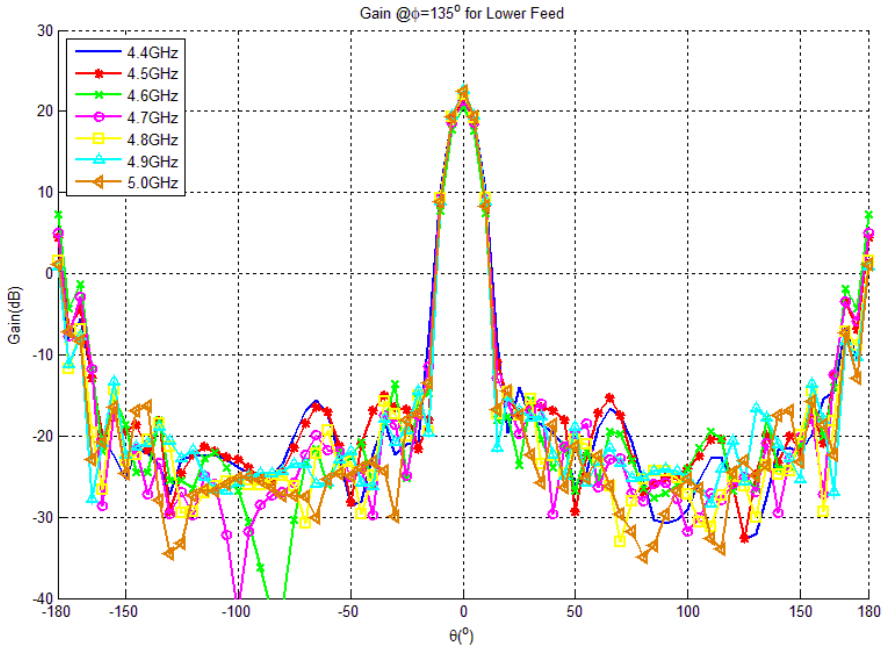

Figure 4.42: The entire array gain pattern at ϕ =135° for the upper feed network in the presence of the grid for various frequencies

The results indicate that together with the grid structure both the couplings among the antenna elements and the effect of grating lobes on SLL can be reduced. It can be seen that reflection coefficients for both upper and lower feed networks are lower than -10dB. Additionally, the cross polarization isolation is better than 40dB. Another point is that, we have SLL lower than -15dB for upper and lower feeds on both cardinal and intercardinal planes. Only at 5GHz, SLL reaches to -14.8dB. With these results, the desired requirements are achieved.

Chapter 5

Conclusion

In this thesis, a C-band dual-polarized strip-fed aperture coupled stacked patch planar antenna array for P2P communication is designed. To satisfy the requirements for P2P communication and MIMO capability; 20dB gain, 40dB cross polarization isolation and -15dB SLL are achieved in both cardinal and intercardinal planes of the antenna array.

At first, a novel antenna element, dual-polarized aperture coupled stacked patch antenna is proposed. The parameters that affect the impedance characteristics of the proposed antenna are provided and investigated with detailed parametric study. Graphical results that indicate the relation between antenna parameters and S-parameters are presented.

After the design of the single element, the amplitude distribution requried for the desired patterns are providied. The design of the feed network that realizes this distribution is given in a step by step fashion together with the related simulations. The resulted array factors and expected array patterns, that are obtained by the multiplication of the antenna element patterns and array factors, are presented.

36 single antenna elements are placed to form a 6x6 in array configuration and they are connected to the feed networks in the continuation. Because the outputs

of the feed networks are not output matched, high reflection coefficients and low SLL values are observed in the array as a result of distortions of amplitude distributions and coupling among the antenna elements, unlike expected results in the design of the feed network. In order to reduce the coupling, a grid structure is designed. In this way, desired patterns and low reflection coefficients are obtained.

The main contribution of this study is the design of a dual-polarized strip-fed aperture coupled stacked patch antenna. In the literature, there are only single polarized ones with stripline feeding. The requirement for strip-fed patch antenna with dual polarization is due to two main reasons. The first one is to prevent distortions on amplitude and phase distributions that occur due to coupling between the feed networks for different polarizations. The second reason is to increase the cross polarization isolation. If microstrip fed patch antennas were used, such a high cross polarization isolation (-40dB) would not be achieved. Additionally, when the feed networks were stacked in order to constitute the dual-polarized feed network, the amplitude and phase distributions on the feed networks would be distorted and the desired array factors and array patterns could not be obtained. Another important point for single antenna element is the vias that are shorting all the ground planes to the others. Without these vias, at the frequencies where patches start to operate and operating of slots is ceasing, a sharp change in the impedance behavior of the antenna element would be observed. The vias eliminate this change by making current distributions on the ground planes equal. Finally, in the array design a grid struture that seperates the antenna elements is presented to increase the inter-element isolation. In this way, ampltiude distortions on the feed network can be reduced and desired array patterns and reflection coefficients can be achieved. Moreover, effect of the grating lobes on SLL can be reduced with this method.

As the future work, the fabrication and measurement of the proposed array will be performed. The fabrication will be performed for single antenna element and antenna array separately. In addition, the grid structure will be fabricated and measurement of the antenna array will be performed in the presence and absence of the grid structure. In this way, the results obtained in the desing process can be followed step by step and compared to measurement results.

Bibliography

[1] T. Koonen, "Trends in optical access and in-building networks," 2008 34th European Conference on Optical Communication, 2008.

[2] G. M. Kizer, *Digital microwave communication: Engineering point-to-point microwave systems*. New Jersey: John Wiley Inc, 2013.

[3] J. Conti, "The 10 greatest communications inventions," *Communications Engineer*, vol. 5, no. 1, pp. 14 – 21, 2007.

[4] A. Hirao, Y. Nomura, and H. Yonezu, "Prim's algorithm based P2MP energy-saving," The 10th International Conference on Optical Internet, 2012.

[5] P. Coulton, C. Khirallah, and S. Qazi, "Increasing the spectral efficiency in fixed point-to-point microwave radio system using multiple antenna arrays," IEE Colloquium on DSP enabled Radio, 2003.

[6] L. Wang, H. Wu, and G. L. Stuber, "Cooperative jamming-aided secrecy enhancement in P2P communications with social interaction constraints," *IEEE Transactions on Vehicular Technology*, vol. 66, no. 2, pp. 1144 – 1158, 2017.

[7] A. Agustin, S. Lagen, and J. Vidal, "Channel training procedures for MIMO interfering point-to-multipoint channel," 2014 IEEE Global Communications Conference, 2014.

[8] H. Moheb, C. Robinson, and N. Moldovan, "Design and development of linear and circular polarized C-band offset Gregorian reflector antenna for

VSAT application," IEEE Antennas and Propagation Society International Symposium 1997, 1997.

[9] M. Q. Tang, K. S. Rao, M. Cuchanski, and R. Pokuls, "Shaped reflector antennas for satellite communications," Symposium on Antenna Technology and Applied Electromagnetics (ANTEM 1994), 1994.

[10] M. Albani, P. Bailing, and et al., "Concepts for polarising sheets and dual-gridded reflectors for circular polarisation," 2010 Conference Proceedings ICECom, 20th International Conference on Applied Electromagnetics and Communications, 2010.

[11] V. Zavodny and P. Kopecky, "Reflector antenna in L band," 2015 Conference on Microwave Techniques (COMITE), 2015.

[12] J. R. Bergmann and F. J. V. Hasselmann, "A reflector antenna synthesis for proposed Brasilsat B3 south american coverage at C and Ku-bands," Microwave and Optoelectronics Conference, 1997. Linking to the Next Century. Proceedings., 1997 SBMO/IEEE MTT-S International, 1997.

[13] B. P. Kumar, C. Kumar, V. S. Kumar, and V. V. Srinivasan, "Design of an axially displaced ellipsoid reflector antenna for a 4.6m diameter ship-borne transportable terminal at S-band," 2015 IEEE Applied Electromagnetics Conference (AEMC), 2015.

[14] V. K. Panasa, R. Chivukula, and et al., "Dual polarized monopulse tracking feed for prime focal reflector antenna at S-band using crossed dipole elements," 2015 European Microwave Conference (EuMC), 2015.

[15] S. Paus, "The INTELSAT-9 C-band hemi/zone antennas," 1999 29th European Microwave Conference, 1999.

[16] J. R. Bergmann and L. P. N. D. Costa, "Shaped beam reflector antennas for the C-band Brasilsat case," SBMO International Microwave Conference/Brazil, 1993.

[17] P. Sarasa, A. Baussois, and P. Regnier, "A compact single horn C/X dual band and circular polarized Tx-Rx antenna system," IEEE Antennas and Propagation Society Symposium, 2004, 2004.

[18] S. A. Muhammad, A. Roland, S. H. Dahlan, R. Sauleau, and H. Legay, "Hexagonal shaped broadband compact scrimp horn antenna for operation in c band," *IEEE Antennas and Wireless Propagation Letters*, vol. 11, pp. 842 – 845, 2012.

[19] B. Du, W. J. Zhang, and K. Z. Yang, "A novel dual-slot structure mode converter for L/C dual-band corrugated horn," IEEE Antennas and Propagation Society Symposium, 2004, 2004.

[20] Z. Zhang, H. Wenhua, and Q. Shi, "The design and optimization of a C band integrated mode converter and horn antenna," 2008 17th International Conference on High Power Particle Beams (BEAMS), 2008.

[21] O. Soykin, A. Kolobov, and et al., "Planar MIMO antenna system with polarization diversity for 2.5-2.7 GHz LTE indoor femtocells," 2015 9th European Conference on Antennas and Propagation (EuCAP), 2015.

[22] I. Acimovic, D. A. McNamara, and A. Petosa, "Dual-polarized microstrip patch planar array antennas with improved port-to-port isolation," *IEEE Transactions on Antennas and Propagation*.

[23] S. Soltani and R. D. Murch, "A compact planar printed MIMO antenna design," *IEEE Transactions on Antennas and Propagation*, vol. 63, no. 3, pp. 1140 – 1149, 2015.

[24] G. Zomchek and S. Laxpati, "S-band phased patch array design for satellite applications," 2005 IEEE Antennas and Propagation Society International Symposium, 2005.

[25] V. K. Lakshmeesha, V. V. Srinivasan, and et al., "C-band microstrip planar array for spaceborne microwave remote sensing," 1991 21st European Microwave Conference, 1991.

[26] H. Ito, Y. Kimura, and M. Haneishi, "Beam shaping of a microstrip array antenna fed by a dogbone slot," 2002 3rd International Conference on Microwave and Millimeter Wave Technology, 2002. Proceedings. ICMMT 2002, 2002.

[27] S. Hsu, Y. Ren, and K. Cheng, "A dual-polarized planar-array antenna for S-band and X-band airborne applications," *IEEE Antennas and Propagation Magazine*, vol. 51, no. 4, pp. 70 – 78, 2009.

[28] A. Vallecchi, "Planar square and diamond microstrip patch array antennas for dual-polarization operation," IEEE Antennas and Propagation Society Symposium, 2004, 2004.

[29] O. Khan, J. Pontes, and et al., "A wideband variable width microstrip grid array antenna," 2014 44th European Microwave Conference, 2014.

[30] K. Feng, N. Li, and et al., "A planar array antenna system design for mobile SATCOM," 2014 IEEE International Conference on Signal Processing, Communications and Computing (ICSPCC), 2014.

[31] Z. Yu-mei, Z. Zu-ji, and L. Xiao-peng, "Design of ultralow sidelobe antenna arrays with inclined slots in the narrow wall of rectangular waveguide," 2003 Proceedings of the International Conference on Radar (IEEE Cat. No.03EX695), 2003.

[32] Z. Yu, G. Wang, and C. Zhang, "A broadband planar monopulse antenna array of C-band," *IEEE Antennas and Wireless Propagation Letters*, vol. 8, no. 3, pp. 1325 – 1328, 2009.

[33] M. M. M. Ali, A. M. Azmy, and O. M. Haraz, "Design and implementation of reconfigurable quad-band microstrip antenna for MIMO wireless communication applications," 2014 31st National Radio Science Conference (NRSC), 2014.

[34] S. C. Gao, W. Li, S. Leong, and T. Yeo, "Dual-polarized slot-coupled planar antenna with wide bandwidth," *IEEE Transactions on Antennas and Propagation*, vol. 51, no. 3, pp. 441 – 448, 2003.

[35] J. B. L. Rao, R. Mital, D. P. Patel, and M. G. Parent, "Low cost multibeam phased array antenna for communication with geostationary satellites," *The WSTIAC Qaurterly*, vol. 10, no. 3, pp. 9 – 12, 2011.

[36] K. Wincza, S. Gruszczynski, and K. Sachse, "Aperture coupled to stripline antenna element for integrated antenna arrays," *Electronics Letters*, vol. 42, no. 3, p. 130, 2006.

[37] D. Pozar, "Microstrip antenna aperture-coupled to a microstripline," *Electronics Letters*, vol. 21, no. 2, p. 49, 1985.

[38] D. Pozar and S. Duffy, "A dual-band circularly polarized aperture-coupled stacked microstrip antenna for global positioning satellite," *IEEE Transactions on Antennas and Propagation*, vol. 45, no. 11, pp. 1618 – 1625, 1998.

[39] S. Padhi, N. Karmakar, C. Law, and S. Aditya, "A dual polarized aperture coupled circular patch antenna using a C-shaped coupling slot," *IEEE Transactions on Antennas and Propagation*, vol. 51, no. 12, pp. 3295 – 3298, 2003.

[40] "ROHACELL HF Product information datasheet."

[41] "ROGERS RT/duroid 5870 5880 datasheet."